DAMPING FROM VIBRATION RECORDS OF TALL BUILDINGS

A THESIS SUBMITTED TO
THE GRADUATE SCHOOL OF NATURAL AND APPLIED SCIENCES
OF
MIDDLE EAST TECHNICAL UNIVERSITY

BY

ANIL CAN GÜMÜŞTEPE

IN PARTIAL FULFILLMENT OF THE REQUIREMENTS
FOR
THE DEGREE OF MASTER OF SCIENCE
IN
CIVIL ENGINEERING

APRIL 2023

Approval of the thesis:

DAMPING FROM VIBRATION RECORDS OF TALL BUILDINGS

submitted by **ANIL CAN GÜMÜŞTEPE** in partial fulfillment of the requirements for the degree of **Master of Science in Civil Engineering, Middle East Technical University** by,

Prof. Dr. Halil Kalıpçılar
Dean, Graduate School of **Natural and Applied Sciences** _____

Prof. Dr. Erdem Canbay
Head of the Department, **Civil Engineering** _____

Assoc. Prof. Dr. Ozan Cem Çelik
Supervisor, **Civil Engineering, METU** _____

Examining Committee Members:

Prof. Dr. Kağan Tuncay
Civil Engineering, METU _____

Assoc. Prof. Dr. Ozan Cem Çelik
Civil Engineering, METU _____

Prof. Dr. Yalın Arıcı
Civil Engineering, METU _____

Prof. Dr. Ahmet Yakut
Civil Engineering, METU _____

Asst. Prof. Dr. Berat Feyza Soysal Albostan
Civil Engineering, Çankaya University _____

Date: 26.04.2023

I hereby declare that all information in this document has been obtained and presented in accordance with academic rules and ethical conduct. I also declare that, as required by these rules and conduct, I have fully cited and referenced all material and results that are not original to this work.

Name, Last name: Anıl Can Gümüştepe

Signature:

ABSTRACT

DAMPING FROM VIBRATION RECORDS OF TALL BUILDINGS

Gümüştepe, Anıl Can
Master of Science, Civil Engineering
Supervisor: Assoc. Prof. Dr. Ozan Cem Çelik

April 2023, 104 pages

With the release of the new Turkish Building Earthquake Code, real-time structural response monitoring of tall buildings became mandatory. As part of two research projects undertaken at Middle East Technical University and Bogazici University to develop the structural health monitoring guidelines, two tall buildings in Izmir and Istanbul were instrumented, respectively. This thesis focuses on the damping estimations of the tallest building in Izmir from its ambient vibration records. Structural response of the building is currently monitored in real time by a dense network of 27 channels of accelerometers. Using the random decrement method, the modal damping ratios of the building were identified for the first four modes in the East-West and North-South translational directions and in the torsional direction. The mean damping ratios were 0.6–1.0% with coefficients of variation in the order of 0.10–0.40 for the first two modes. The identified modal damping ratios were compared with the values from code and other formulations in literature as well as other instrumented tall buildings. The time history analyses were performed to reproduce the recorded strong motion responses of the building during the 2019 M_w 5.0 Ayvacik, Canakkale and M_w 5.8 Marmara Sea, Istanbul earthquakes using both

identified and code-specified damping ratios in the existing finite element model of the building to evaluate the impact of damping on structural responses.

Keywords: Ambient Vibration, Damping, Earthquake Response, Random Decrement Method, Structural Health Monitoring, System Identification

ÖZ

YÜKSEK BİNALARIN TİTREŞİM KAYITLARINDAN SÖNÜM HESAPLAMALARI

Gümüştepe, Anıl Can
Yüksek Lisans, İnşaat Mühendisliği
Tez Yöneticisi: Doç. Dr. Ozan Cem Çelik

Nisan 2023, 104 sayfa

Yeni Türkiye Bina Deprem Yönetmeliğinin yürürlüğe girmesiyle yüksek binaların yapı tepkilerinin gerçek zamanlı olarak izlenmesi zorunlu hale gelmiştir. Orta Doğu Teknik Üniversitesi ve Boğaziçi Üniversitesi'nde yapı sağlığı izleme yönergesi hazırlanması amacıyla yürütülen iki araştırma projesi kapsamında sırasıyla İzmir ve İstanbul'da iki yüksek binaya yapı sağlığı izleme sistemleri kurulmuştur. Bu tez, İzmir'in en yüksek binasının çevresel titreşim kayıtlarından sönüm hesaplarına odaklanmaktadır. Binanın yapısal tepkisi ivmeölçerlerden oluşan 27 kanallı kapsamlı bir yapı sağlığı izleme sistemi ile gerçek zamanlı olarak izlenmektedir. Rassal azalma metodu kullanılarak binanın Doğu-Batı ve Kuzey-Güney yönlerindeki ilk dört öteleme modları ve binanın ilk dört burulma modlarına ait modal sönüm oranları tespit edilmiştir. İlk iki mod için ortalama sönüm oranları %0,6–1,0 arasındadır ve ilgili varyasyon katsayıları 0,10–0,40 mertebesindedir. Tespit edilen modal sönüm oranları, yönetmeliklerde verilen değerler ve literatürde bulunan formülasyonların yanı sıra yapı sağlığı izleme sistemine sahip diğer yüksek binaların sönüm oranları ile karşılaştırılmıştır. Tespit edilen ve yönetmelikte verilen modal sönüm oranları binanın mevcut sonlu eleman modelinde kullanılarak zaman

tanım alanında yapılan analizlerle binanın 2019 M_w 5,0 Ayvacık, Çanakkale ve M_w 5,8 Marmara Denizi, İstanbul depremleri sırasında kaydedilen kuvvetli hareket tepkileri elde edilmeye çalışılmış ve sönüm oranlarının bina tepkilerine etkisi değerlendirilmiştir.

Anahtar Kelimeler: Çevresel Titreşim, Deprem Tepkisi, Rassal Azalma Metodu, Sistem Tanılaması, Sönüm, Yapı Sağlığı İzleme

To my family,

ACKNOWLEDGMENTS

The author wishes to express his deepest appreciation to his supervisor Dr. Ozan Cem Çelik for his unwavering guidance, invaluable support, constructive criticism and continuous encouragement throughout this research.

The author is deeply grateful to the jury members for their time, effort and expertise invested in evaluating this thesis. Their thoughtful comments and recommendations have been instrumental in shaping and refining the research.

Mistral Izmir Office Tower was instrumented by funding received from the Disaster and Emergency Management Authority of Turkey under grant UDAP-G-17-04. This support is gratefully acknowledged. The author thanks Mistral Izmir Management for authorizing the deployment of the structural health monitoring system.

The author would like to present his sincere thanks to his parents for their continuous support, understanding and patience. Their continuous faith has been a driving force behind the author's determination and perseverance.

Finally, the author would like to thank everybody who were important to the successful realization of this thesis, and also express his apologies for not mentioning everybody one by one.

TABLE OF CONTENTS

CHAPTERS

LIST OF TABLES

TABLES

LIST OF FIGURES

FIGURES

CHAPTER 1

INTRODUCTION

1.1 Background

The growing population, urbanization and increased demand for housing and office spaces have pushed people to build taller buildings. Advances in technology and building materials have made this possible. Constructing tall buildings is also economically beneficial for contractors and landlords due to the potential for higher rents and occupancy rates. Furthermore, tall buildings can also symbolize a city's prosperity and modernization. Considering their importance, such buildings should be maintained well. Especially in the seismic zones, tall buildings are needed to be monitored in real time to assess their condition after a seismic event and to reduce the time required for this assessment. With the release of the new Turkish Building Earthquake Code, TBEC 2018, [AFAD 2018], it became mandatory to install real-time structural response monitoring systems on the buildings of earthquake design class 1 or 2 (i.e., design earthquake spectral acceleration parameter at short periods, $S_{DS} \geq 0.50$) that are taller than 105 m. The Disaster and Emergency Management Authority of Turkey (AFAD) funded two research projects that were undertaken at Middle East Technical University and Bogazici University to develop the guidelines for installing these so-called structural health monitoring (SHM) systems. As part of these research projects, two tall buildings in Izmir and Istanbul are permanently instrumented [Gumus 2021]. Besides the rapid assessment benefit, continuous structural response recordings allow structural engineers to further study the dynamic properties of buildings such as natural vibration frequencies, vibration mode shapes and damping ratios. Damping ratios, in particular, can not be calculated numerically in the design stage. They can be estimated from structural response

recordings; however, the estimations contain high uncertainty. There is a clear need for a robust method to identify the damping ratios.

This study focuses on damping ratio estimations from continuous ambient vibration recordings of tall buildings. For this purpose, this study uses the recorded responses of an instrumented tall building in Izmir, estimates the modal damping ratios, quantifies the uncertainty in the estimations and performs time history analysis of the building using its 3-D finite element structural model with the identified damping ratios to reproduce the recorded earthquake responses.

1.2 Objectives and Scope

The main goals of this study are listed below:

1) Review the literature on instrumented tall buildings with a particular focus on damping ratio estimations using ambient vibration records.
2) Identify the dynamic properties of a tall building from its ambient vibration records for use in damping estimations.
3) Estimate the modal damping ratios of the building and quantify the uncertainty on the estimations.
4) Perform time history analyses using the estimated modal damping ratios in the finite element model to reproduce the recorded earthquake responses of the building and evaluate the effect of the damping ratios in the earthquake responses.
5) Perform time history analyses using the code-based damping ratio in the finite element model and compare the results with the recorded earthquake responses.

1.3 Thesis Outline

This chapter has presented the background and objectives and scope of this study.

Chapter 2 reviews the literature on previously instrumented buildings and damping ratio estimation methods using ambient vibration records.

Chapter 3 briefly presents the studied tall building and its instrumentation system, describes the random decrement method, and estimates the modal damping ratios of the building and compares them with the values from the literature.

Chapter 4 briefly presents the existing finite element model of the building and performs time history analyses to reproduce the recorded earthquake strong motion responses.

Finally, Chapter 5 presents a summary of the research, conclusions and possible future contributions to the study.

CHAPTER 2

LITERATURE REVIEW

2.1 Introduction

This chapter lists the benefits of instrumenting tall buildings for monitoring their structural responses and presents examples of instrumented tall buildings around the world together with the findings of system identification studies conducted using the recorded acceleration responses. The widely used methods to identify the damping ratios from ambient vibration records in the literature are also critically reviewed.

2.2 SHM on Tall Buildings

SHM systems on tall buildings can play a critical role after an earthquake event. Approximately 300 buildings were subjected to inspection of their structural members and connections after the 1994 Northridge earthquake, which is a costly and time-consuming process [Limongelli and Celebi 2019]. If those buildings were instrumented, significant amount of time and money could have been saved. In addition to the practical benefits, SHM systems help us enlarge our knowledge of civil engineering structures.

The primary benefits and justifications for placing SHM systems on tall buildings were summarized below [Limongelli and Celebi 2019, Shan et al. 2020, Su et al. 2020]:

1) Perform rapid and accurate damage assessment in a tall building immediately after extreme events to decide on the evacuation and future retrofit or repair works.

2) Validate the design assumptions and parameters, finite element models and laboratory tests using the identified dynamic properties from SHM system records, i.e., natural vibration frequencies, vibration mode shapes, and damping ratios.
3) Improve understanding of the structural response mechanisms in the real world and help developing structural design codes.
4) Collect mass amount of invaluable in-situ data for further research in structural engineering.

With the realization of the benefits listed above, an increasing number of buildings have been instrumented and continuously monitored. In the United States, the accelerometers were installed first by the U.S. Department of Commerce, Coast and Geodetic Survey at the beginning of 1930s. The importance of the SHM systems was started to be acknowledged after the 1933 Long Beach earthquake and the network of instrumentations was expanded rapidly [USGS 2023]. The first permanently instrumented building is the Hollywood Storage Building, which was instrumented in 1933 [Trifunac and Todorovska 2001]. Currently, the National Seismic Monitoring Program (NSMP) under the U.S. Geological Survey (USGS) and the California Strong Motion Instrumentation Program (CSMIP) under the California Geological Survey (CGS) are the two largest instrumentation programs in the United States. Both programs have different types of instrumented structures such as buildings, dams, tunnels and bridges in their inventory. The CSMIP and NSMP inventories include 248 and 95 instrumented buildings, respectively [Celebi 2022]. In addition to the buildings in the United States, more than 100 buildings in Japan and more than 40 buildings in Taiwan have been instrumented for recording their seismic responses and assessing their post-earthquake damages [Su et al. 2020].

In the following sub-sections, examples of instrumented tall buildings around the world are presented and the system identification studies conducted using the recorded acceleration responses are summarized.

2.2.1 One Rincon Hill Tower

The acceleration responses of One Rincon Hill Tower were recorded under ambient vibrations and several earthquakes including the 2014 M_w 6.0 Napa earthquake [Celebi et al. 2013, Celebi et al. 2017]. One Rincon Hill Tower is a 188 m tall 64-story building in San Francisco, California, which was completed in 2008. The building has a 34.4 m by 41.8 m rectangular footprint. It is the tallest building in the United States designed using a performance-based seismic design procedure. The structural system of the building is composed of reinforced concrete (RC) core shear walls and columns, with added RC outrigger columns, which are connected to the core shear walls with buckling restrained braces (BRBs) at floors 28–32 and 51–55 (Figure 2.1). In addition, two tuned liquid sloshing dampers (TSDs) are located at floor 62.

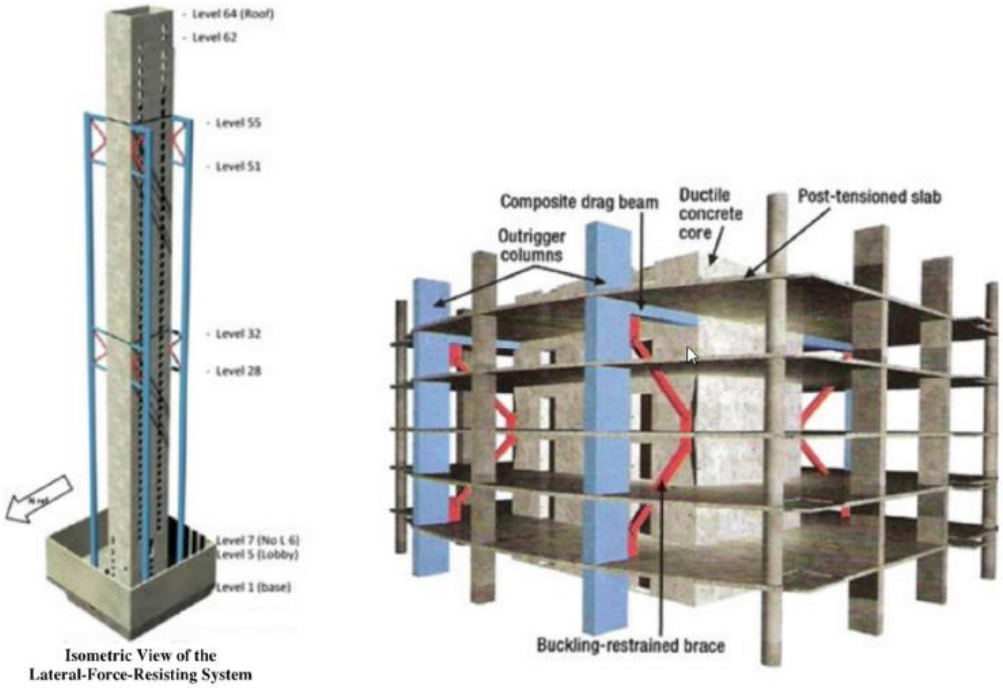

Figure 2.1 Isometric view of the structural system and BRB system of One Rincon Hill Tower [Celebi et al. 2013]

The building was instrumented by 72 channels of accelerometers to monitor its structural responses within the scope of CSMIP (Figure 2.2). The dynamic properties such as natural frequencies, mode shapes and modal damping ratios were identified using spectral analysis methods and subspace methods under ambient vibrations at first [Celebi et al. 2013], then under earthquake excitations [Celebi et al. 2017]. Under ambient excitations, the fundamental natural frequencies and corresponding modal damping ratios were identified as 0.30 Hz and 0.9%, 0.28 Hz and 0.3–0.9% and 0.70 Hz and 0.4% for the North-South (N-S) translational, East-West (E-W) translational and torsional modes, respectively. On the other hand, under earthquake excitations, the fundamental natural frequencies and corresponding modal damping ratios were identified as 0.29 Hz and 1.2%, 0.26 Hz and 2.2–4.1% and 0.68 Hz and 0.8% for the N-S translational, E-W translational and torsional modes, respectively. During the 2014 Napa earthquake, the maximum top floor acceleration was 0.17 g. Furthermore, it was observed that BRBs and TSDs did not change the mode shapes or the overall dynamic characteristics of the building under ambient and low-level earthquake excitations and no non-linearities were observed.

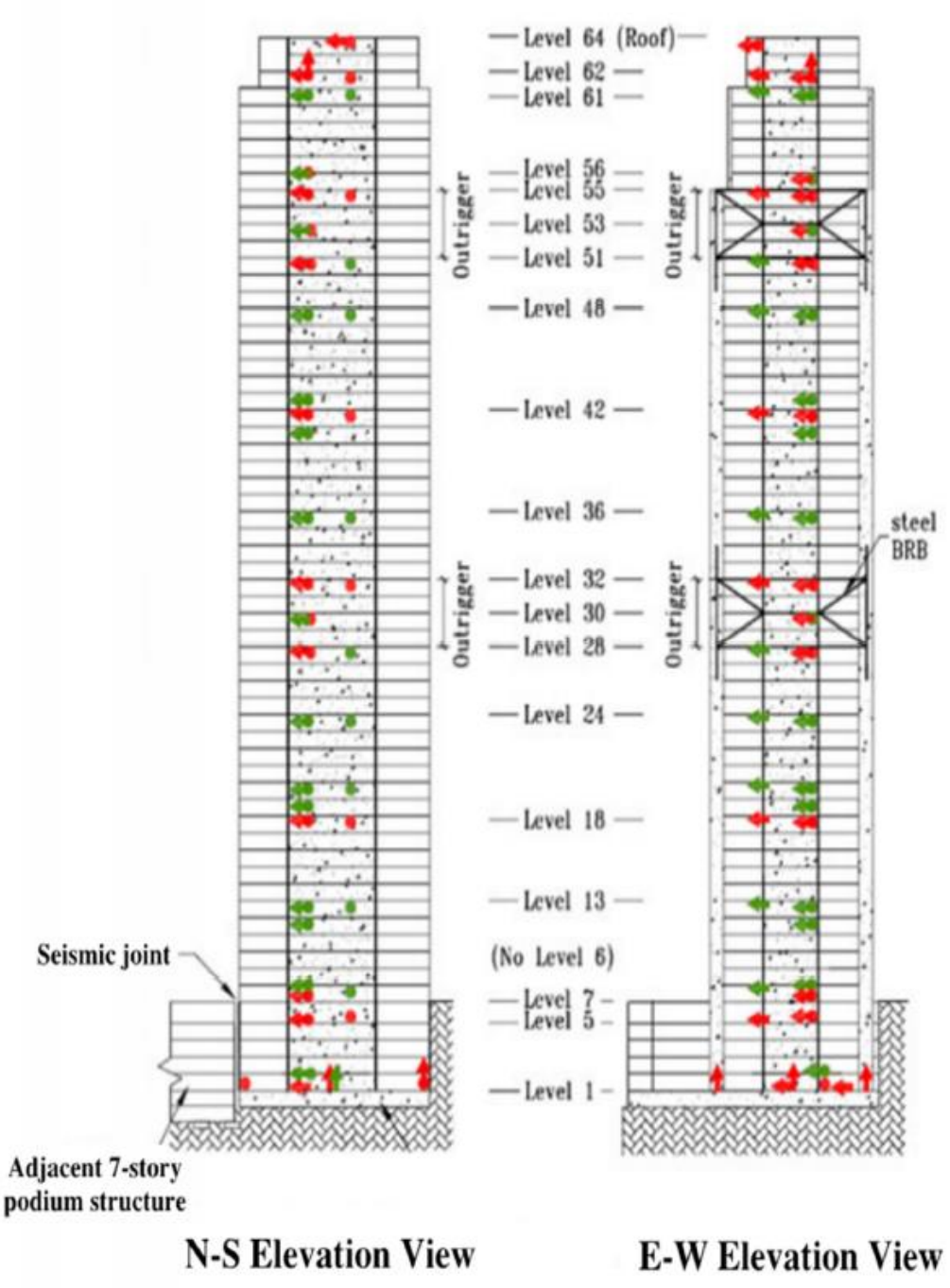

Figure 2.2 Instrumentation scheme of One Rincon Hill Tower (adopted from Celebi et al. [2013])

2.2.2 Ping-An Finance Center

The acceleration response of Ping-An Finance Center was recorded during Typhoon Haima (2016) [He et al. 2017]. Ping-An Finance Center is a 600 m tall 118-story building in Shenzen, China. The building has a square footprint with 56.4 m sides, which decrease gradually to 46.0 m along the height of the building. It is the second tallest building in China and the fourth tallest in the world [Zhang and Li 2019]. The structural system of the building is composed of a tube-in-tube system, wherein the inner tube is made of RC shear walls and the outer tube consists of eight composite columns and seven belt trusses. The tubes are connected to each other with four outriggers. Two uniaxial accelerometers placed on floor 81 were used (Figure 2.3) to identify the dynamic properties and evaluate the performance of the building before, during and after Typhoon Haima. The fundamental natural frequency of the building was identified using the peak picking method as 0.12 Hz. The associated damping ratio was calculated as 0.7% from the ambient vibration records (before the typhoon) and 0.9% during the typhoon using the half-power bandwidth method and 0.6–1.2% during the typhoon using the random decrement method. The recorded maximum floor acceleration during the typhoon was 0.003 g. It was concluded that 0.5–1.5% damping ratio is reasonable for the design of the building under wind-induced excitations. The serviceability performance of the building during the typhoon was shown to meet upper limits given in ISO-6897-1984 standard [ISO 1984].

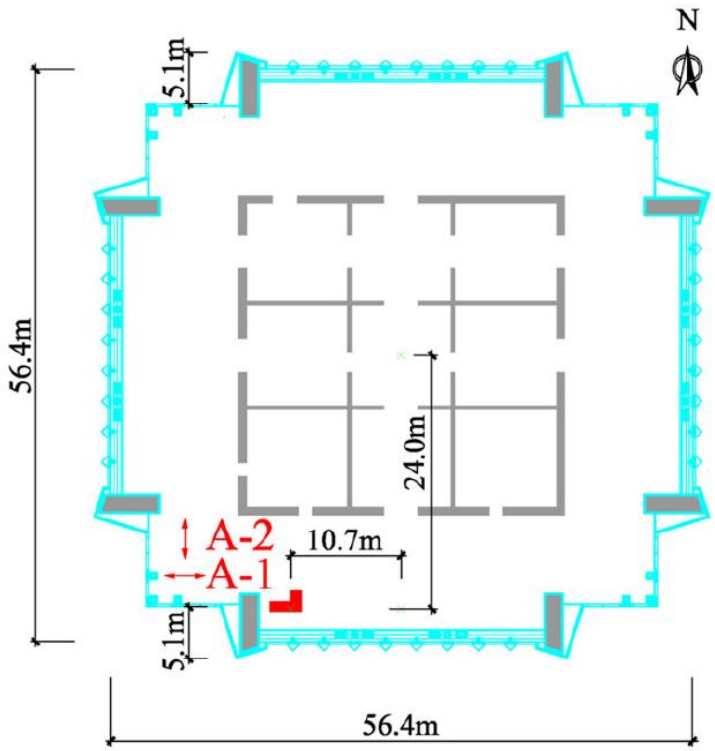

Figure 2.3 Accelerometer locations on floor 81 [He et al. 2017]

2.2.3 Atwood Building

The acceleration responses of Atwood building under multiple small to medium earthquakes in 2003–2006 were recorded [Celebi 2006]. Atwood building is an 81 m tall 20-story building, which was constructed in 1980, in Anchorage, Alaska. The building has a square footprint with 39.6 m sides. The structural system of the building is composed of steel moment resisting frames. It was instrumented by 31 accelerometers (Figure 2.4). Using the N4SID system identification procedure and spectral methods, the natural frequencies and modal damping ratios of the building were identified under the 2005 M_w 4.9 Tazlina Glacier earthquake. The first two natural frequencies were 0.47 Hz and 1.56 Hz for the E-W translational modes, 0.58 Hz and 1.83 Hz for the N-S translational modes and 0.47–0.58 Hz and 1.5–1.9 Hz for the torsional modes, respectively. The similarity in the natural vibration frequencies for the translational and torsional modes indicated possible coupling and

resulted in beating. Corresponding modal damping ratios were 4.2% and 2.8% for the E-W translational modes, 2.7% for both N-S translational modes. The fundamental site frequency was identified as 1.5 Hz, close to the second translational and torsional modes; however, no significant soil-structure interaction effect was observed.

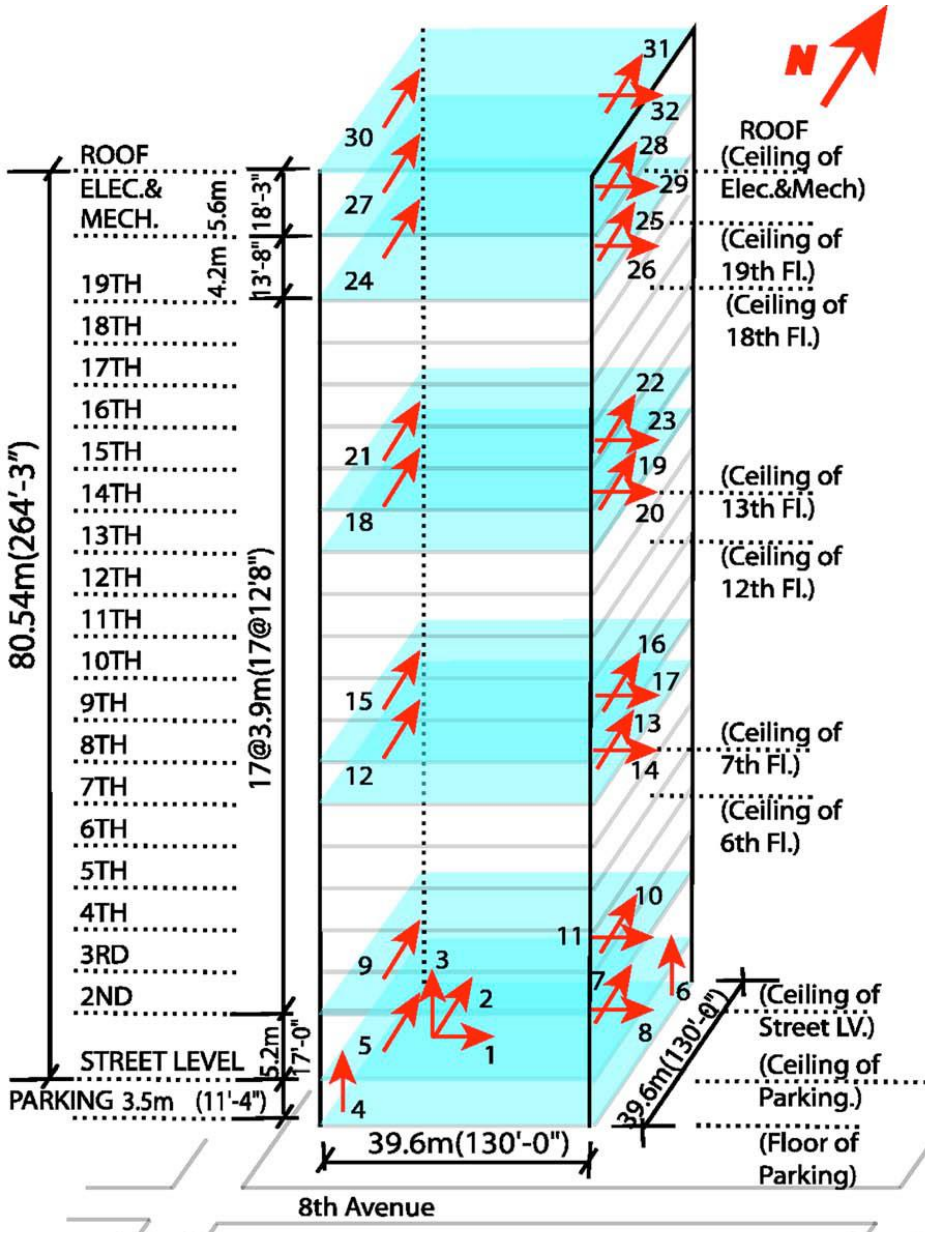

Figure 2.4 Instrumentation scheme of Atwood Building [Celebi 2006]

2.2.4 51-Floor Residential Building

The acceleration response of the 165 m tall 51-story residential building in Los Angeles, California was recorded under the 2019 M_w 7.1 Ridgecrest earthquake [Celebi et al. 2021]. The footprint of the tower part of the building is a parallelogram with 47.7 m by 29.1 m sides. The structural system of the building consists of RC dual-core shear wall and perimeter column systems, which are interconnected by post-tensioned cast-in-place flat slabs. The building is instrumented by a 30 channel SHM system (Figure 2.5). The recorded maximum floor acceleration was 0.067 g. Natural vibration frequencies and modal damping ratios were identified using the N4SID system identification procedure and spectral methods. The first two natural frequencies were 0.21 Hz and 0.94 Hz for the N-S translational modes, 0.28 Hz and 1.21 Hz for the E-W translational modes and 0.45 Hz and 1.22 Hz for the torsional modes, respectively. Beating effect was observed in the E-W direction. Corresponding modal damping ratios were 2.4% and 1.6% for the N-S translational modes, 2.1% and 2.0% for the E-W translational modes and 2.2% and 1.7% for the torsional modes. The maximum drift ratio was around 1.5% and no structural damage was reported. Rocking of the foundation about the N-S and E-W axes were insignificant.

2.2.5 Shanghai World Financial Center

Ambient and forced vibration tests were performed on Shanghai World Financial Center using the active tuned mass dampers of the building located at floor 90 [Shi et al. 2012]. Shanghai World Finance Center is a 492 m tall 101-story building in Shanghai, China. The building has a square floor plan with 58.0 m sides. The structural system of the building consists of a mega-frame structure, RC and braced steel cores and outrigger trusses (Figure 2.6).

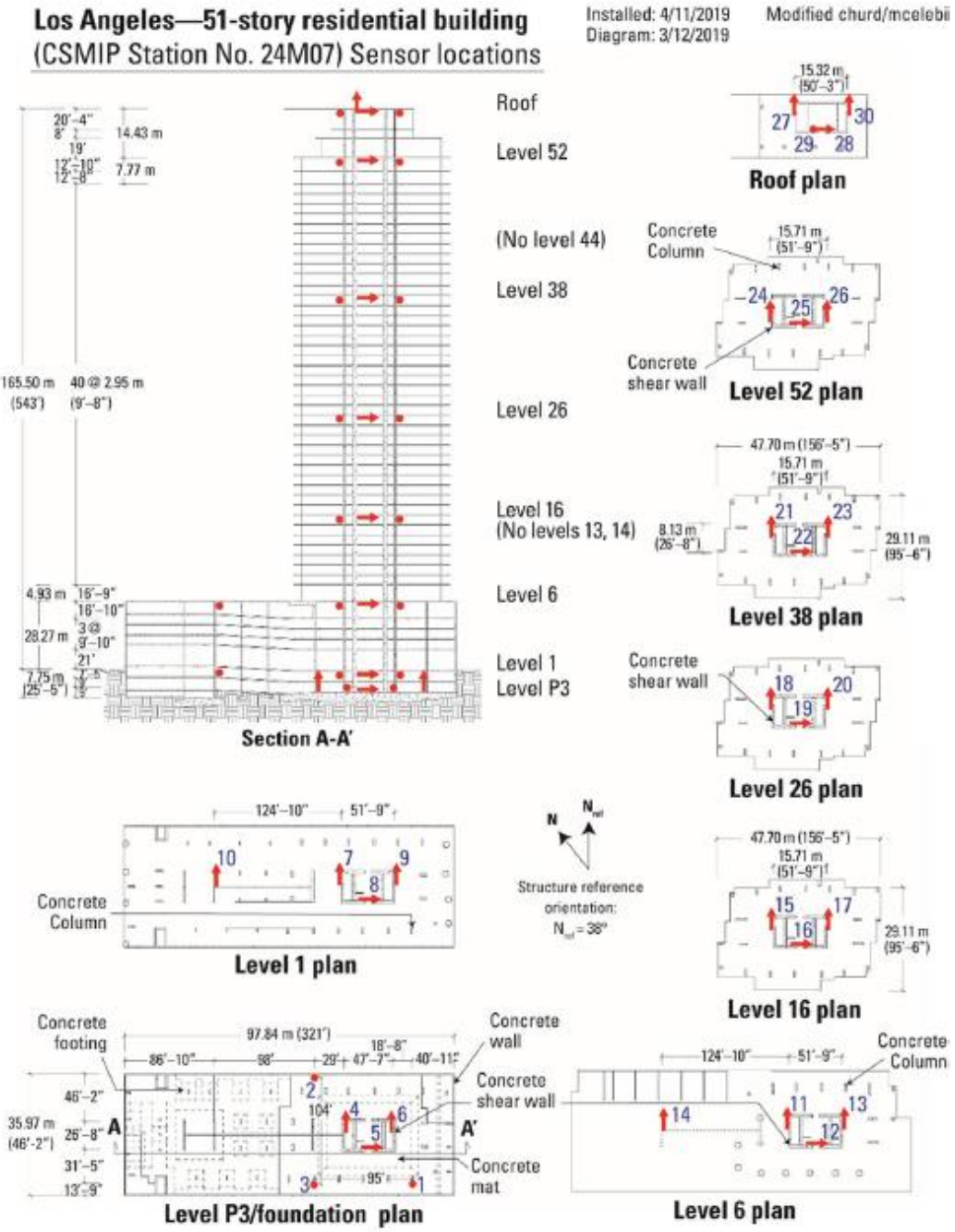

Figure 2.5 Instrumentation scheme of 51-floor residential building [Celebi et al. 2021]

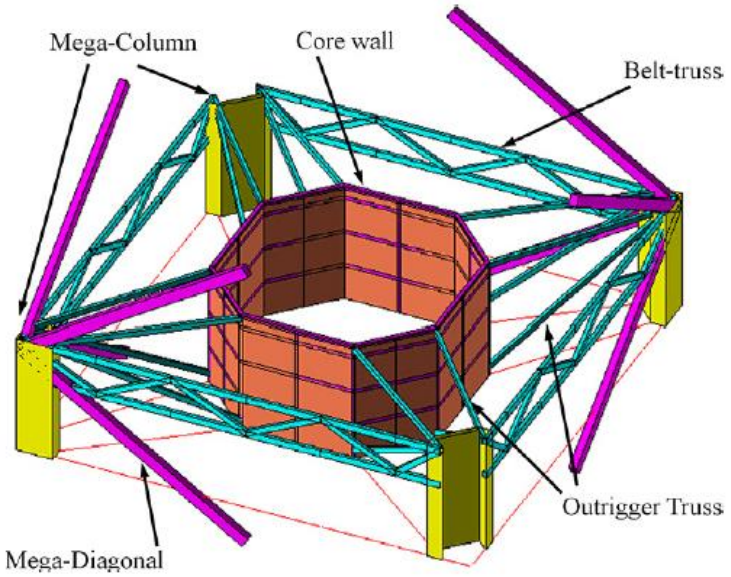

Figure 2.6 Three parallel structural systems of Shanghai World Financial Center [Shi et al. 2012]

The vibration tests were performed in two setups, in which accelerometers were roved (Figure 2.7). Random decrement and Hilbert-Huang transform methods were used to identify the natural frequencies and damping ratios from the forced vibration test. The fundamental natural mode frequencies were 0.16 Hz for both X and Y directions and the corresponding damping ratios were 0.5% and 0.4% for the X and Y directions, respectively, as identified from both methods. Peak picking and Hilbert-Huang transform methods were used for the ambient vibration test. The fundamental natural frequencies were 0.16 Hz for both X and Y directions and the corresponding damping ratios were 0.6% and 0.5% for the X and Y directions, respectively, as identified from both methods. It was also shown that when the active tuned mass dampers were activated, the damping ratios were increased to 3.4% and 3.9% for the X and Y directions, respectively. Furthermore, the developed finite element model and the performed shaking table tests of the building yielded similar dynamic properties.

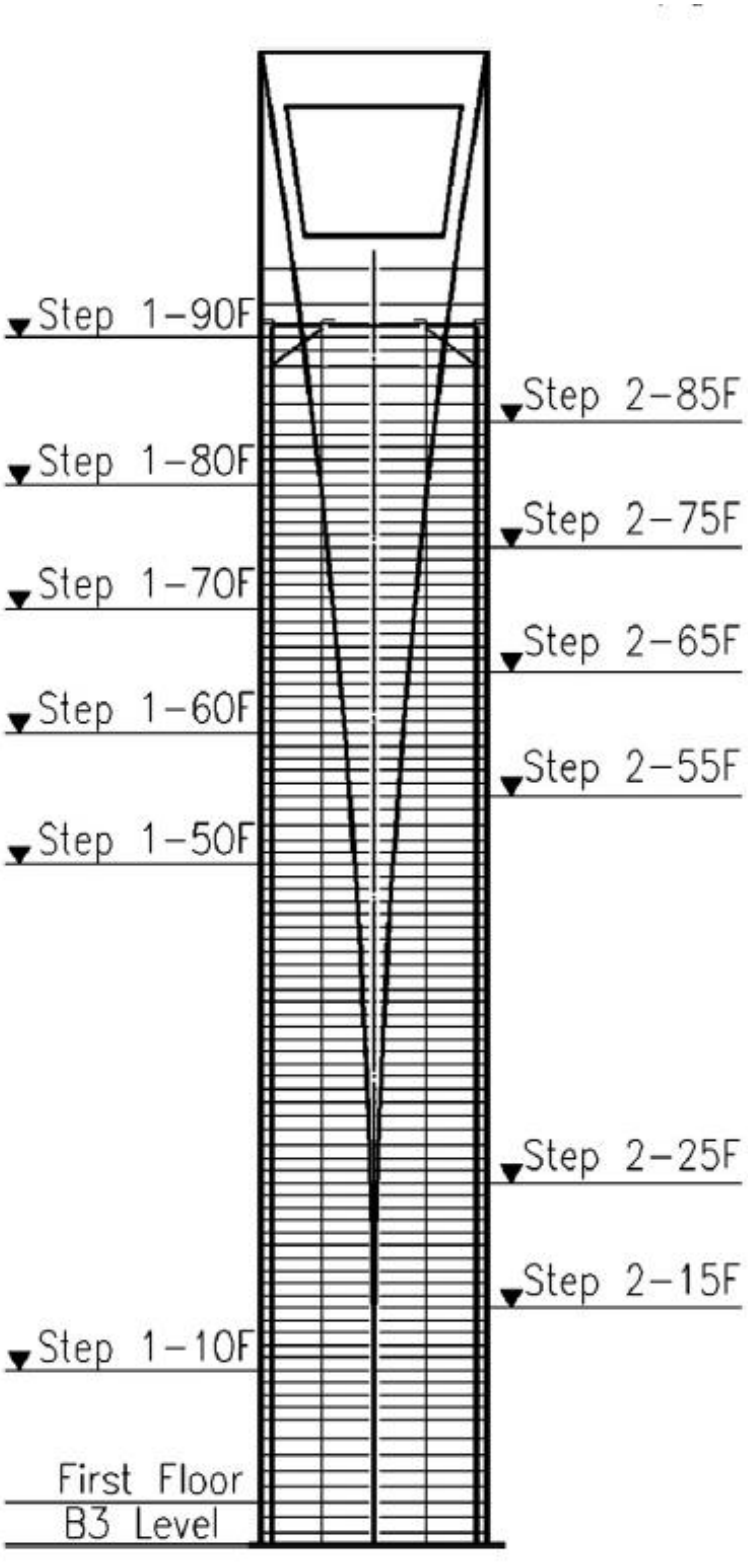

Figure 2.7 The elevation view of Shanghai World Finance Center and accelerometer locations used in the tests [Shi et al. 2012]

Further examples and state of the art of SHM in tall buildings can be found in Shan et al. [2020] and Su et al. [2020].

2.3 Damping (on Tall Buildings)

The equation of motion of a linear elastic single degree of freedom (SDOF) system under an earthquake ground motion is given by [Chopra 2011]:

$$m\ddot{u} + c\dot{u} + ku = -m\ddot{u}_g \tag{2.1}$$

where m, c and k are the mass, damping constant and stiffness of the SDOF system, respectively, $\ddot{u}$, $\dot{u}$ and u are the acceleration, velocity and displacement of the SDOF system, respectively and $\ddot{u}_g$ is the ground acceleration. The damping constant can be expressed as [Chopra 2011]:

$$c = 4\pi\xi m f_n \tag{2.2}$$

where ξ is the damping ratio and f_n is the natural frequency. The natural frequency can also be expressed in terms of mass and stiffness. Therefore, the damping constant is proportional to the damping ratio, mass and stiffness. Mass and stiffness can be calculated numerically using the mechanical and geometrical properties of the structure. However, the damping ratio cannot be calculated. It affects the dynamic response significantly. It is also highly uncertain due to its dependence on many different aspects of the structures such as the soil type, the foundation type, construction materials, joint types, structural system, interior and exterior walls, claddings, non-structural members and vibration amplitude [Tamura 2012, Tamura and Kareem 2013].

Different types and physical causes of damping in building structures can be classified as follows [Tamura and Kareem 2013]:

1) Internal friction damping which is caused by energy dissipation due to internal friction of solid materials.

2) Plasticity damping which is caused by energy dissipation due to plasticity of solid materials.
3) External friction damping which is caused by energy dissipation due to friction between solids.
4) Radiation damping which is caused by energy transfer and radiation due to soil-structure interaction.
5) Aerodynamic damping which is caused by aerodynamic interaction between building and air.

External friction damping and radiation damping dominate the total damping in building structures.

2.3.1 Damping Estimation Methods

Damping ratios of buildings can be estimated using their acceleration response recordings. There are numerous methods available; however, these methods should be selected carefully and implemented appropriately. Otherwise, the estimated damping ratios will be much different than the actual values [Tamura 2012]. Some of the common methods are explained below.

2.3.1.1 Half-Power Bandwidth Method

The half-power bandwidth method is one of the most common and simplest methods available to estimate the damping ratios [He et al. 2017]. The method can be classified as a frequency domain method since the method transforms the response history in time domain to the frequency domain using the Fourier amplitude spectra (FAS) [Safak and Cakti 2014]. The modal damping ratio can then be identified using

$$\xi = \frac{f_a - f_b}{2f_n} \tag{2.3}$$

where f_a and f_b are the frequencies on either side of the resonant frequency, i.e., the modal frequency, at which the amplitude is $1/\sqrt{2}$ times the resonant amplitude, as

illustrated in Figure 2.8. The method is only accurate at low damping ratios [Chopra 2011, Casiano 2016] and generally used for forced vibration testing. The smoothing of the FAS of the ambient vibration responses to facilitate the peak picking for identifying the natural vibration frequencies, changes the bandwidth of the response and hence the damping ratios. The frequency resolution also has a significant influence on the damping ratio estimations; larger frequency resolutions (i.e., shorter response recordings) generally tend to yield overestimated damping ratios [Shi et al. 2012].

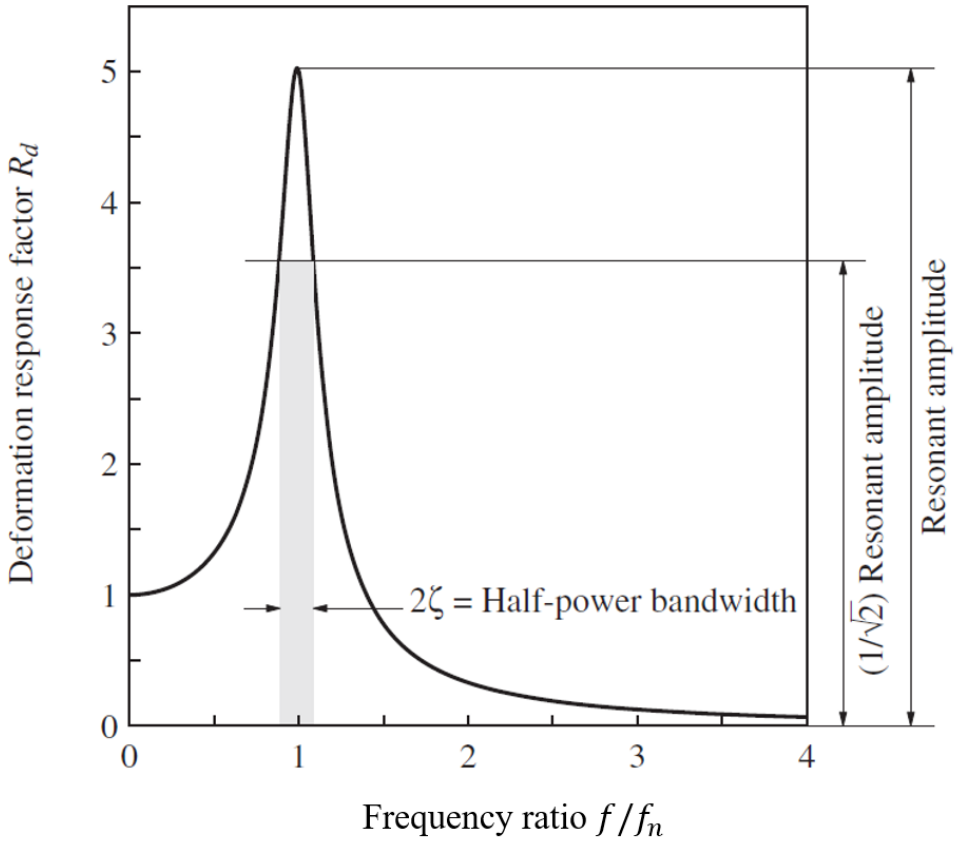

Figure 2.8 Illustration of the half-power bandwidth method (adopted from Chopra [2011])

2.3.1.2 Autocorrelation-Based Methods

Autocorrelation-based methods for estimating the damping ratios of civil engineering structures have been used since 1950s [Tanaka et al. 1969]. Output autocorrelation functions for an SDOF system is proportional to the response function of the system to an impulse. These methods estimate damping ratios by fitting exponential decay functions to the peaks of decaying part of the autocorrelation outputs, often referred to as the logarithmic decrement method [Safak and Cakti 2014, Shi et al. 2012]. First, the acceleration response of the structure is narrow bandpass filtered around modal vibration frequencies to obtain the SDOF responses. Then, autocorrelation outputs of these filtered responses are calculated. Finally, using the logarithmic decrement method, the damping ratios for all vibration modes are identified [Safak and Cakti 2014]. Frequency domain decomposition method, which was proposed by Brincker et al. [2001a], is another example of autocorrelation-based methods. The method was later improved for the cases involving closely spaced modes [Brincker et al. 2001b] and called the enhanced frequency domain decomposition method. Casiano [2016] presented a similar damping estimation method for aerospace structures under random inputs. Numerous other damping estimation methods use autocorrelation functions of modal response recordings. Autocorrelation functions can be very sensitive to the changes in the amplitude of the structural response. Therefore, the changes in the amplitude and the shape of autocorrelation functions should be monitored continuously in longer response recordings.

2.3.1.3 Random Decrement Method

Random decrement method is another widely used method for identifying modal damping ratios. The method was first introduced by Cole [1973] for on-line damage detection and damping estimation of aerospace structures. The method depends on ensemble averaging of structural response segments of finite length that have the

same initial amplitude and slope. When large number of segments are averaged, the random component in the response and the initial velocity response reduce to zero; leaving only the initial displacement response which is called the random decrement signature (RDS) [Li et al. 2020, Mikael et al. 2013, Zhou and Li 2021, Rodrigues and Brincker 2005]. The simplified mathematical formulation of RDS can be given by [Mikael et al. 2013, Li et al. 2020]

$$RDS(\tau) = \frac{1}{N}\sum_{i=1}^{N} s(t_i + \tau) \tag{2.4}$$

where N is the number of averaged segments having the same initial conditions, s is the ambient vibration segment for a duration of τ, and t_i is the time satisfying the initial conditions. RDSs are estimates of autocorrelation functions [Cole 1973, Kijewski and Kareem 2002]. Therefore, similar to autocorrelation-based methods, damping ratios can be estimated using the logarithmic decrement method on RDSs. The main advantage of using the random decrement method is its ability to overcome the requirements for stationary data assumption unlike the spectral methods, which allows better estimations using shorter structural response recordings [Kijewski and Kareem 2000, Kijewski and Kareem 2002]. Some significant parameters are needed to be set carefully before applying the method for damping estimation. Detailed explanation of the method, the parameters and application of the method are given in Chapter 3.

2.4 Summary

In this chapter, the benefits of installing SHM systems on tall buildings were presented. The history and development of SHM systems were briefly summarized. Examples of instrumented buildings around the world were presented and the system identification studies conducted using the recorded acceleration responses were summarized. The examples were selected considering the structural system of the buildings, their instrumentation scheme, the system identification method used and the type of recorded response used in the system identification. The system

identification results were presented highlighting the identified damping ratios. In the examples, the identified damping ratios were less than 1.0% under ambient vibrations and less than 5.0% under earthquake excitations indicating the amplitude dependency of damping. This dependency is considered in the guidelines of LATBSDC [2020], which recommends damping ratios larger than 2.5% for maximum considered earthquakes, whereas damping ratios smaller than 2.5% for service-level earthquakes. Finally, the chapter critically reviewed the widely used system identification methods.

CHAPTER 3

DAMPING ESTIMATION OF MISTRAL IZMIR OFFICE TOWER USING THE RANDOM DECREMENT METHOD

3.1 Introduction

This chapter briefly introduces the studied tall building and its SHM system, describes the random decrement method in detail highlighting its parameters, which is subsequently used to identify the modal damping ratios of the building from its ambient vibration records. The identified modal damping ratios are also compared with the values from code and other formulations as well as other instrumented tall buildings.

3.2 Mistral Izmir Office Tower

Mistral Izmir Office Tower (Figure 3.1) is a 216 m tall 48-story building in Konak, Izmir (38.4480^{o} N, 27.1794^{o} E), which is the tallest building in Izmir and the eighth tallest in Turkey [CTBUH, 2023]. It was opened in December 2017. The typical floor height is 4 m, except the two basement floors and two podium floors above the ground. The building has a trapezoidal floor plan at the basement having parallel edges along the N-S direction, with an area of nearly 1900 m^2 (Figure 3.2a). The tower part has a square floor plan with an area of almost 710 m^2 (Figure 3.2b), which reduces gradually above floor 45. The facade of the building is covered with sloped glass panels.

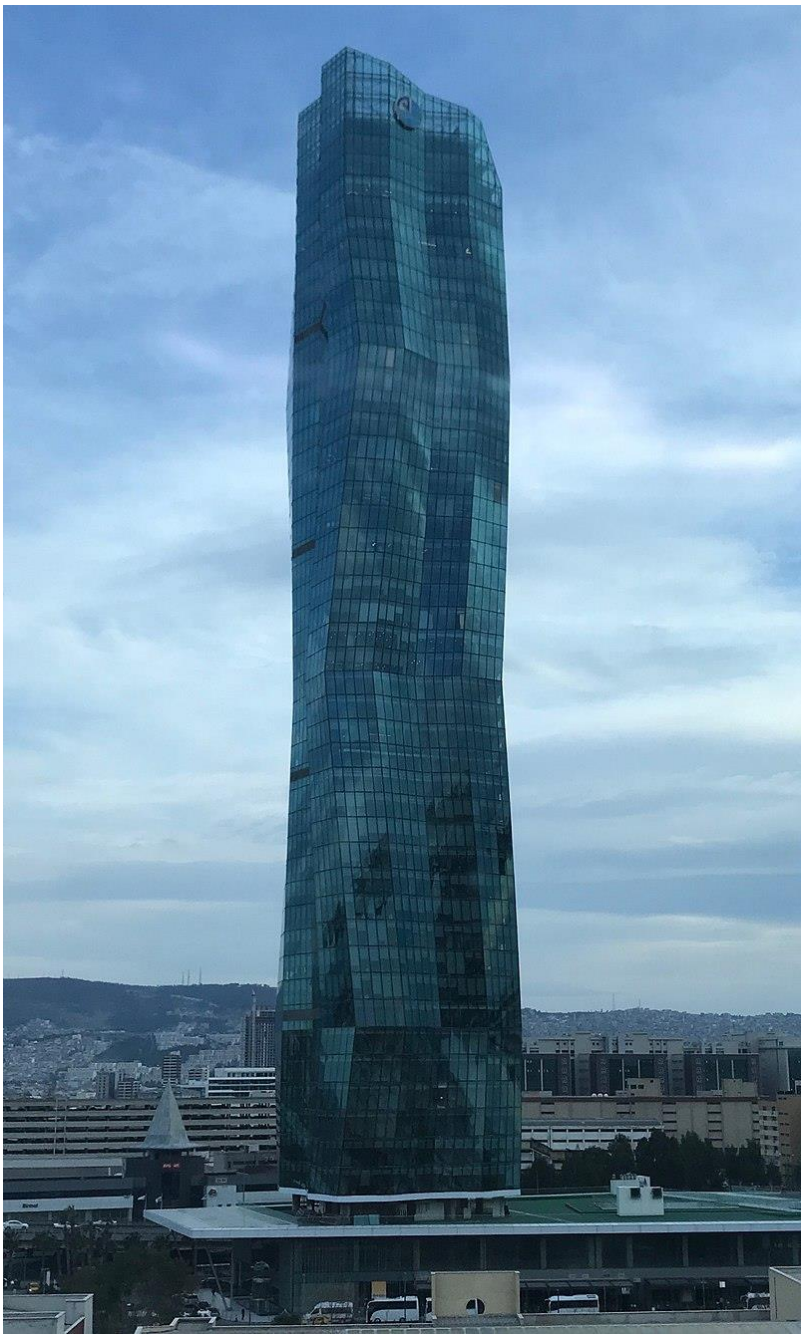

Figure 3.1 View of the building from the north

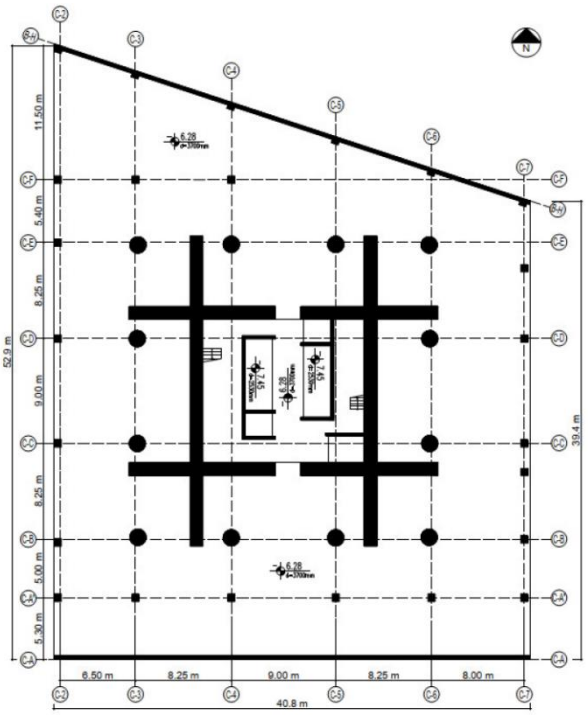

(a)

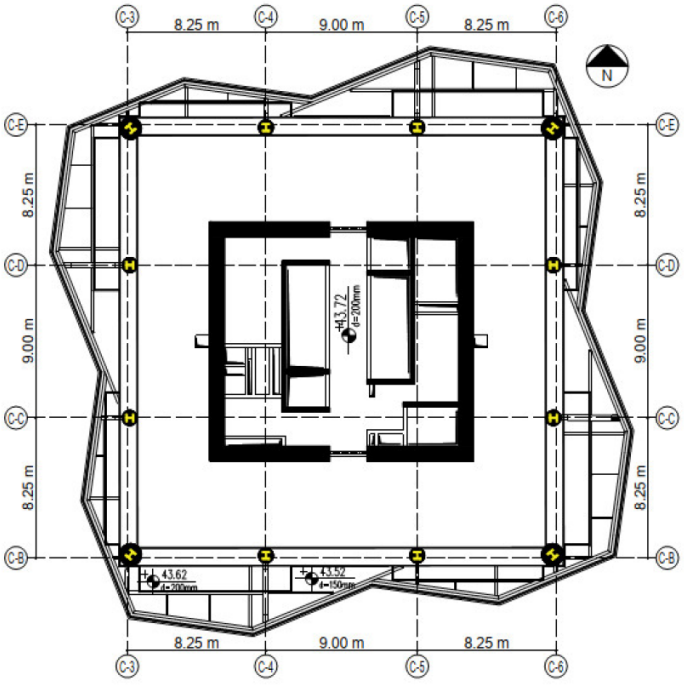

(b)

Figure 3.2 (a) Footprint of the building and (b) 10th floor plan

3.2.1 Structural system

The structural system of the tower consists of two U-shaped RC core shear walls with steel coupling beams and peripheral composite columns. At two mechanical floors, i.e., floors 19 and 39, there are BRB-outrigger systems that connect the corner columns to the closest corners of the core shear walls (Figures 3.3 and 3.4). Concentric X-braced steel frames are encased within the core shear walls below and above the mechanical floors at floors 18–20 and 38–40. Core shear wall thicknesses gradually reduce from 1.1 m at the basement levels to 0.5 m at the top levels of the tower. Composite columns are circular in shape with encased W steel sections. Similar to the core shear walls, their size decreases at the upper stories: the largest columns are 1.4 m in diameter and the smallest columns are 0.8 m in diameter. HEM/HEB 800 steel sections are used as coupling beams except at basement 1 and ground floors. Tower perimeter beams are RC with varying cross sections. The foundation of the building is composed of a 3.7 m thick mat foundation on 0.80 × 2.80 m barette piles.

Figure 3.3 BRB-outrigger system

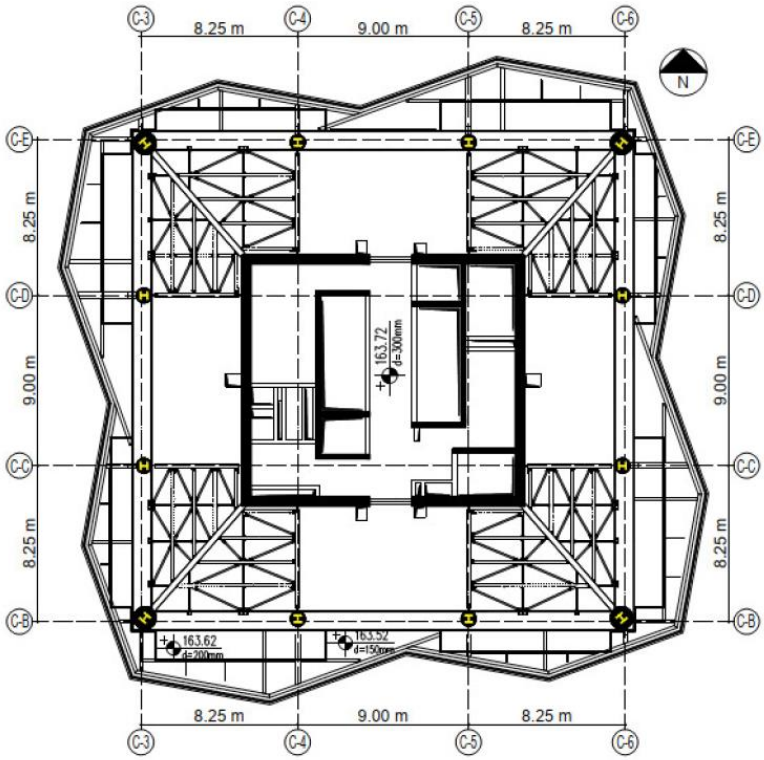

Figure 3.4 Typical plan of floors 19 and 39

C50, C40 and C30 grade concrete are used for the building, the foundation and the overhang slabs, respectively. S420, S460, S355 and S275 grade steels are used for the reinforcing steel, the composite columns, the built-up steel plates and the overhang beams, respectively. More information about the structural system of the Mistral Izmir Office Tower can be found in Gumus [2021].

3.2.2 SHM System

Mistral Izmir Office Tower is instrumented with a 27-channel SHM system (Figure 3.5) as part of a research project funded by the Disaster and Emergency Management Authority of Turkey [Gumus and Celik 2019]. The building has been monitored in real time since January 27, 2019. There are 24 uniaxial accelerometers connected to eight three-channel digital recorders and one triaxial accelerometer in the SHM

system. Time synchronization of the records are performed by a network time protocol server and a GPS antenna.

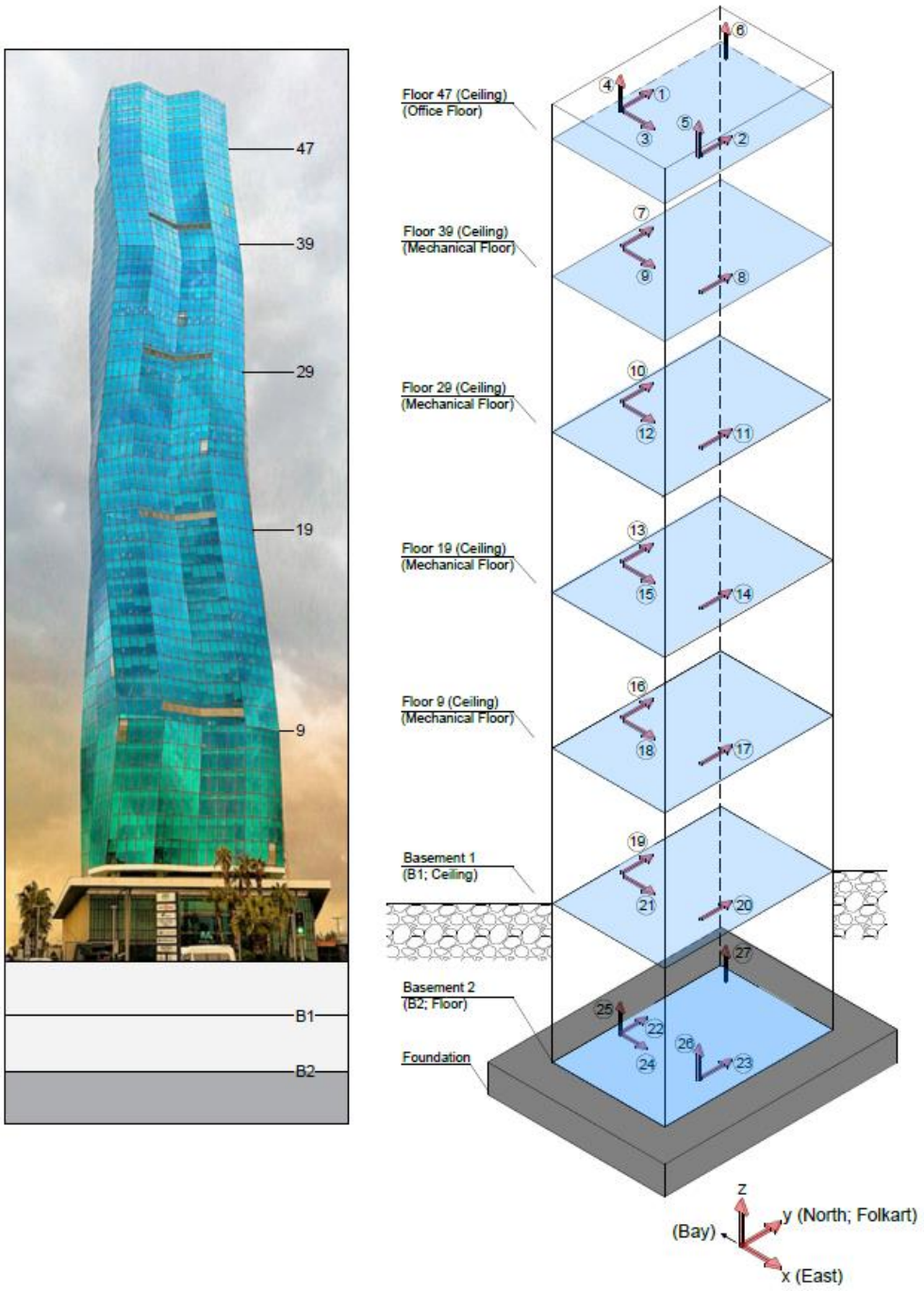

Figure 3.5 View of the building from the east and instrumentation scheme [Gumus 2021]

The accelerometers are installed on seven different floor levels: floors 48, 40, 30, 20, 10, and ground (G) and basement 2 (B2) levels. On each instrumented floor, except B2, there are two uniaxial accelerometers placed parallel in the N-S direction and one uniaxial accelerometer placed in the E-W direction. Additionally, floor 48 is instrumented by three uniaxial accelerometers in the vertical direction at three corners. Moreover, B2 is instrumented by one triaxial accelerometer in one corner, two uniaxial accelerometers, one in the E-W direction and another in the vertical direction, at another corner, and one uniaxial accelerometer in the vertical direction at a third corner (Figure 3.6). More information about the SHM system on the Mistral Izmir Office Tower can be found in Gumus [2021].

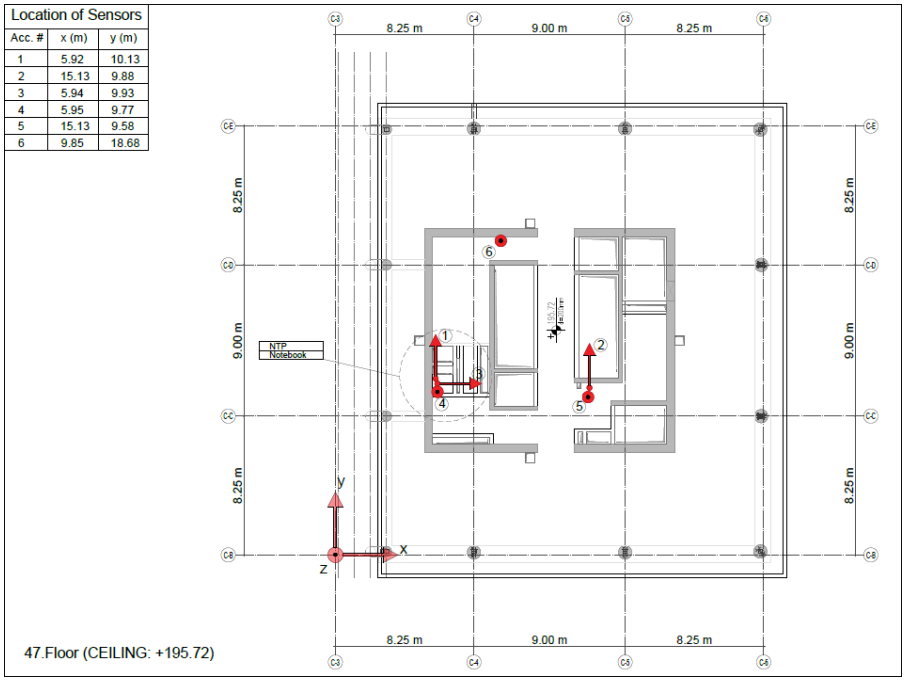

(a) Floor 48

Figure 3.6 Location and orientation of accelerometers at the instrumented floors [Gumus 2021]

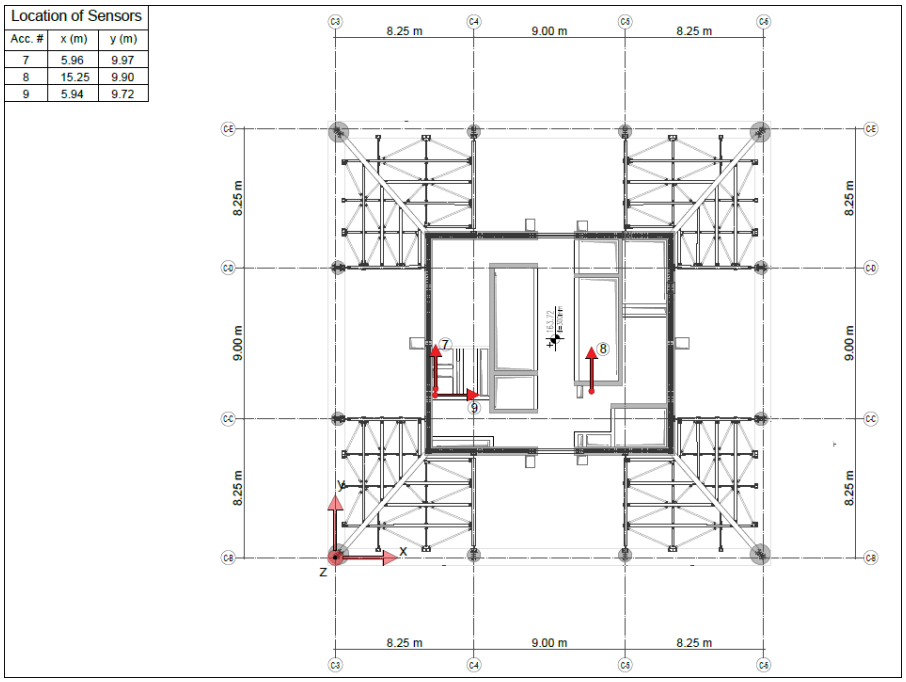

(b) Floor 40

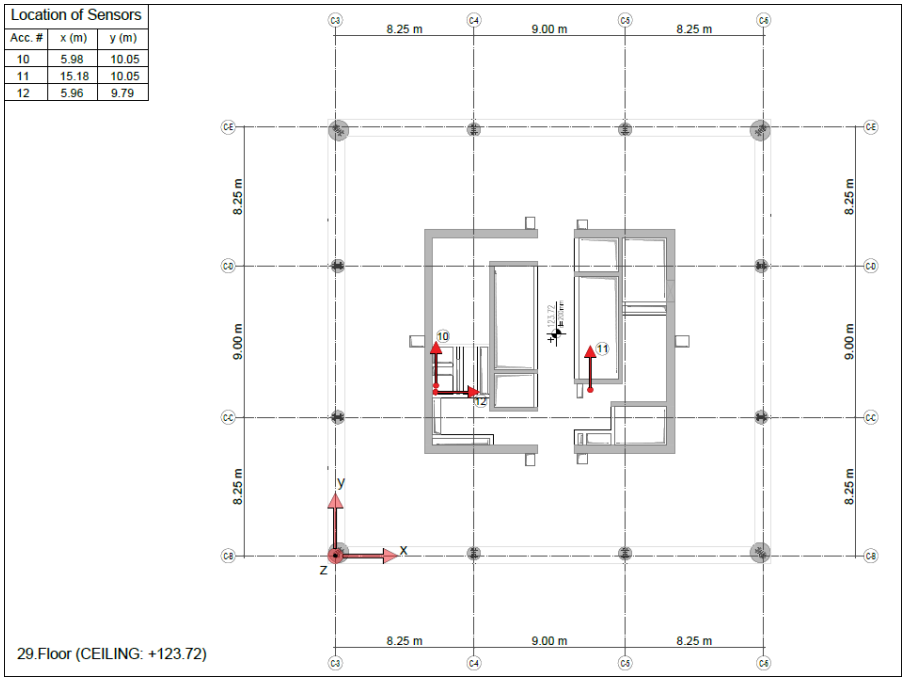

(c) Floor 30

Figure 3.6 Location and orientation of accelerometers at instrumented floors [Gumus 2021] (continued)

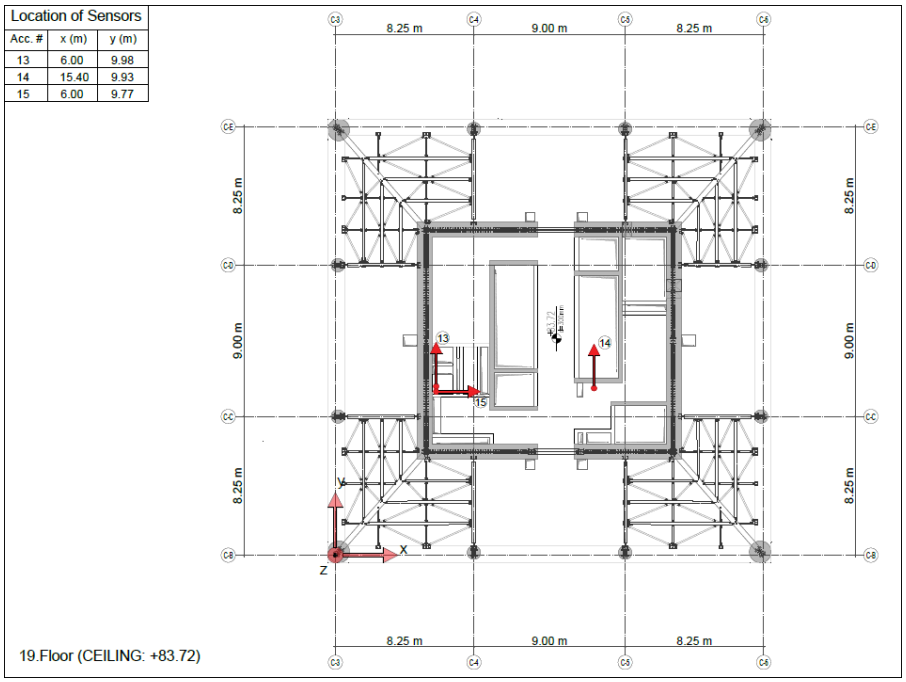

(d) Floor 20

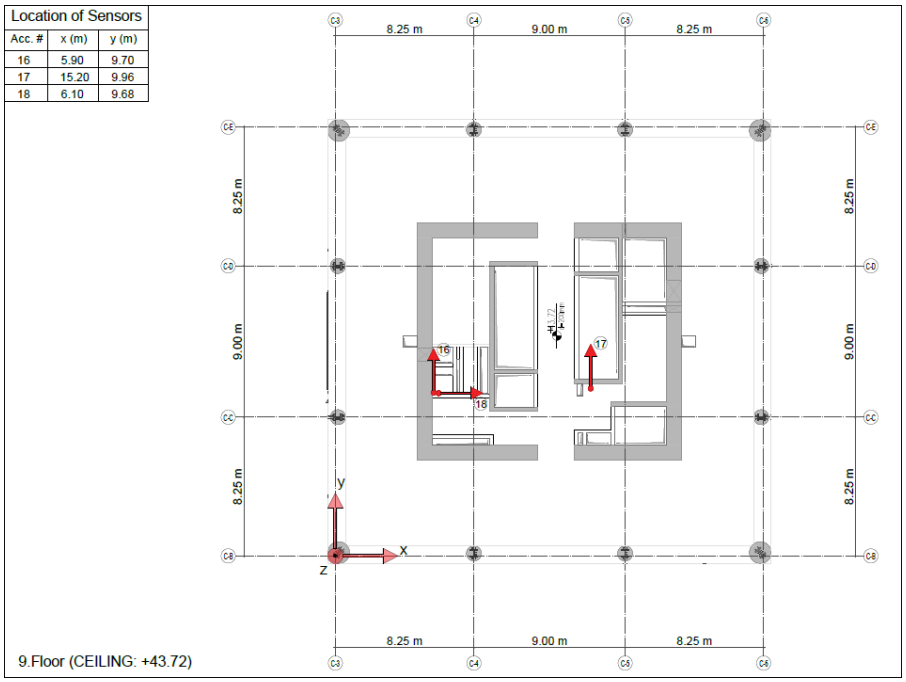

(e) Floor 10

Figure 3.6 Location and orientation of accelerometers at instrumented floors [Gumus 2021] (continued)

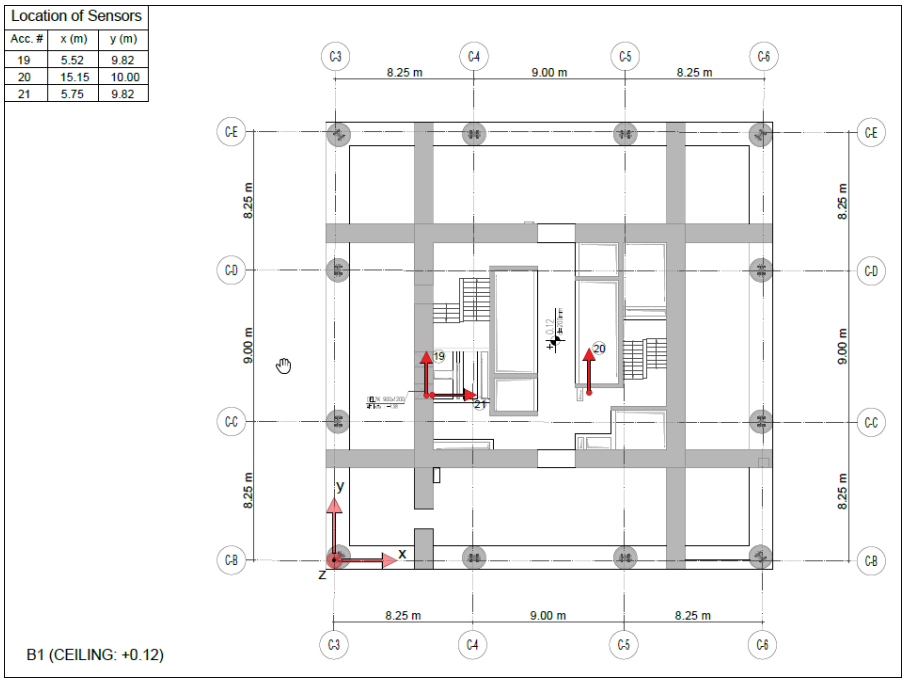

(f) Floor G

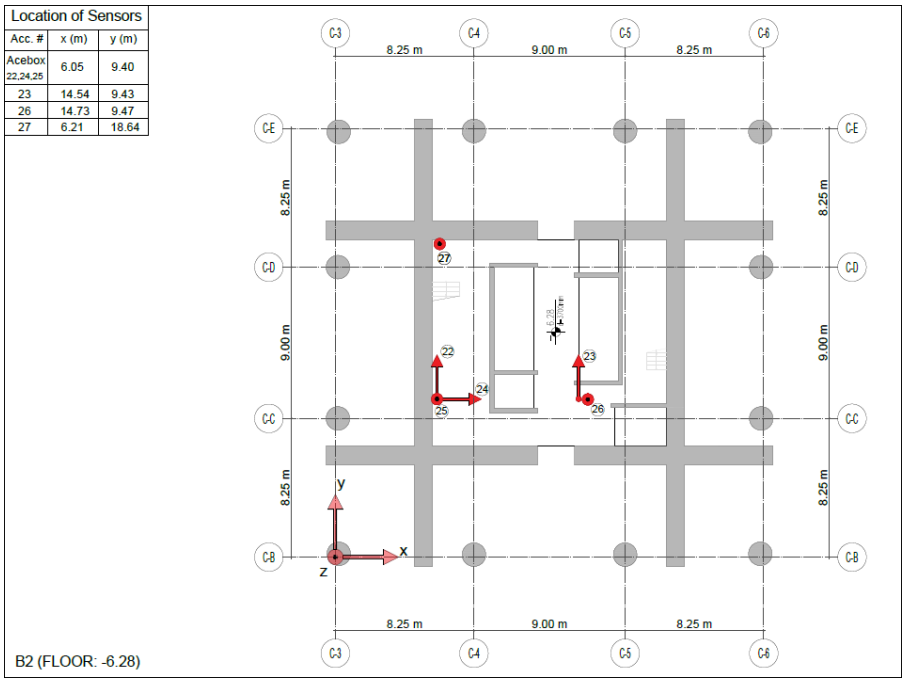

(g) Floor B2

Figure 3.6 Location and orientation of accelerometers at instrumented floors [Gumus 2021] (continued)

3.3 Random Decrement Method

In the early 1970s, researchers in the aerospace industry were using Fourier transform and half-power bandwith methods to gather information from in-service responses of aircrafts. In 1973, Henry A. Cole, who was a researcher at NASA, came up with the random decrement method. Using this method, unique RDSs of the aircraft components were obtained. Cole [1973] showed that these signatures are stable in form and scale. Subsequently, the method was used for on-line damage detection and damping estimation in the aerospace industry.

The method is quite practical and can be used for any random structural response. In 1980s, Jeary [1986] introduced this method to civil engineering structures for damping estimation under random inputs. Thereafter, the random decrement method has become one of the most common structural identification methods in civil engineering due to its effectiveness and practicality in damping estimation [Zhou and Li 2021, Rodrigues and Brincker 2005]. Hence, the random decrement method has also been used in this study to estimate the modal damping ratios of the Mistral Izmir Office Tower.

The random decrement method is based on the hypothesis that the response of a linear SDOF system is composed of three parts: step, impulse and random responses [Cole 1973]. The step response is the response due to the initial displacement, the impulse response is the response due to the initial velocity and the random response is the response due to the random input force applied to the structure (Figure 3.7).

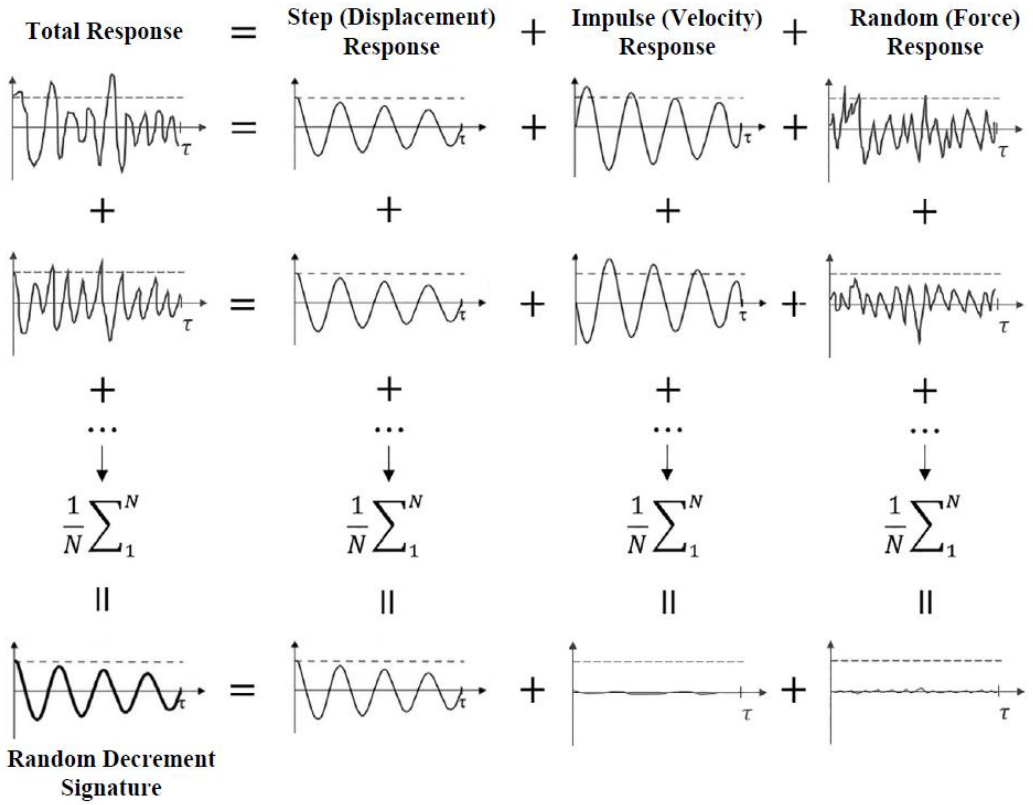

Figure 3.7 Principles of the random decrement method (adopted from Zhou and Li [2021])

The random decrement method proposes that, if a large number of structural response segments having similar initial conditions are to be averaged, the impulse and random responses reduce to zero while the step response remains. This averaged response is called the RDS. The signature is representative of the free decay damped response, from which the damping ratio of the SDOF system can easily be estimated.

A set of RDS plots are presented in Figure 3.8, which show the evolution of the free decay damped response. As the number of segments used is increased, the RDS gains free decay damped response properties gradually while the impulse and random responses reduce to zero.

Random decrement method is suggested for linear elastic SDOF systems; however, the method can be used for multi-degree-of-freedom systems (MDOF) by applying a bandpass filter to determine the modal responses [Kijewski and Kareem 2002].

Hence, structural engineers can use the random decrement method to estimate modal damping ratios of different types of civil structures. To initiate the calculations, modal frequencies must be calculated. Algorithms that use Fourier transform can be used for this purpose [Safak and Cakti 2014].

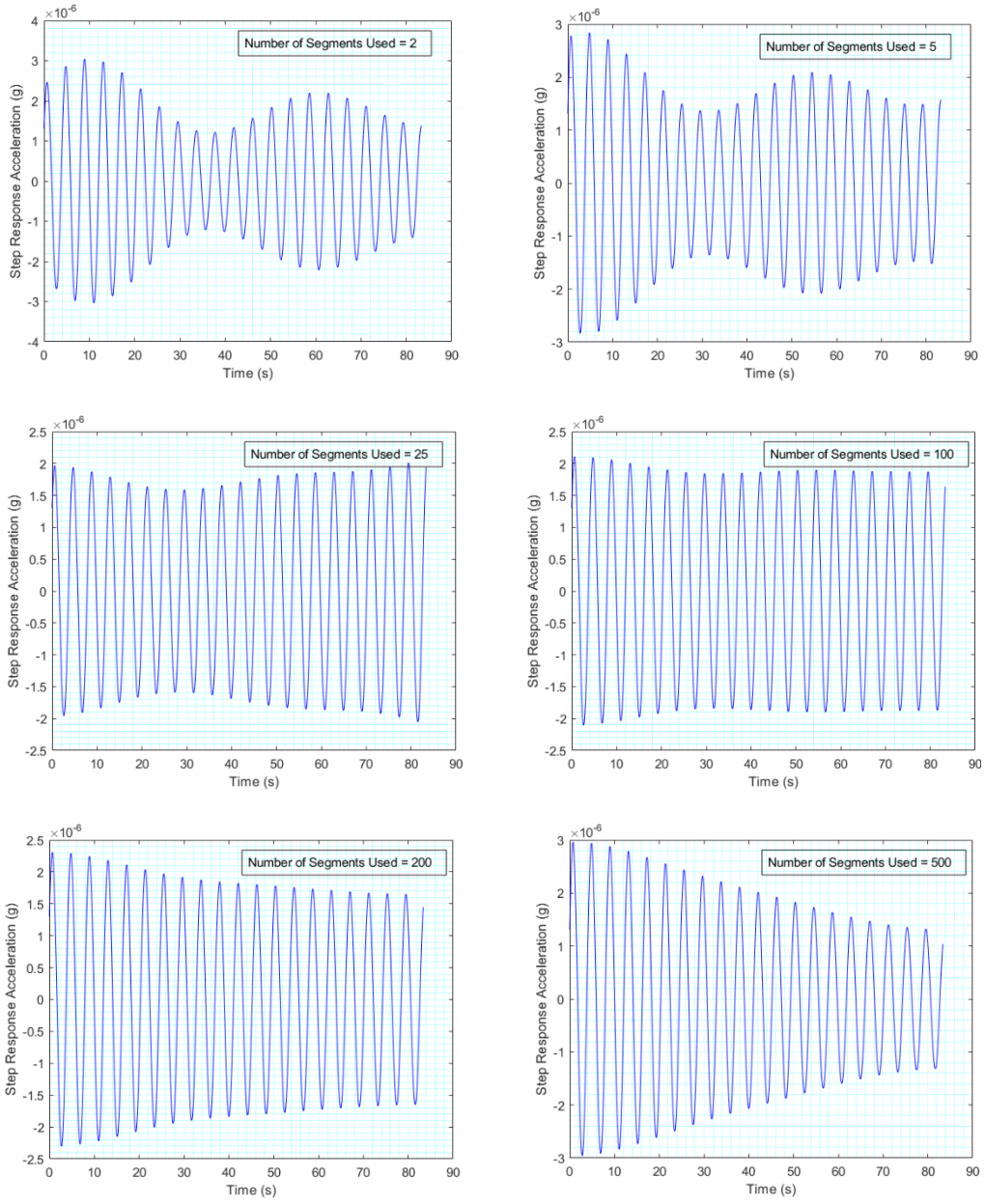

Figure 3.8 RDSs obtained with different numbers of segments: X direction 1st mode 11.02.2019 00:00:00 GMT

In this study, MATLAB software [The MathWorks Inc, 2019] is used for signal processing of the recorded ambient vibration responses. Firstly, the raw data from the accelerometers in counts are converted to acceleration in g. To do this, calibration coefficients provided by the SHM system manufacturer are used. Then, the accelerations at the floor geometric center are computed using the transformation given below, which is based on the rigid floor assumption:

$$\begin{bmatrix} A_x \\ A_y \\ A_T \end{bmatrix} = \begin{bmatrix} 0 & 1 & x_1 - x_c \\ 0 & 1 & x_2 - x_c \\ 1 & 0 & y_c - y_3 \end{bmatrix}^{-1} \begin{bmatrix} A_1 \\ A_2 \\ A_3 \end{bmatrix} \tag{3.1}$$

where A_x, A_y and A_T are the E-W translational, N-S translational and torsional floor accelerations, respectively, A_1, A_2 and A_3 are the accelerations recorded by accelerometers #1 (N-S translational), #2 (N-S translational) and #3 (E-W translational), respectively, x_c and y_c are the x and y coordinates of the floor geometric center, x_1, x_2, and y_3 are the x coordinates of accelerometers #1 and #2 and the y coordinate of accelerometer #3, respectively (Figure 3.9).

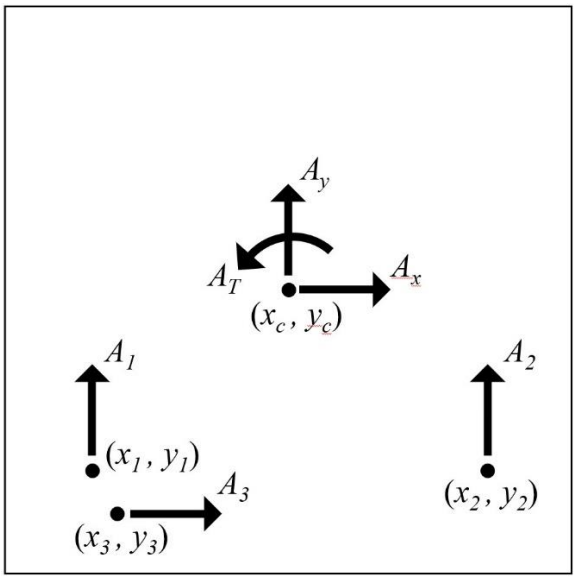

Figure 3.9 Points of recorded and computed accelerations on a floor

As stated previously, in order to apply the random decrement method to the building structures, modal frequencies are needed to be identified. Peaks of the Fourier

amplitude spectra of the computed floor accelerations correspond to the modal vibration frequencies. Figure 3.10 presents the Fourier amplitude spectra of the ambient vibration responses recorded at floor 48 of the Mistral Izmir Office Tower. In order to facilitate the peak picking, smoothing method given in Petrovic [2018] can be used.

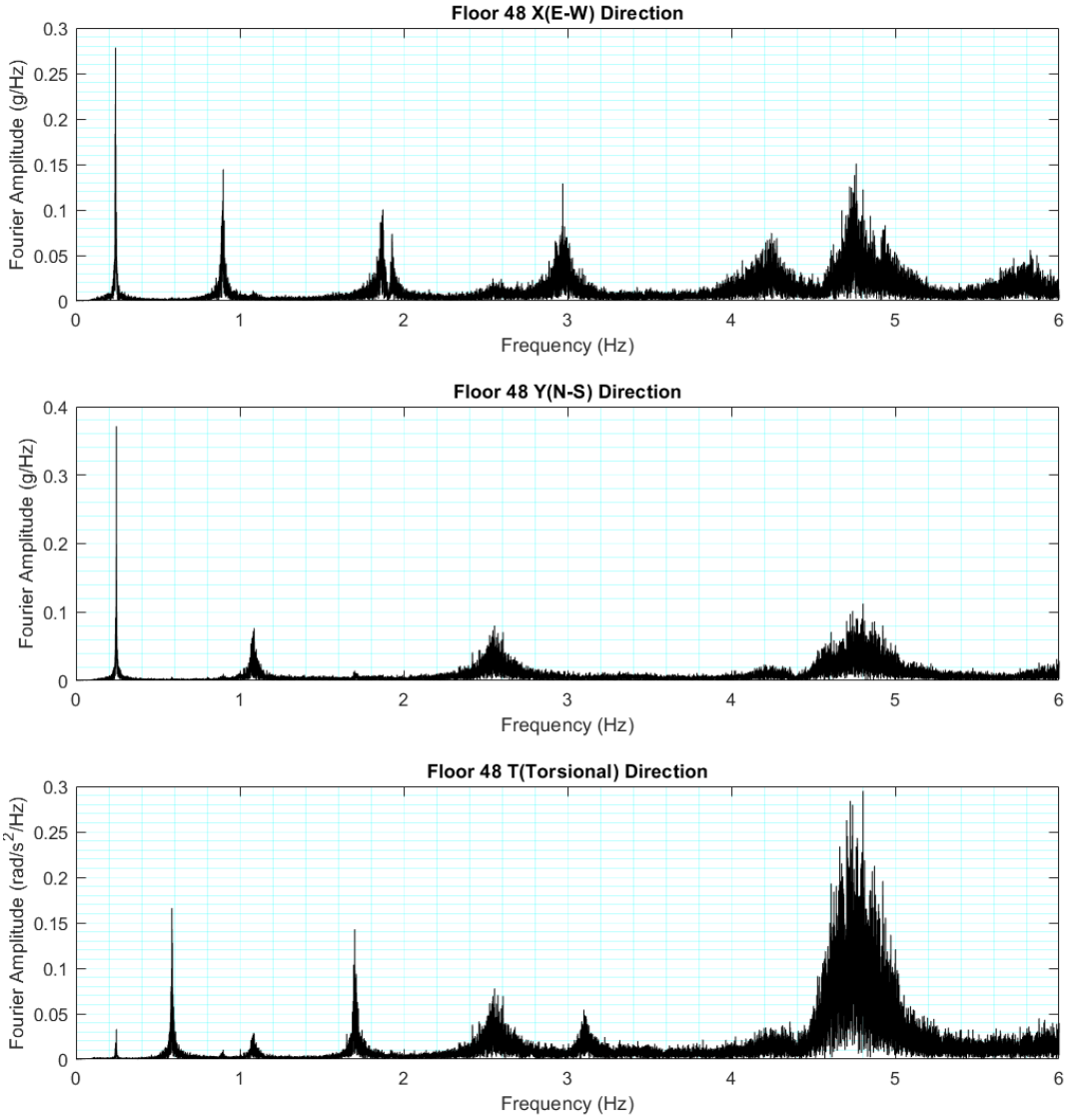

Figure 3.10 Fourier amplitude spectra of floor 48 accelerations: 11.02.2019 02:00:00 GMT

The algorithm is summarized below:

1) Divide the data into windows of 120 s with 50% overlap.
2) Apply a Hanning window to each window using the “Hann” function in MATLAB.
3) Calculate the Fourier amplitude spectrum of each window using the “fft” function in MATLAB.
4) Calculate the average of the Fourier amplitude spectra of all windows using the “mean” function in MATLAB.

Figure 3.11 presents the smoothed Fourier amplitude spectra of the recorded ambient accelerations at floor 48. The first four modal frequencies in each of the translational directions as well as the torsional direction are marked on the figure and listed in Table 3.1. Table 3.2 lists the corresponding modal periods.

Random decrement method parameters need to be set to their respective proper values to identify the modal damping ratios accurately. The first important point is the triggering condition. In order to obtain the RDSs, structural response segments with the same initial conditions should be extracted from the ambient vibration records. Therefore, there must be a triggering condition to define the starting point of a segment. Two of the most commonly used triggering conditions are “level-peak” and “level-crossing” [Zhou and Li 2021]. The level-peak condition is a strict condition to satisfy; only the peaks with the specified amplitude can trigger a segment. This condition makes sure that both the initial amplitudes and the initial slopes of the segments be the same. However, it is difficult to identify such segments. Hence, longer ambient vibration records are needed to obtain the required number of segments. On the other hand, the level-crossing condition is a much simpler, conventional triggering condition in which only a threshold level is required. Triggering happens whenever the structural response crosses the threshold level. In this condition, the initial amplitudes of the segments are the same but the initial slopes are different from each other. To alleviate this, only the crossings with positive slopes can be extracted. This triggering condition is relatively easy to satisfy

and longer ambient vibration records are not needed. In this study, an hour-long ambient vibration records are used with the latter triggering condition.

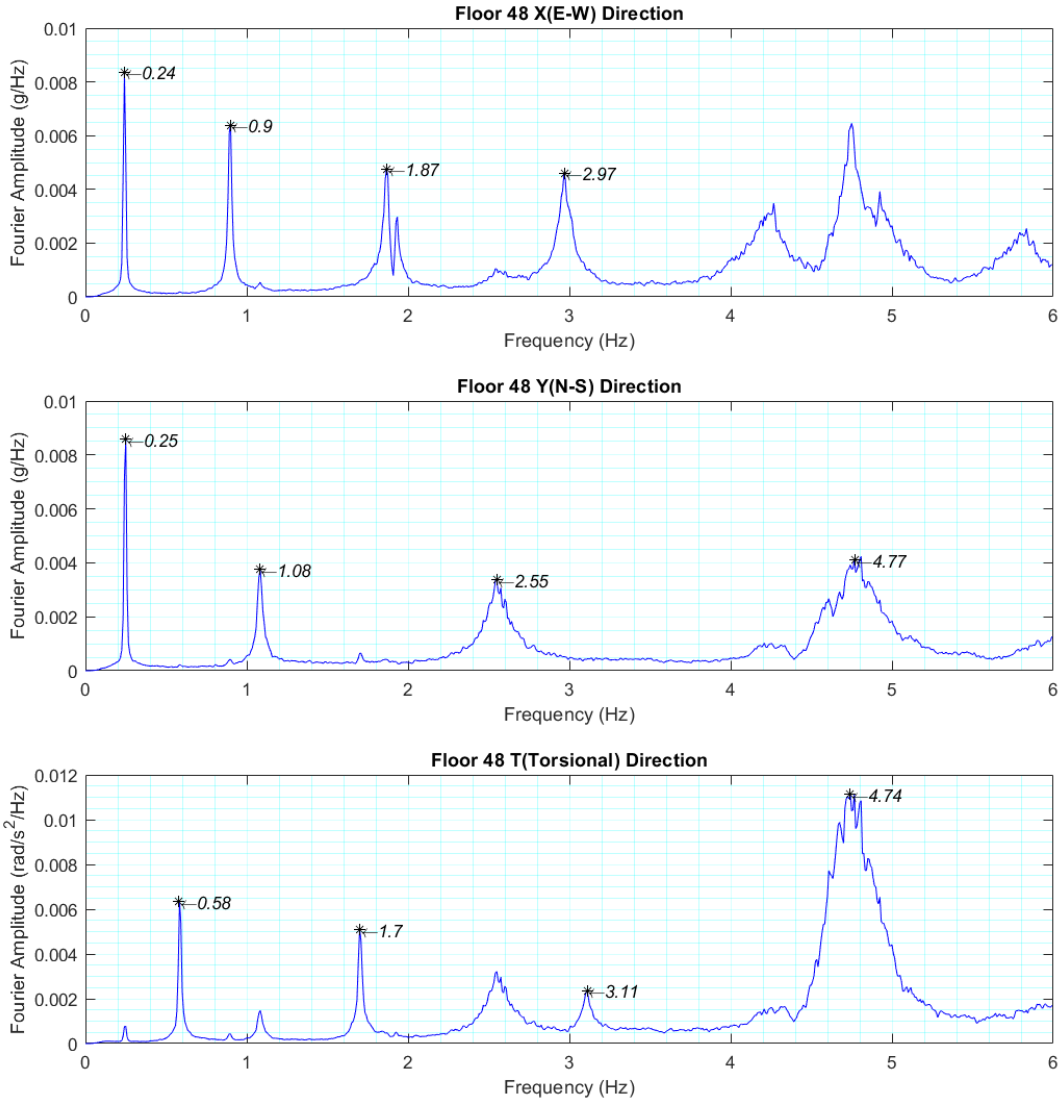

Figure 3.11 Smoothed Fourier amplitude spectra of floor 48 accelerations

Overlapping between segments is allowed to increase the number of segments extracted. Furthermore, in practice, random decrement method using level-crossing triggering condition with overlap can provide the most reliable damping estimate among other triggering conditions [Zhou and Li 2021].

Table 3.1 Natural vibration frequencies (Hz)

Mode	X(E-W)	Y(N-S)	T(Torsional)
1	0.24	0.25	0.58
2	0.90	1.08	1.70
3	1.87	2.55	3.11
4	2.97	4.77	4.74

Table 3.2 Natural vibration periods (s)

Mode	X(E-W)	Y(N-S)	T(Torsional)
1	4.17	4.00	1.72
2	1.11	0.93	0.59
3	0.53	0.39	0.32
4	0.37	0.21	0.21

A threshold value must be set to use the level-crossing triggering condition. Threshold value directly affects the number of segments (suggested values will be mentioned subsequently) that are extracted from finite-length ambient vibration records, such as the hour-long ambient vibration records used in this study, which greatly changes the form of the RDS as illustrated in Figure 3.8. The optimum level for the threshold was proposed by Tamura [2012] as one standard deviation 1σ of the modal filtered ambient vibration record, whereas Rodrigues and Brincker [2005] proposed $\sqrt{2}\sigma$ as an optimum value.

In this study, different threshold values are examined to determine a suitable threshold level for the available data. Firstly, the proposed threshold values were used. Since the natural frequencies of the first vibration modes in both translational directions are quite low (making the natural periods quite long), there are much less cycles in the filtered response of the first translational modes than the other modes. This naturally results in less number of segments compared to the other modes.

Consequently, this played a major role in determining the threshold value. Both of the proposed threshold values yield less number of segments than the suggested number of segments. Hence, the threshold value was selected as 0.5σ to obtain adequate number of segments for computing RDSs for the first translational modes. To keep consistency among the computations, 0.5σ threshold was used for all modes.

Damping estimations from hour-long records over a week together with the number of segments used in each estimation are presented in Figure 3.12. Threshold value of 2.5σ was used to demonstrate the effects of a high threshold value on the damping estimations. Most of the outlier damping ratio values are from the 2.5σ threshold case. As threshold value gets smaller, the number of segments increases and the damping ratio estimations converge to each other. For 2.5σ, $\sqrt{2}\sigma$ and 1σ threshold values, approximately 50, 275 and 450 segments are used per hour on average, respectively. On the other hand, for 0.5σ threshold value, approximately 700 segments are used, which is a better figure than the other values. The suggested values for the number of segments will be mentioned later in this section.

The second important random decrement method parameter is the length of the extracted segments that are averaged, which, in turn, is the length of the RDS. Since the method applies to modal responses, the length of the segments can also be expressed in terms of the number of vibration cycles of motion. Kijewski and Kareem [2000] suggested that the segments include five vibration cycles. Rodrigues and Brincker [2005] suggested that the RDS incorporates the complete decay of the motion.

In this study, the use of different numbers of vibration cycles in computing the damping ratios were examined as shown in Figure 3.13. Using 5 cycles results in underestimation of the damping ratio, whereas using 30 cycles tends to overestimate the damping ratio. Using 10–20 cycles gives more consistent damping ratios at each hour. Segments including 20 cycles will be used to compute the RDSs and estimate the damping ratios subsequently.

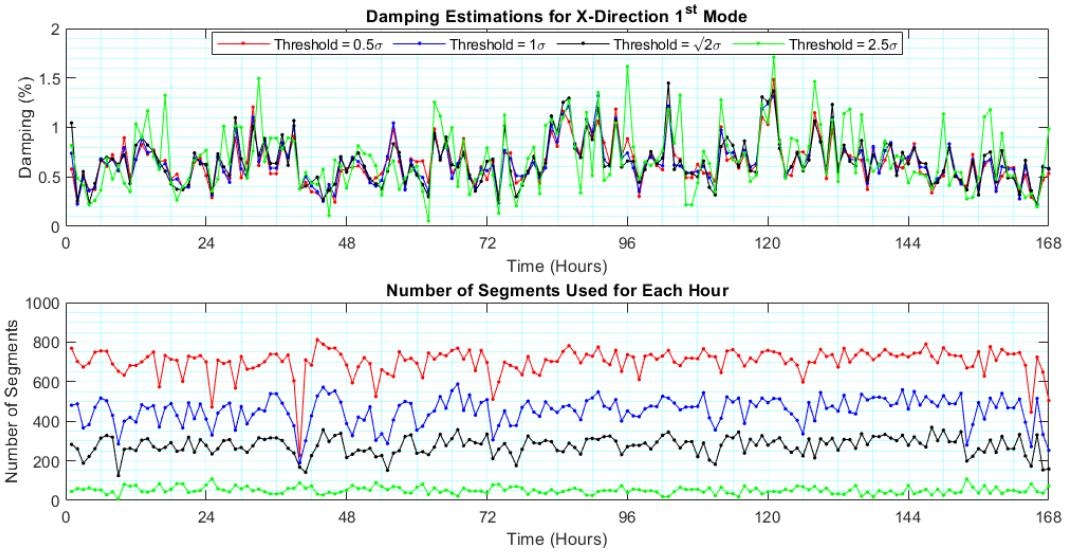

Figure 3.12 Hourly damping estimations and numbers of segments with different threshold values used for X direction 1st mode: 11.02.2019 00:00:00–17.02.2019 23:59:59 GMT

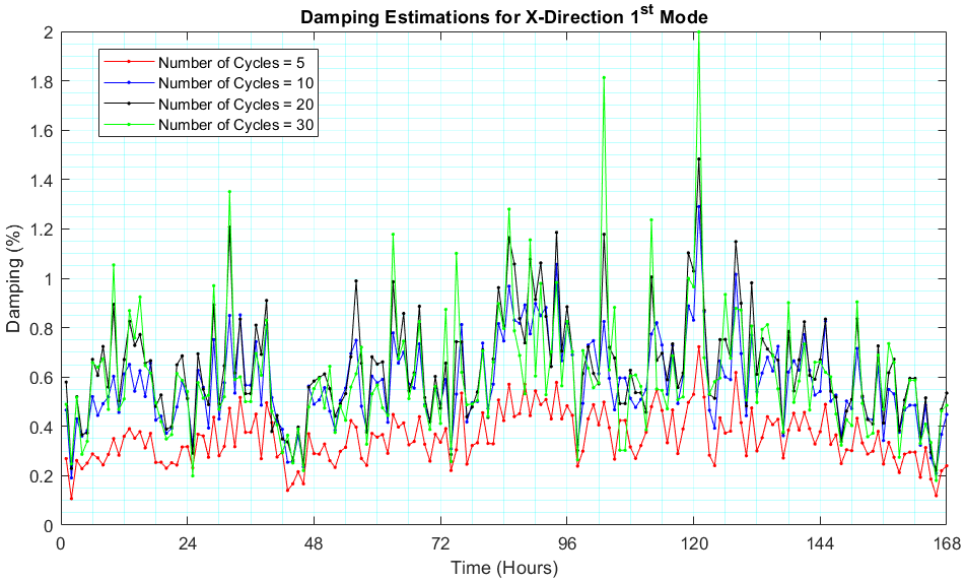

Figure 3.13 Hourly damping estimations with different numbers of vibration cycles used for X direction 1st mode: 11.02.2019 00:00:00–17.02.2019 23:59:59 GMT

The third important random decrement method parameter is the bandpass filter width. Since the objective is to identify the modal damping ratios, the structural response is narrow bandpass filtered to determine the modal response. Here, upper

and lower bounds of the bandpass filter are to be decided. Filter properties can significantly affect the RDSs. Using a too narrow filter results in underestimation of damping ratios [Tamura 2012]. On the other hand, using a too wide filter prevents extracting a single mode.

In this study, different filter bandwidths were examined and the findings are similar to those in Tamura [2012]. Here, the bandwidth of the filter can be expressed as a percentage of the modal frequency. For example, for the first translational mode in the X direction, which has a natural frequency of 0.24 Hz, when the bandpass filter width is set to 20%, the lower and upper bound frequencies of the bandpass filter are 0.216 Hz and 0.264 Hz. Figure 3.14 shows the identified damping ratios using different bandpass filter widths. Using a narrow bandpass filter width as 2% results in underestimation of damping ratios. Damping ratios start to converge beyond 10% bandpass filter widths. 10% bandpass filter width will be used subsequently.

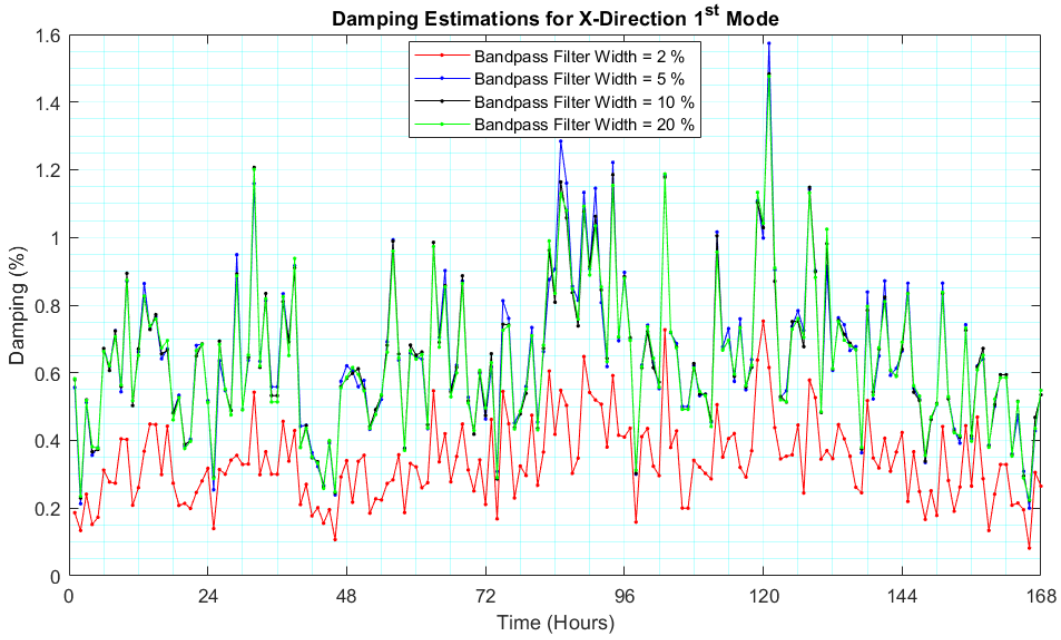

Figure 3.14 Hourly damping estimations with different bandpass filter widths used for X direction 1st mode: 11.02.2019 00:00:00–17.02.2019 23:59:59 GMT

Another parameter that has a significant effect on the RDS is the number of averaged segments, which depends on the length of the original structural response and the

threshold level. Low numbers of segments may lead to erratic results. Therefore, it is important to make sure that adequate numbers of segments are used while computing the RDSs. For example, Cole [1973] suggested that at least 500 segments are used to get stable RDSs. Kijewski and Kareem [2002] also stated that damping estimates steadily improve with increasing number of segments and the use of more than 500 segments results in damping ratios within 10% of the actual values. The RDS computed using the above selected values of the parameters, i.e., threshold set to 0.5σ, length of the segments taken as 20 vibration cycles and bandpass filter width set to 10%, includes the number of segments shown in Figure 3.15. The number of segments is greater than 500 and on average approximately 700 per hour.

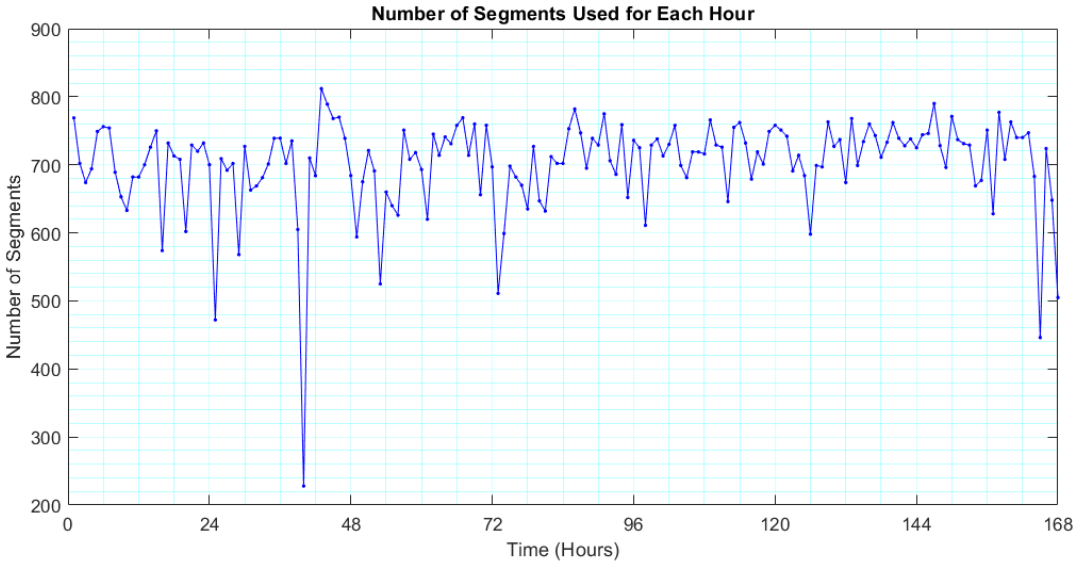

Figure 3.15 Number of segments used for estimating damping for X direction 1st mode for each hour: 11.02.2019 00:00:00–17.02.2019 23:59:59 GMT

After deciding on the values of the important parameters as explained above, the damping ratios can be estimated from the peak points of the RDSs using the logarithmic decrement method [Safak and Cakti 2014] as illustrated in Figure 3.16:

$$\ln[P(t)] = -2\pi\xi f_n + \ln(C) \tag{3.2}$$

where $P(t)$ is the peak points of the RDS, ξ is the damping ratio, C is a constant and f_n is calculated as:

$$f_n = 1 \Big/ \left[\frac{1}{n-1} \sum_{i=1}^{n-1} (t_{i+1} - t_i) \right] \tag{3.3}$$

where n is the number of peak points in the RDS and t_i is the time of peaks.

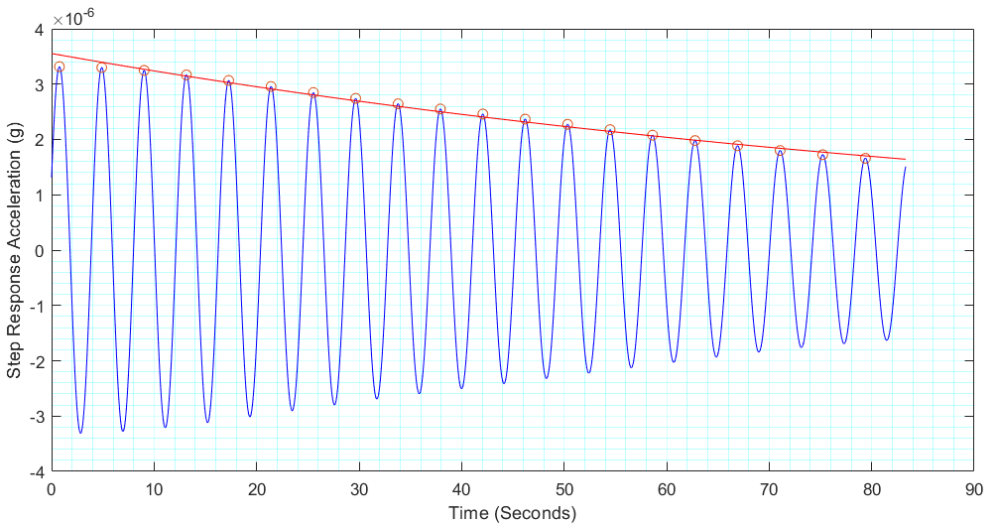

Figure 3.16 Damping computation from the RDS for X direction 1st mode: 11.02.2019 00:00:00 GMT

An overview of the algorithm that was used to compute RDSs and damping ratios is provided below:

1) Calculate the modal responses using a narrow bandpass filter centered around modal frequencies.
2) Extract the segments when the triggering condition is satisfied.
3) Average the segments to compute the RDS.
4) Gather the peak points of the RDS.
5) Calculate the frequency from the RDS using the peak points.
6) Calculate the damping ratio using the logarithmic decrement method.

This procedure is repeated for computing the damping ratios for the first four modes in each direction for the weeks of 11.02.2019 and 16.09.2019. Modal frequencies used in the damping ratio computations are presented in Figures 3.17 and 3.18, and computed modal damping ratios are presented in Figures 3.19 and 3.20, respectively. The histograms of modal damping ratios are presented in Figures 3.21 and 3.22,

respectively. On each histogram plot, mean damping value, standard deviation and coefficient of variation (CoV) values are given, which are also listed in Tables 3.3 and 3.4. The coefficients of variation do not exceed 0.40 for all modes and have a mean of 0.23.

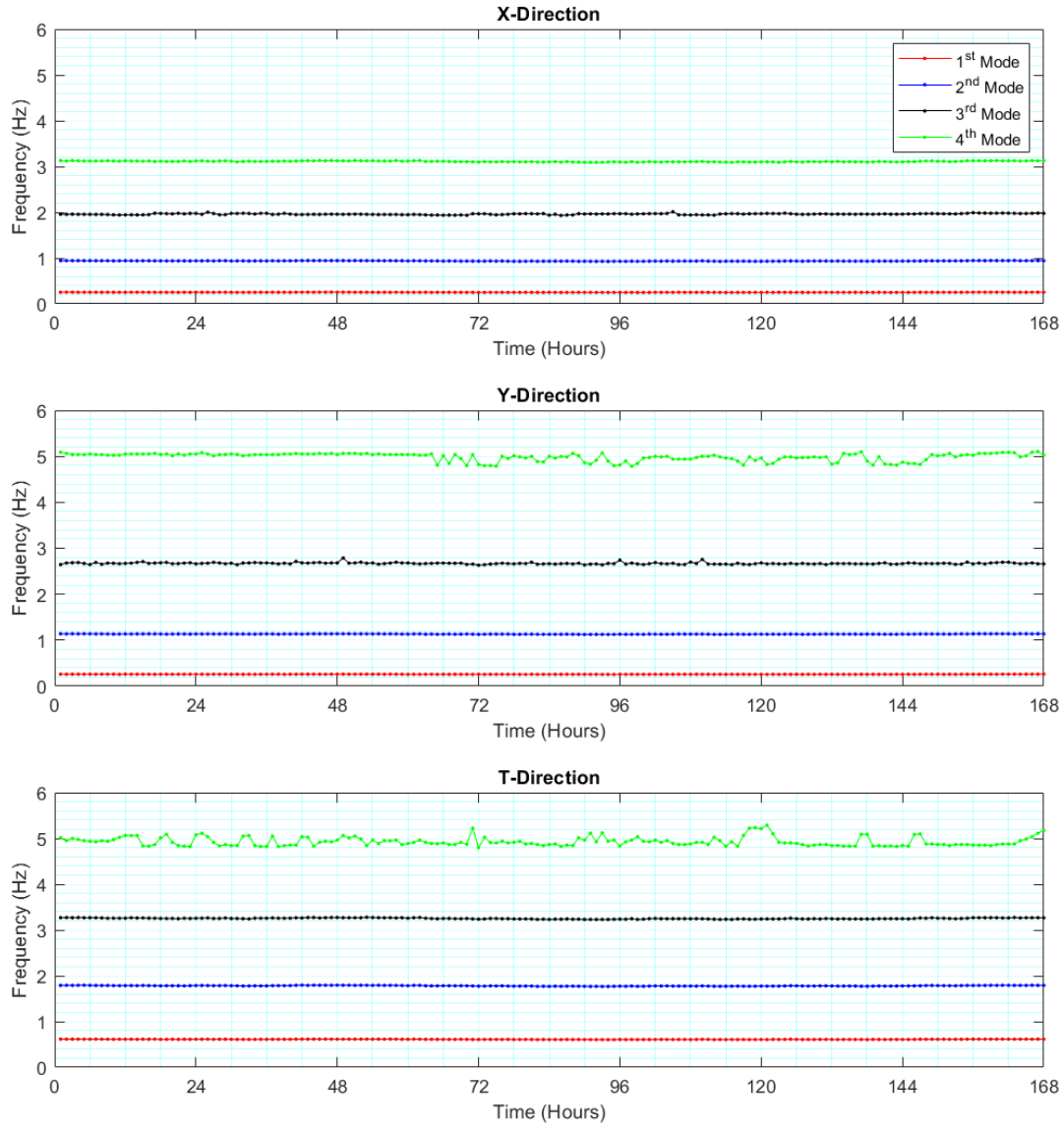

Figure 3.17 Modal frequencies: 11.02.2019 00:00:00–17.02.2019 23:59:59 GMT

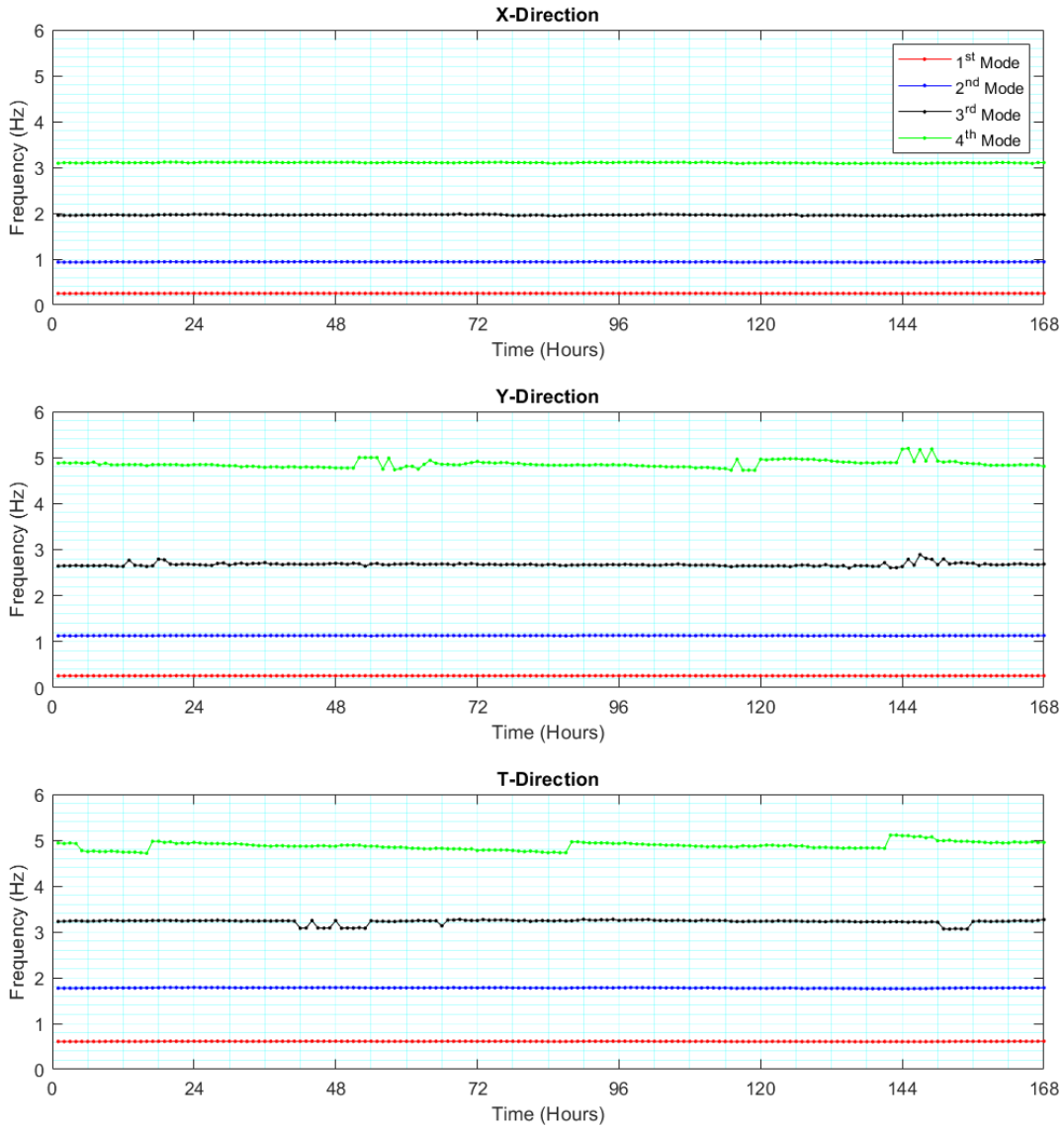

Figure 3.18 Modal frequencies: 16.09.2019 00:00:00–22.09.2019 23:59:59 GMT

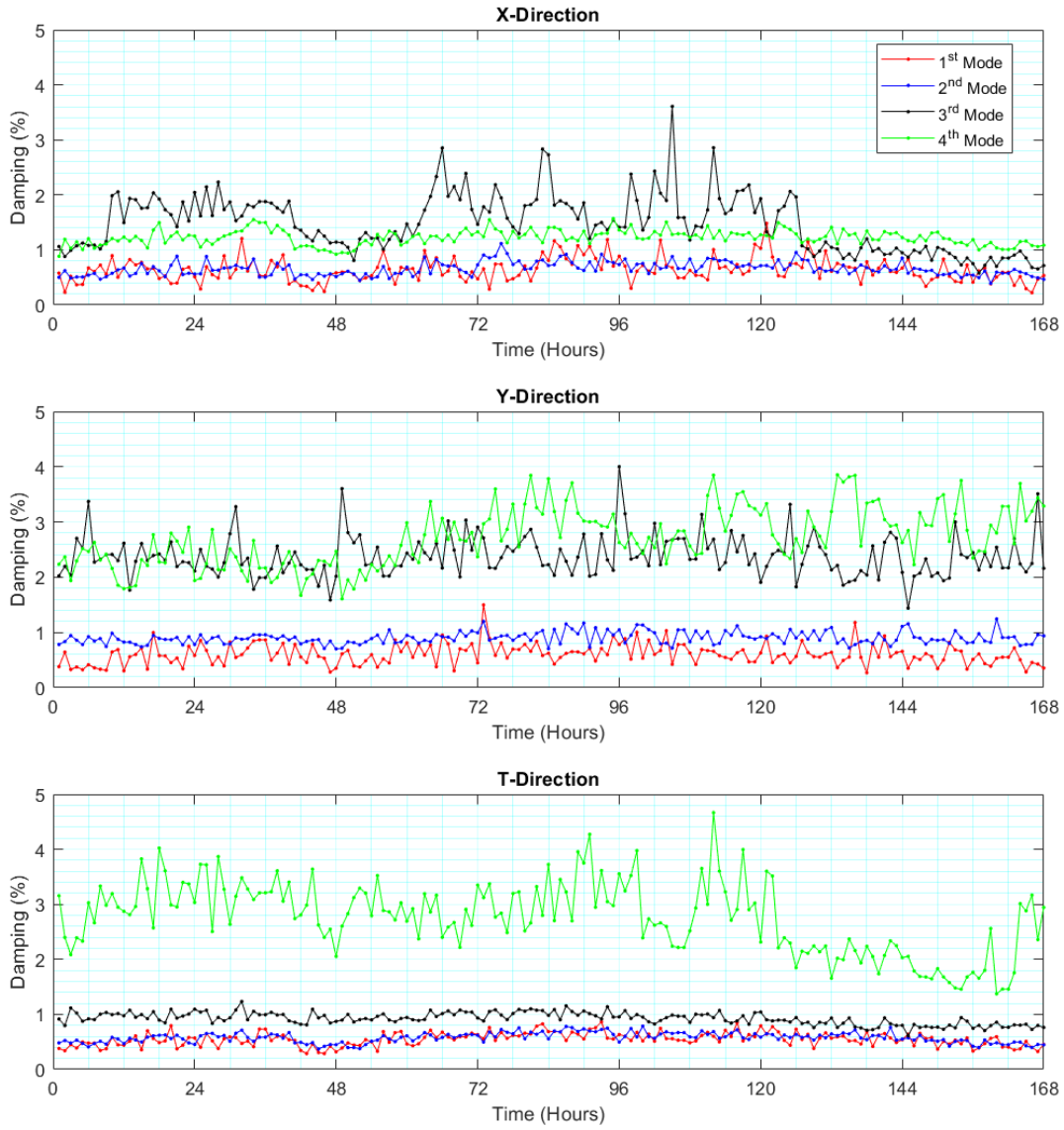

Figure 3.19 Damping ratios: 11.02.2019 00:00:00–17.02.2019 23:59:59 GMT

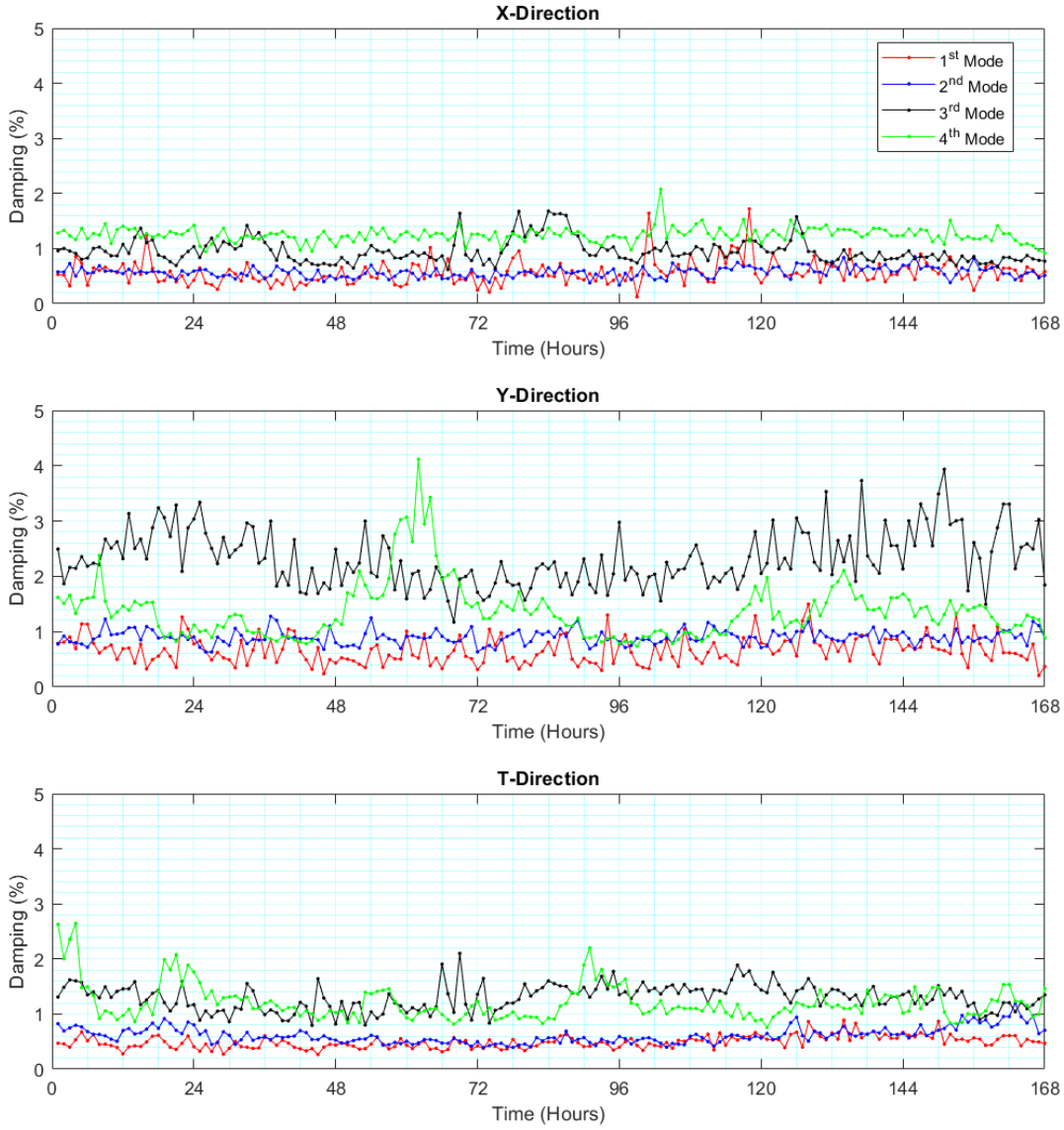

Figure 3.20 Damping ratios: 16.09.2019 00:00:00–22.09.2019 23:59:59 GMT

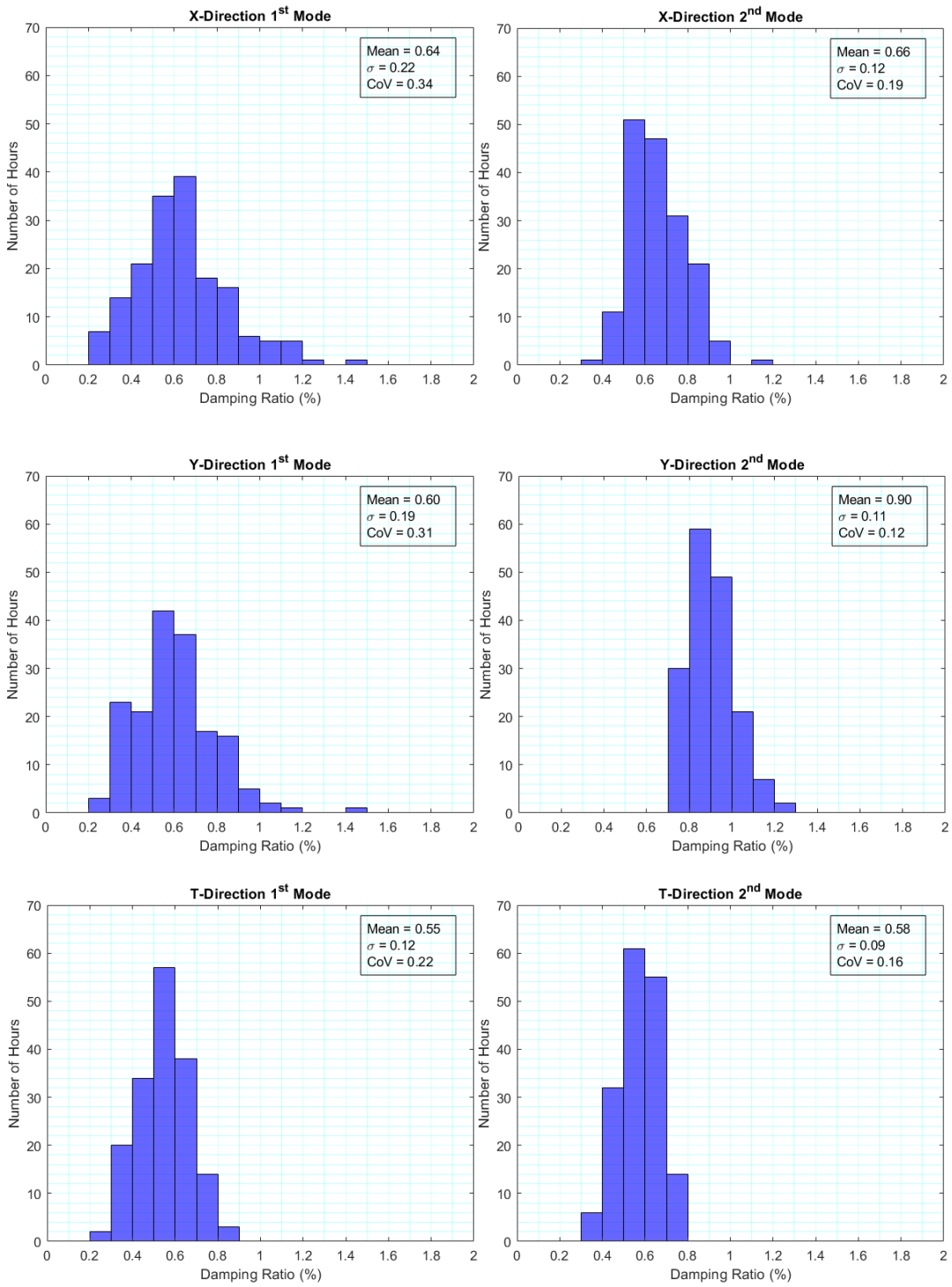

Figure 3.21 Histograms of modal damping ratios over a week: 11.02.2019 00:00:00–17.02.2019 23:59:59 GMT

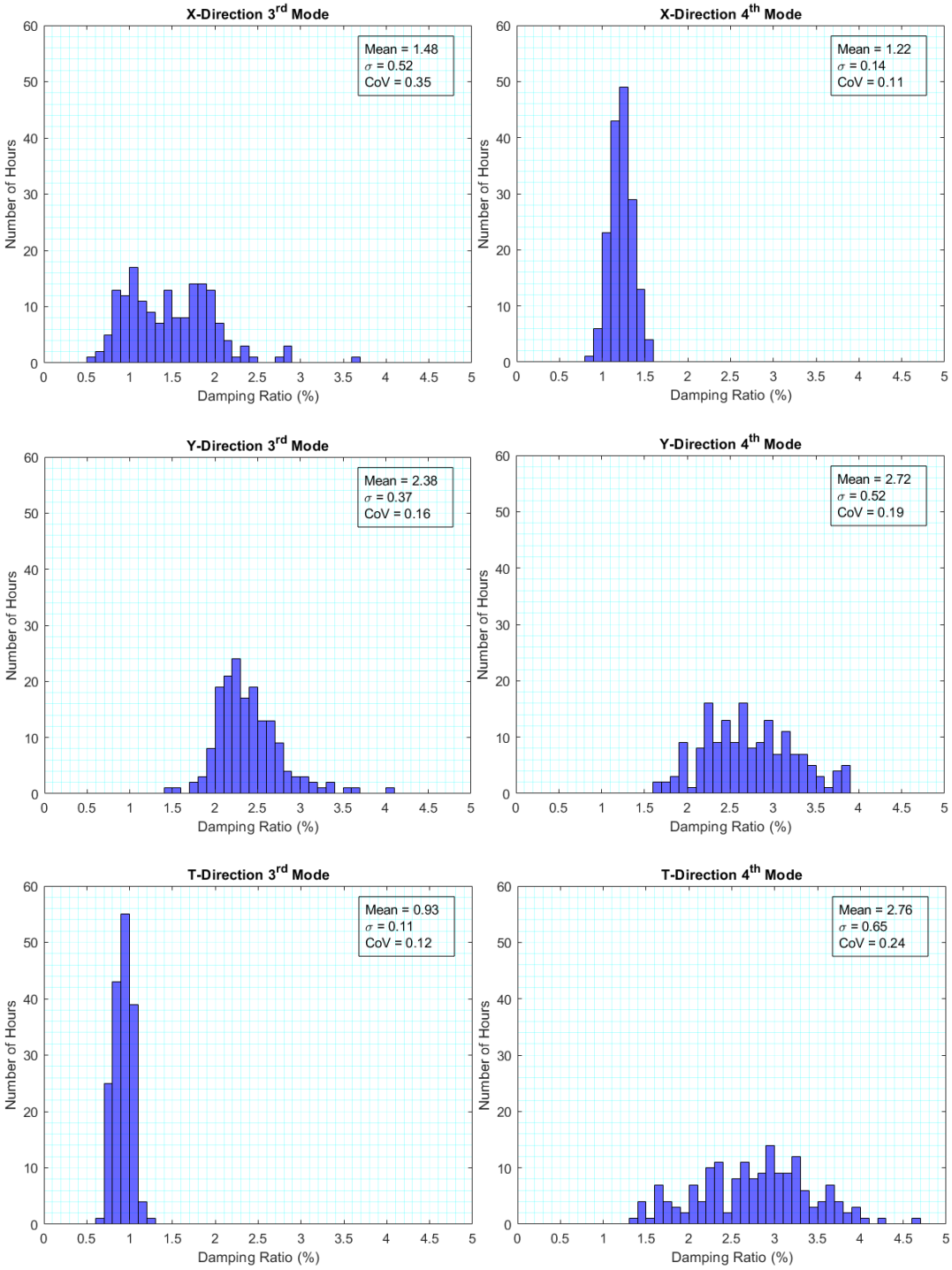

Figure 3.21 Histograms of modal damping ratios over a week: 11.02.2019 00:00:00–17.02.2019 23:59:59 GMT (continued)

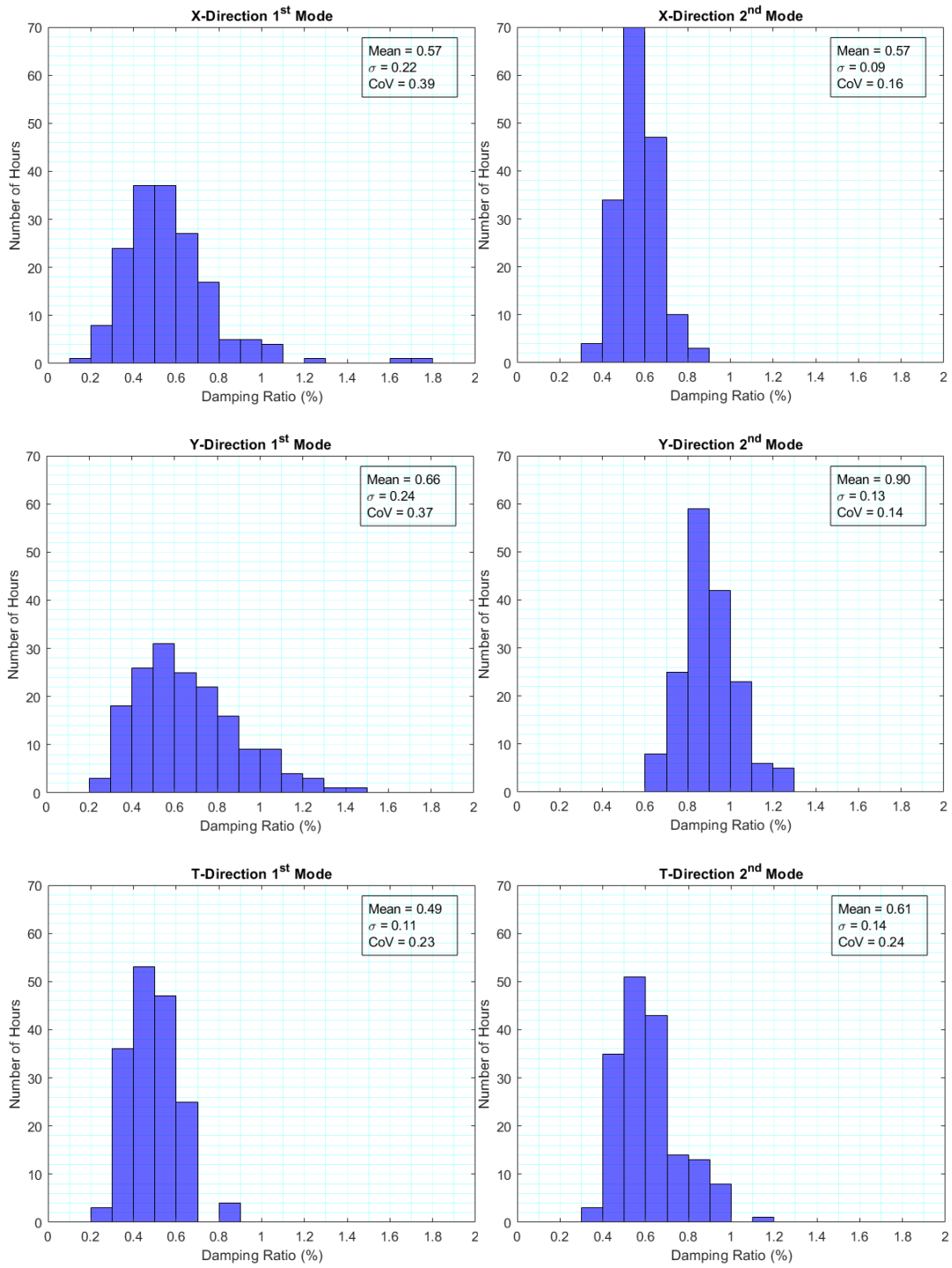

Figure 3.22 Histograms of modal damping ratios over a week: 16.09.2019 00:00:00–22.09.2019 23:59:59 GMT

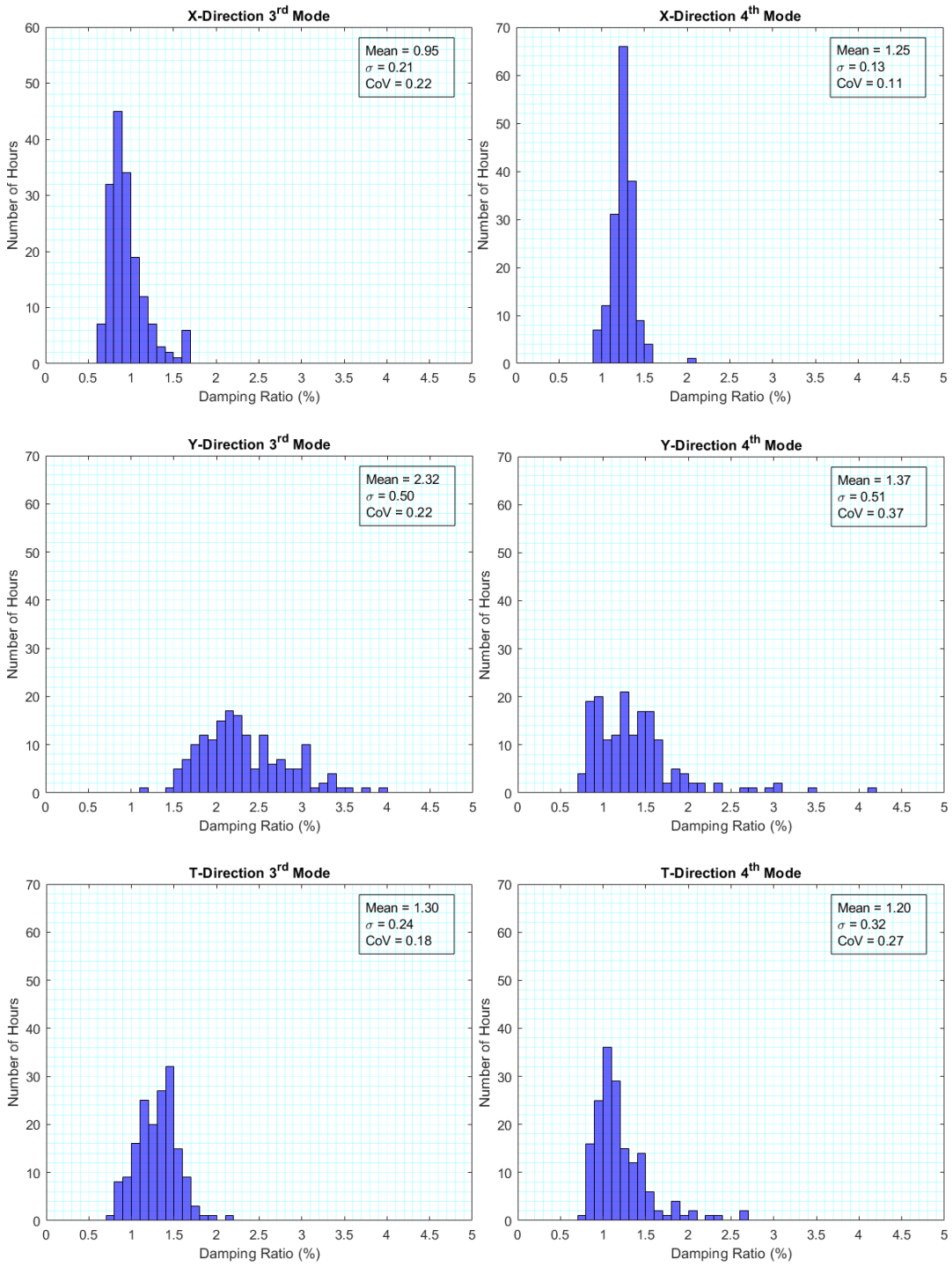

Figure 3.22 Histograms of modal damping ratios over a week: 16.09.2019 00:00:00–22.09.2019 23:59:59 GMT (continued)

Table 3.3 List of statistical properties of damping ratios: 11.02.2019 00:00:00–17.02.2019 23:59:59 GMT

Direction	Mode	Mean (%)	σ (%)	CoV
X	1	0.64	0.22	0.34
	2	0.66	0.12	0.19
	3	1.48	0.52	0.35
	4	1.22	0.14	0.11
Y	1	0.60	0.19	0.31
	2	0.90	0.11	0.12
	3	2.38	0.37	0.16
	4	2.72	0.52	0.19
T	1	0.55	0.12	0.22
	2	0.58	0.09	0.16
	3	0.93	0.11	0.12
	4	2.76	0.65	0.24

Table 3.4 List of statistical properties of damping ratios: 16.09.2019 00:00:00–22.09.2019 23:59:59 GMT

Direction	Mode	Mean (%)	σ (%)	CoV
X	1	0.57	0.22	0.39
	2	0.57	0.09	0.16
	3	0.95	0.21	0.22
	4	1.25	0.13	0.11
Y	1	0.66	0.24	0.37
	2	0.90	0.13	0.14
	3	2.32	0.50	0.22
	4	1.37	0.51	0.37
T	1	0.49	0.11	0.23
	2	0.61	0.14	0.24
	3	1.30	0.24	0.18
	4	1.20	0.32	0.27

3.4 Comparisons of the Identified Damping Ratios with the Code and Other Formulations

Tables 3.3 and 3.4 show that damping ratios generally increase for the higher modes. This trend can also be verified from Figure 3.13 by considering the principles of the half-power bandwidth method.

Jeary [1986] expressed the modal damping for tall buildings as a function of the modal frequency f_n (in Hz):

$$\xi = 0.01 f_n \tag{3.4}$$

Tamura et al. [2000] modified this equation for steel and RC frames, respectively:

$$\xi = 0.013 f_n \tag{3.5}$$

$$\xi = 0.014 f_n \tag{3.6}$$

The damping ratios identified in the previous section are compared with the calculated values from these equations in Table 3.5. Except the first translational modes, these equations predict higher damping ratios.

Table 3.5 Comparison of the damping results

Direction	Mode	Random Decrement Method (%)*	Jeary [1986] (%)	Tamura et al. [2000] (%)
X	1	0.61	0.24	0.31
	2	0.62	0.90	1.17
	3	1.22	1.87	2.43
	4	1.24	2.97	3.86
Y	1	0.63	0.25	0.33
	2	0.90	1.08	1.40
	3	2.35	2.55	3.32
	4	2.05	4.77	6.20
T	1	0.52	0.58	0.75
	2	0.60	1.70	2.21
	3	1.12	3.11	4.04
	4	1.98	4.74	6.16

* Mean damping ratios from both weeks

Ha et al. [2020] proposed an equation for the first-mode damping ratio for use in the wind design of buildings:

$$\xi = 0.2467/H + 0.0067 \tag{3.7}$$

where H is the roof height above grade in m. This equation gives 0.79% for Mistral Izmir Office Tower.

Furthermore, Li et al. [2020] proposed an equation for the first-mode damping ratio for buildings taller than 200 m:

$$\xi = 2.05 - 0.28\,H/s \tag{3.8}$$

where s is the total number of floors. This equation gives 0.84% for Mistral Izmir Office Tower.

Los Angeles Tall Buildings Structural Design Council (LATBSDC) also proposed an equation for the damping ratio [LATBSDC, 2020]:

$$\xi = 0.20/\sqrt{H} \tag{3.9}$$

which gives 1.4% for Mistral Izmir Office Tower under service-level earthquakes. On the other hand, LATBDSC recommends a minimum 2.5% damping ratio for the maximum considered earthquake.

Ha et al. [2020] collected the damping ratio equations for tall buildings from structural codes around the world and compared them as shown in Figure 3.23. As can be deduced from this figure, the predicted damping ratio for Mistral Izmir Office Tower is 2.0% per ASCE 7-10, 1.6% per Eurocode 1, 1.2% per ISO 4354 and 1.0% per AS/NZS 1170. Furthermore, TBEC 2018 provides the damping ratio for tall buildings as 2.5%. Note that these damping ratios are for design-level earthquakes, whereas the identified damping ratios using the random decrement method in this study are based on ambient vibration records.

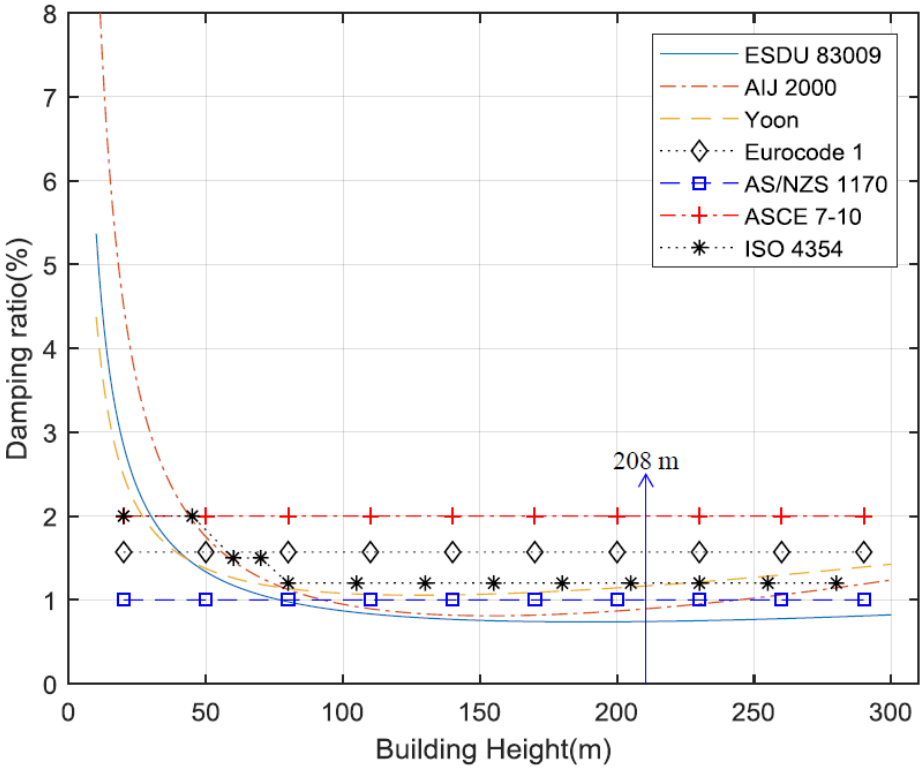

Figure 3.23 Damping ratios for tall buildings (Adopted from Ha et al. [2020]).

Ha et al. [2020] investigated structural response recordings from 36 different tall buildings in Korea and identified their natural periods and damping ratios using the stochastic subspace identification method. Among these buildings, the ones having similar heights and natural periods as the Mistral Izmir Office Tower are listed in Table 3.6.

3.5 Summary

In this chapter, the structural system and the SHM system of the Mistral Izmir Office Tower were presented. The random decrement method used for identifying the modal damping ratios of the building from its ambient vibration records was explained in detail highlighting the selection of its parameters for accurate damping identification with the algorithm used. Then, the identified modal damping ratios for the first four modes in both translational directions and in the torsional direction were

presented. The histograms were also provided showing the distributions and statistical properties of the identified modal damping ratios from two weeks of ambient vibration records. The mean values of the identified modal damping ratios were 0.6–2.9% and the corresponding CoVs were 0.10–0.40. Generally, the damping ratios were higher for the higher modes. Finally, the identified modal damping ratios were compared with the values from code and other formulations in literature. In general, the identified damping ratios from ambient vibration records were lower than the calculated values recommended for seismic or wind design of tall buildings, pointing the amplitude dependency of damping.

Table 3.6 List of buildings from Ha et al. [2020]

Building Name	Number of Floors	Building Height (m)	Natural Period (s)	Damping Ratio (%)
Mistral Izmir	48	208	4.17	0.61
Centrum Star	60	210	4.28	0.60
Leaders' View	57	217	4.44	1.22
Central Star A	58	207	4.33	0.47
I-Park T3	45	202	2.97	0.75
Star City	60	204	4.05	0.84

CHAPTER 4

SIMULATED VERSUS RECORDED EARTHQUAKE RESPONSES

4.1 Introduction

This chapter briefly presents a pre-existing finite element model of the Mistral Izmir Office Tower and the earthquake strong motion records of the building used in this study with this model. The time history analyses are performed using the identified modal damping ratios in the finite element model to reproduce the recorded strong motion responses. The analyses are repeated by setting the code-specified damping ratios in the finite element model.

4.2 Finite Element Structural Model

A 3-D linear elastic finite element model of the building (Figure 4.1) was previously developed by Gumus [2021] using ETABS [Computers and Structures 2018]. Gumus [2021] developed four versions of the model with different stiffness parameters to consider cracking in structural members at varying levels of earthquake intensities. The eigenvalue analysis results of these models were subsequently compared with the dynamic properties identified from the ambient vibration records of the building. Natural vibration periods and mode shapes determined from the finite element model that used the gross section properties, i.e., the uncracked section properties, matched the in-situ dynamic properties. Hence, this version of the finite element model is used in the current study for further investigation of the in-situ dynamic properties, particularly the modal damping ratios.

A brief comparison of the eigenvalue analysis results with the system identification results (see Chapter 3) is given in Table 4.1. The natural vibration frequencies

identified from the ambient vibration records and those determined from the 3-D finite element model are in good agreement. In the model, beams and columns were modeled using frame members whereas shear walls and slabs were modeled using shell elements that combine membrane and thin plate behavior. Truss elements were used in the modeling of BRBs at floors 19 and 39. P-Delta effects were considered in the model based on the gravity load combination $1.0D + 0.3L$ (D and L stand for the dead and live loads, respectively; TBEC 2018). Fixed support conditions were used at the basement level.

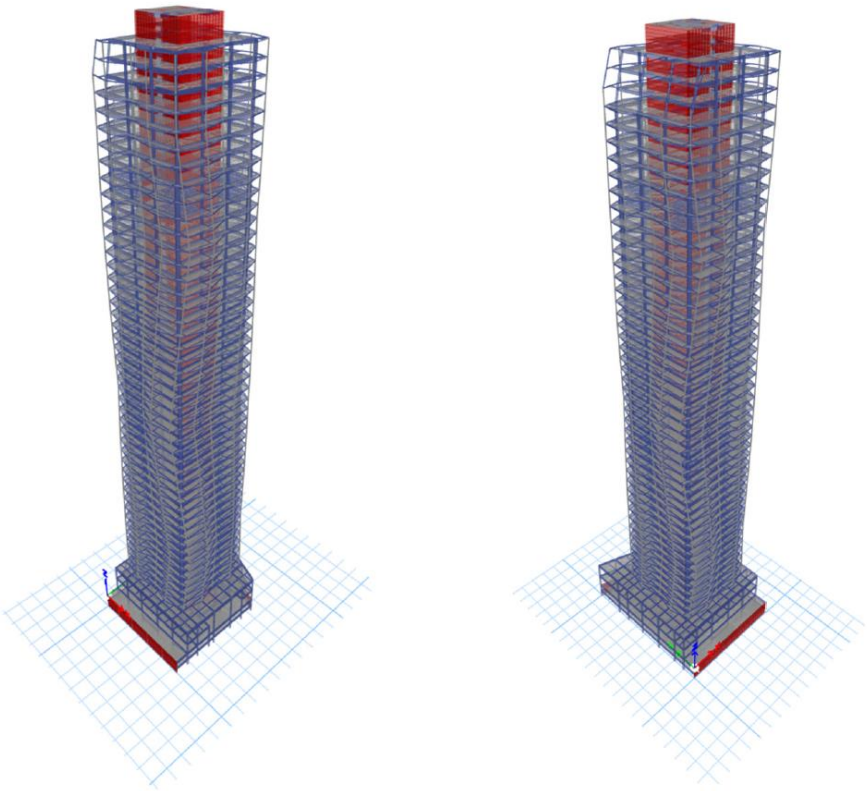

(a) (b)

Figure 4.1 3-D views of the finite element model from the (a) southeast and (b) southwest corners [Gumus 2021]

Table 4.1 Natural vibration frequencies identified from the ambient vibration records and those determined from the finite element model

Direction	Mode	Natural Vibration Frequency (Hz)	
		Ambient Vibration	Finite Element Model
X	1	0.24	0.24
	2	0.90	0.90
	3	1.87	1.92
	4	2.97	2.95
Y	1	0.25	0.24
	2	1.08	1.09
	3	2.55	2.58
	4	4.77	4.45
T	1	0.58	0.58
	2	1.70	1.70
	3	3.11	3.06
	4	4.74	4.56

4.3 Earthquake Strong Motion Records

A number of earthquake strong motions were recorded on the building since the installation of the SHM system. The records captured in 2019 are presented in Gumus [2021]. Two of these earthquake strong motion records are used in this study. The first record belongs to the M_w 5.0 Ayvacik, Canakkale earthquake, which occurred on February 20, 2019, with epicenter 144 km away from the building. The second record belongs to the M_w 5.8 Marmara Sea, Istanbul earthquake, which occurred on September 26, 2019, with epicenter 283 km away from the building. Both earthquakes can be classified as frequent earthquakes (TBEC 2018) in terms of their intensities at the building site. The acceleration time histories of the building base motions are presented in Figures 4.2 and 4.3. The acceleration amplitude of the Canakkale earthquake is significantly larger than that of the Istanbul earthquake.

Peak ground acceleration values at the building base were 0.003 g and 0.001 g during the Canakkale and Istanbul earthquakes, respectively. Figure 4.4 presents the 5% damped acceleration response spectra of the building base motions. The Istanbul earthquake is more dominant than the Canakkale earthquake at higher periods (lower frequencies) and would excite the lower vibration modes of the building more. On the contrary, the Canakkale earthquake is more dominant at lower periods (higher frequencies) and would excite the higher vibration modes more. Similar comparisons can be made for the velocity and displacement response spectra presented in Figure 4.5. This is the main motivation behind selecting these two particular earthquake strong motion records for this study.

4.4 Simulated Earthquake Responses using the Identified Damping Ratios

Linear elastic time history analyses of the building using the earthquake ground motion records presented in Figures 4.2 and 4.3 are performed using ETABS. "Linear Modal" subtype is selected for the time history analyses as the building remained in the elastic range during these earthquakes (the natural frequencies and mode shapes did not alter after the earthquakes). The other linear subtype available, "Linear Direct Integration," is computationally costly and gives similar results when P-Delta effects are insignificant. In the "Linear Modal" subtype, the response is computed using closed-form integration of the modal equations assuming linear behavior. The first 25 vibration modes are included in the response. The time step is selected the same as the earthquake records, i.e., 0.01 s.

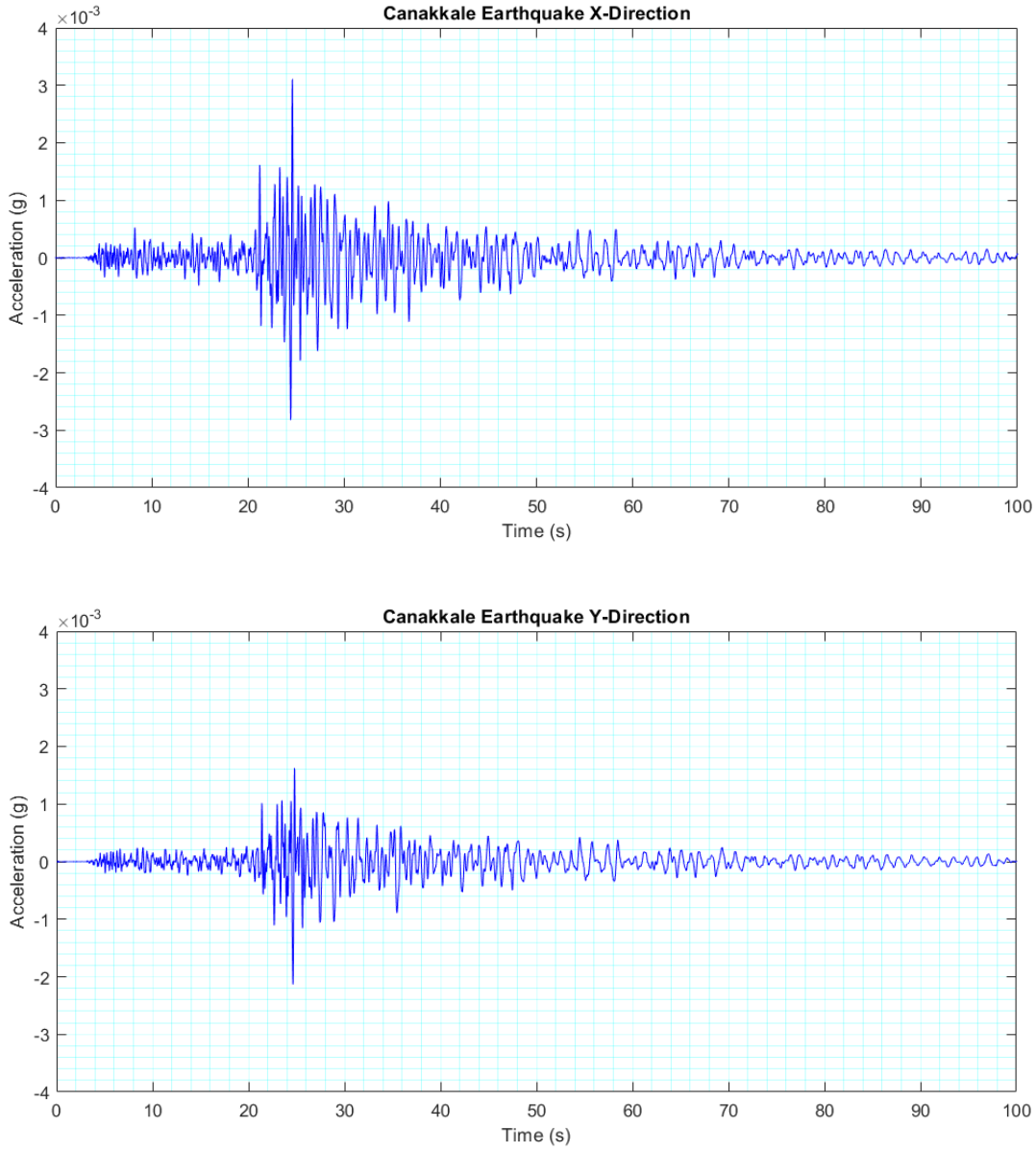

Figure 4.2 Building base motions during the 2019 Mw 5.0 Canakkale earthquake

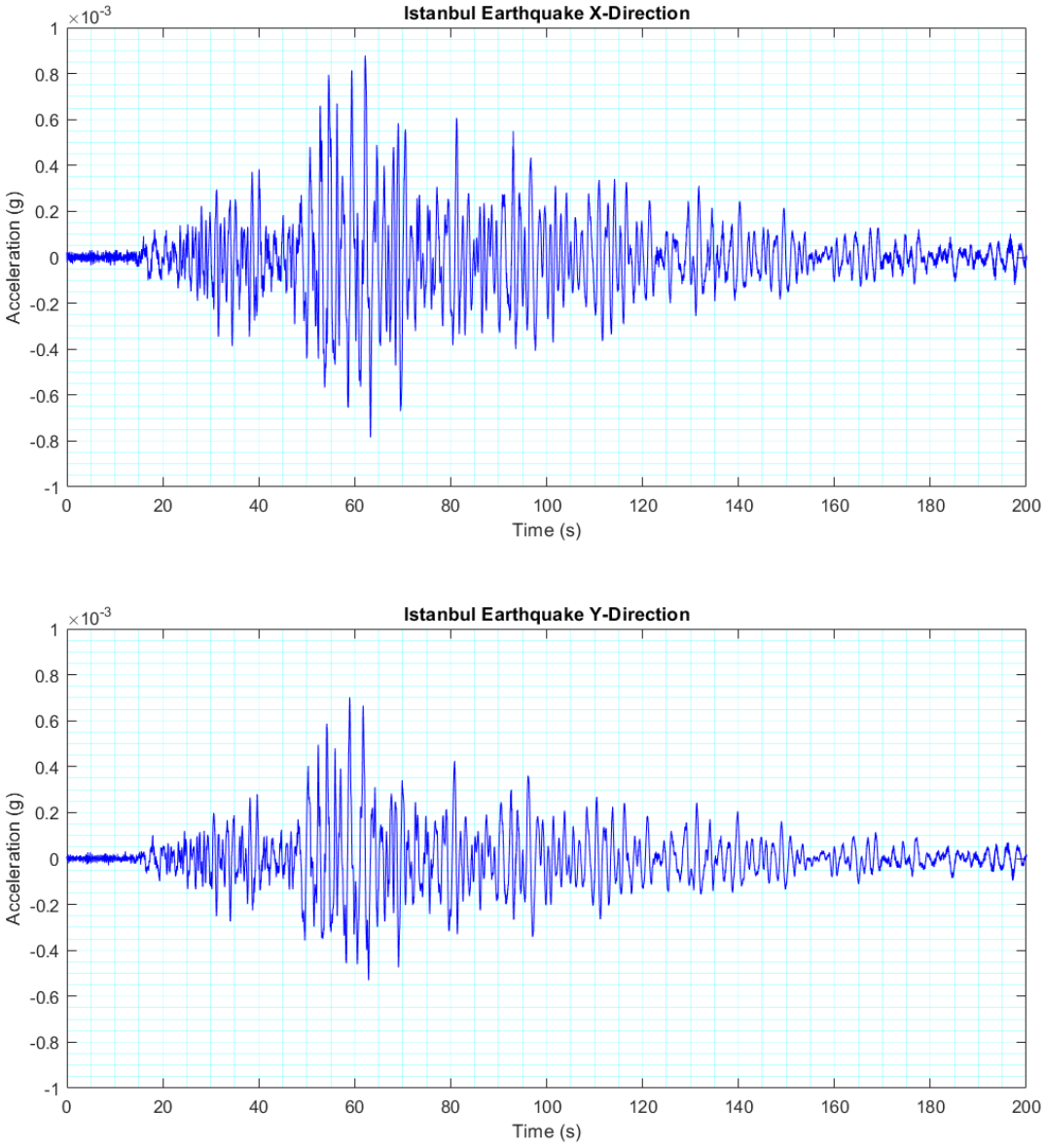

Figure 4.3 Building base motions during the 2019 Mw 5.8 Istanbul earthquake

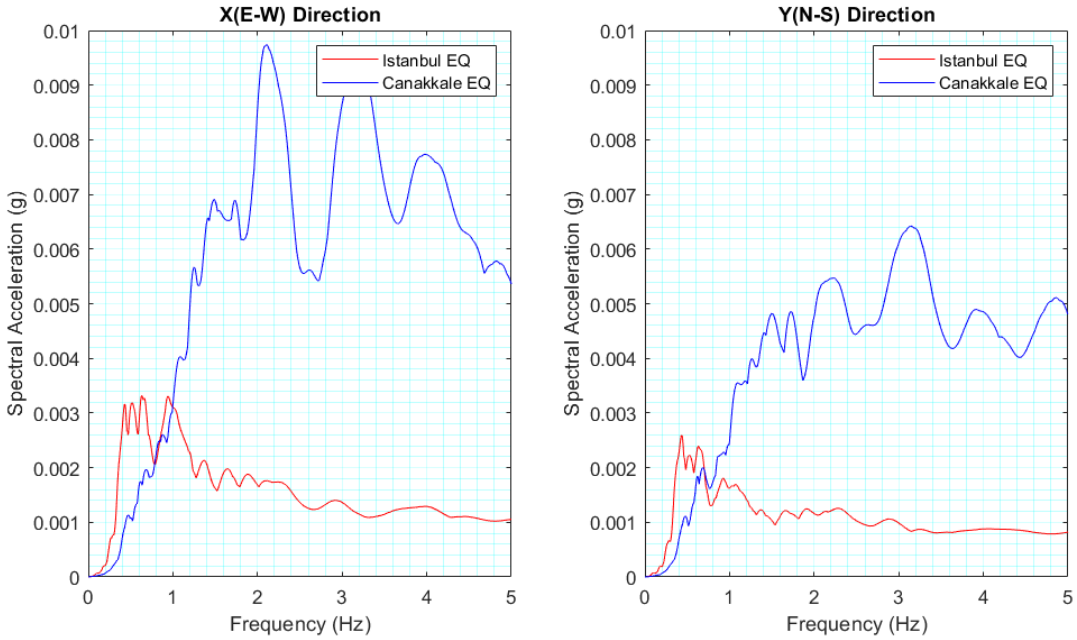

(a)

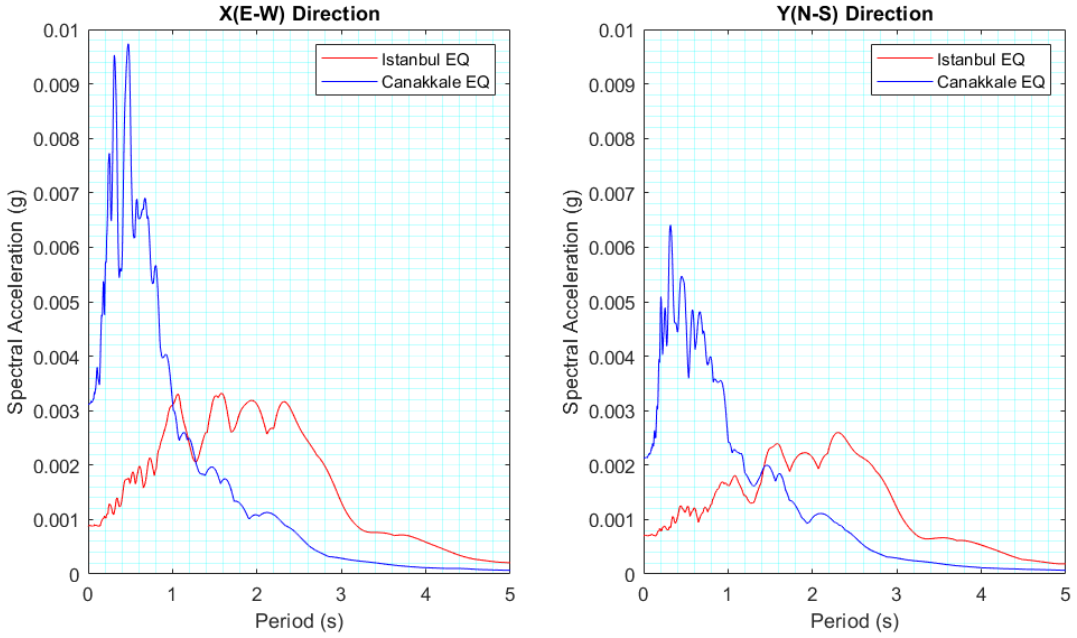

(b)

Figure 4.4 Response spectra of the building base motions recorded during the 2019 M_w 5.0 Canakkale and 2019 M_w 5.8 Istanbul earthquakes, as functions of natural vibration (a) frequency and (b) period

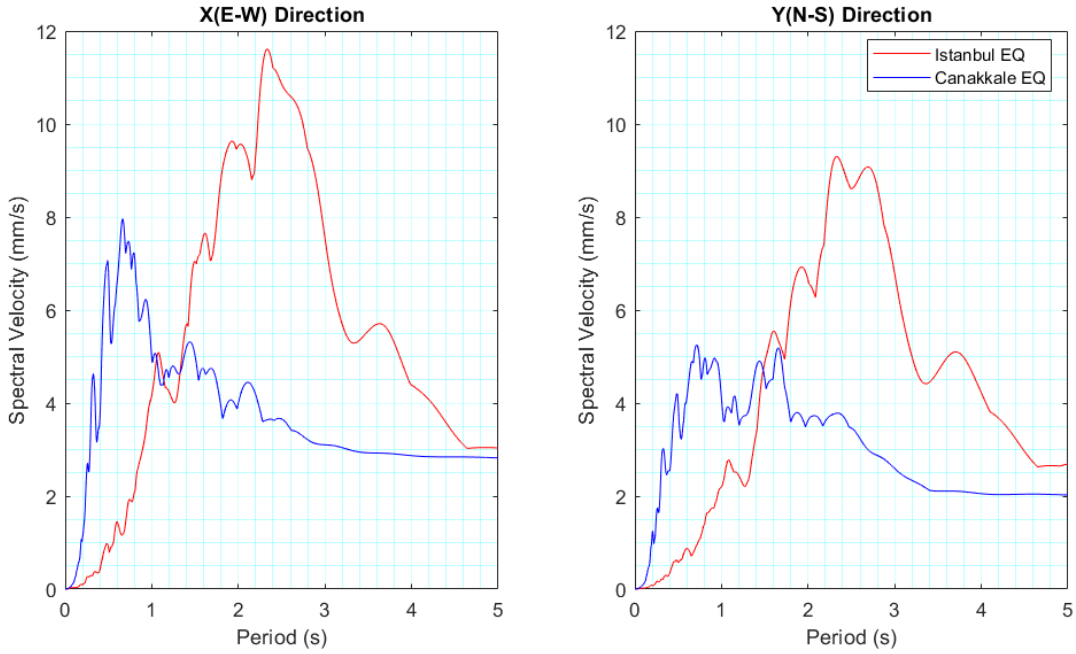

(a)

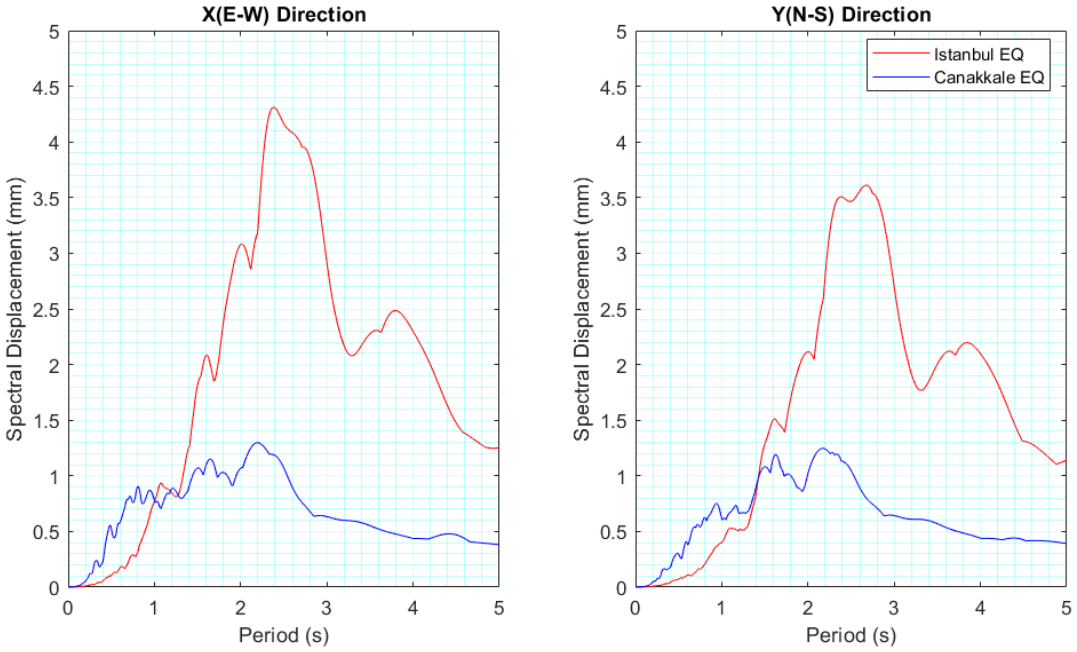

(b)

Figure 4.5 (a) Velocity and (b) displacement response spectra of the building base motions recorded during the 2019 M_w 5.0 Canakkale and 2019 M_w 5.8 Istanbul earthquakes

There are three different options for defining the damping ratios in linear elastic time history analysis using ETABS. The first one is constant damping for all modes, where a single damping ratio is defined for all modes. The second option is interpolated damping by frequency, where modal damping ratios are linearly interpolated between the specified damping-frequency pairs. The third option is mass and stiffness proportional damping, i.e., Rayleigh damping. Whichever option is selected, modal damping ratios can be overwritten for the specified modes. In this study, a constant damping of 5% for all modes is defined and then specific values of damping ratios are defined using the overwrites option for the first four E-W translational, N-S translational and torsional modes that contributed significantly to the overall response during the earthquakes. In this section, the mean damping ratios identified from the ambient vibration records for the first four modes in each direction (see Tables 3.3 and 3.4) are used in the time history analyses.

4.4.1 Simulated versus Recorded Canakkale Earthquake Responses

Figure 4.6 compares the simulated acceleration responses with the recorded responses of the instrumented floors when the finite element model is subjected to the Canakkale earthquake ground motions. The vibration amplitudes increase from the ground floor to floor 20, then decrease between floors 20 and 40. The amplitudes eventually peak at floor 48. These show that higher mode effects exist in the response of the building to the earthquake.

In the X direction, the differences between the simulated and recorded responses become evident with increasing floors. The simulated responses significantly underestimate the recorded responses between 35 and 60 s, whereas they overestimate the recorded responses between 70 and 90 s. Both differences are more evident at floors 48 and 20, a sign for possible higher mode effects.

In the Y direction, the simulated responses are in better agreement with the recorded responses. Especially at the ground floor, the simulated responses almost perfectly

follow the recorded responses. However, at the upper floors, there are differences between 55 and 75 s, where the simulated responses underestimate the recorded responses. Similar to the X direction, these differences are more evident at floors 48 and 20, again indicating possible higher mode effects.

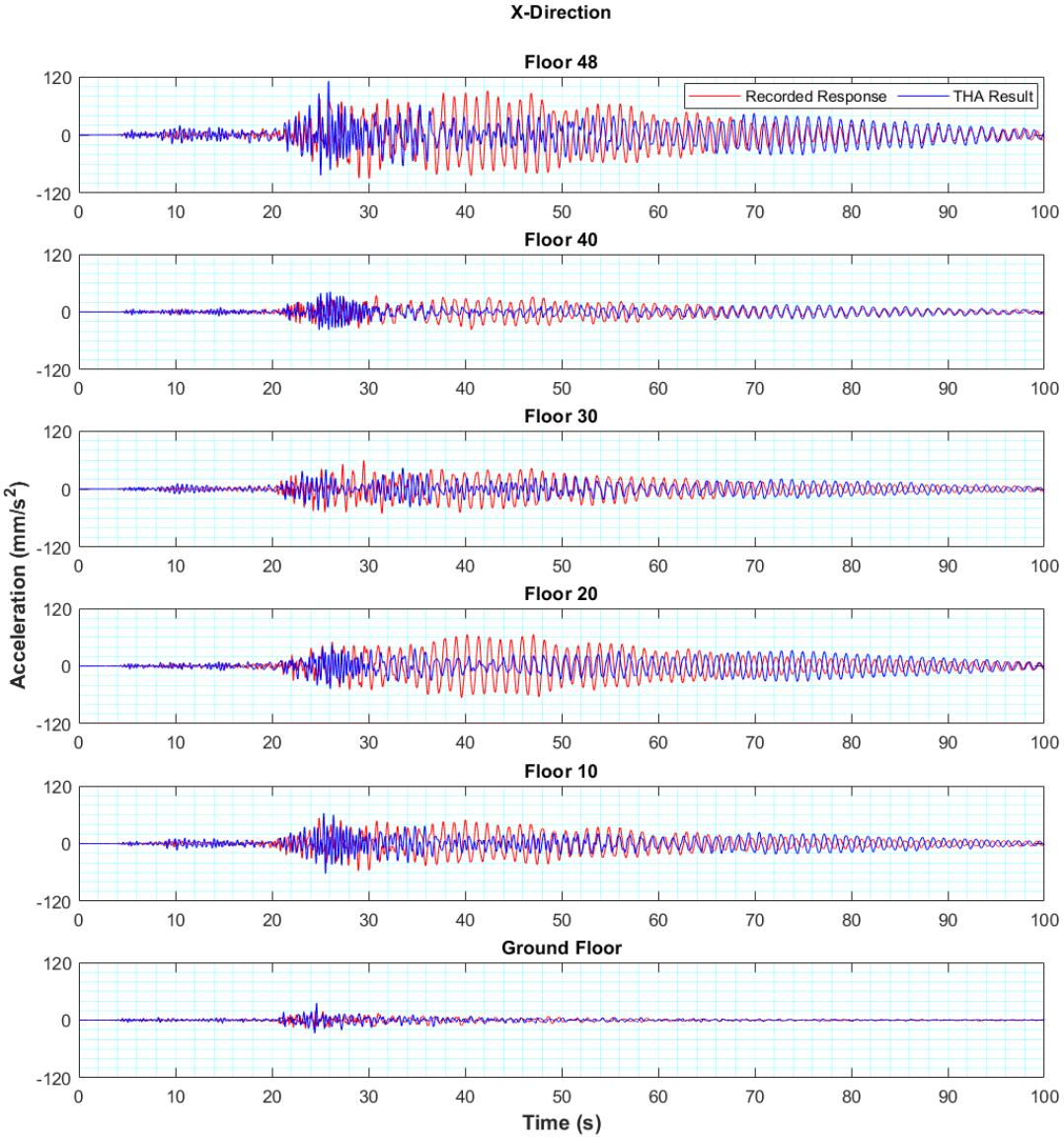

(a)

Figure 4.6 Simulated versus recorded acceleration responses of the instrumented floors for the Canakkale earthquake: (a) X and (b) Y directions

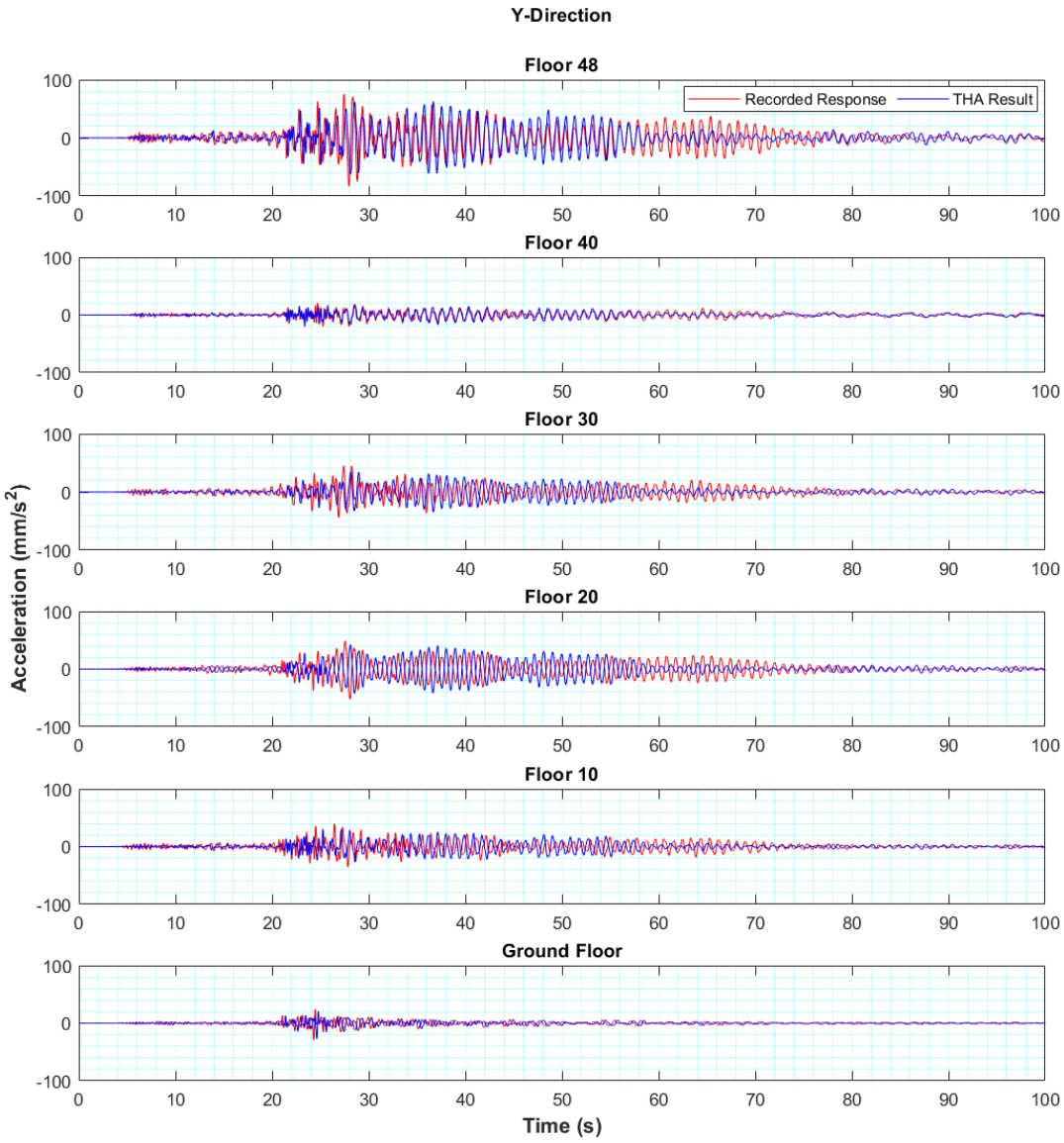

(b)

Figure 4.6 Simulated versus recorded acceleration responses of the instrumented floors for the Canakkale earthquake: (a) X and (b) Y directions (continued)

To examine the torsional responses, the recorded responses by accelerometers #7 and #8, two horizontal accelerometers placed parallel on floor 40, are compared in Figure 4.7. The amplitudes and the frequency content are almost the same; hence, the torsional responses are insignificant during the Canakkale earthquake.

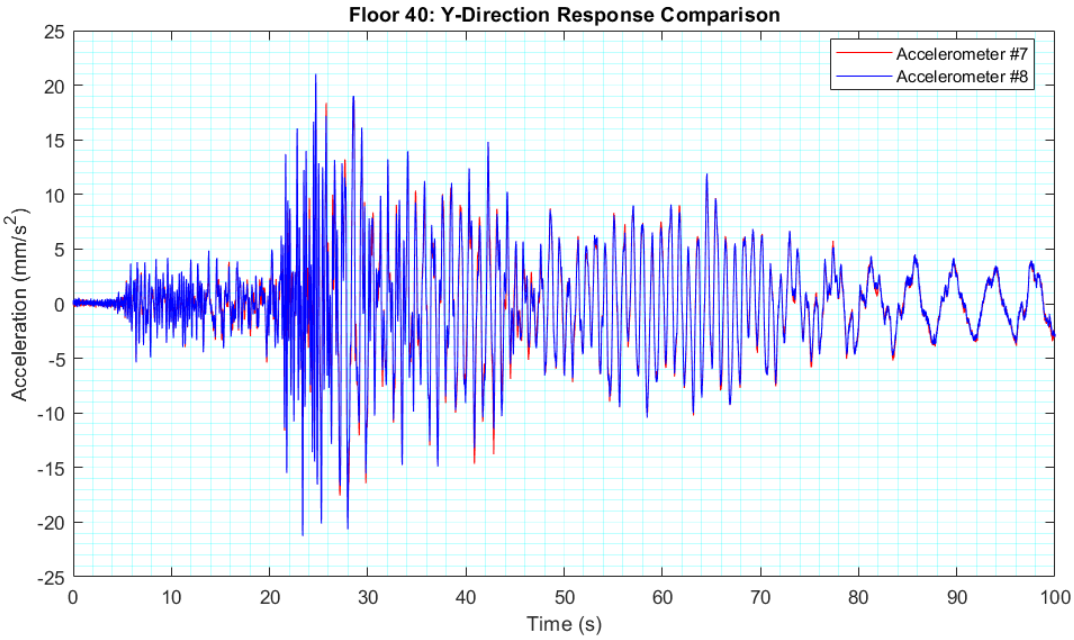

Figure 4.7 Comparison of the accelerations recorded by accelerometers #7 and #8 during the Canakkale earthquake

To investigate the modal contributions to the total building response during the earthquake, the short time Fourier transform (STFT) of the recorded acceleration response of floor 48 is calculated as shown in Figure 4.8. The STFT is calculated using the "stft" function in MATLAB with a Hanning window of 1024 data points with 75% overlap. The second translational modes in the X and Y directions (with the identified natural frequencies of 0.90 and 1.08 Hz, respectively; see Table 3.1) significantly contribute to the building response. The third and fourth translational modes also have noticeable contributions. On the other hand, the first translational modes (0.24 and 0.25 Hz in the X and Y directions, respectively) have limited contributions during the earthquake. However, these contributions do not die out unlike the higher mode contributions following the earthquake. Although the torsional response amplitudes are insignificant, a rich frequency content is apparent.

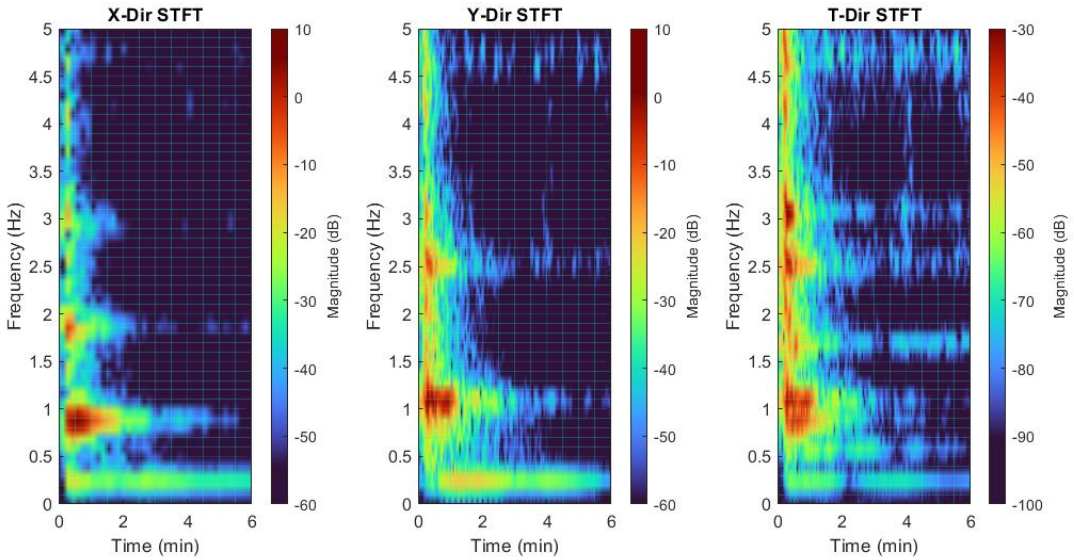

Figure 4.8 STFTs of the recorded floor 48 accelerations during the Canakkale earthquake

To further investigate the individual contributions of the modal responses on the total building response, the simulated and recorded acceleration responses of floor 48 in the X and Y directions are narrow bandpass filtered around the identified modal frequencies to compute the modal responses as shown in Figure 4.9. The second translational modes dominate the total responses while the third and the fourth translational modes have noticeable contributions. The first translational modes, on the other hand, have limited contributions to the total responses.

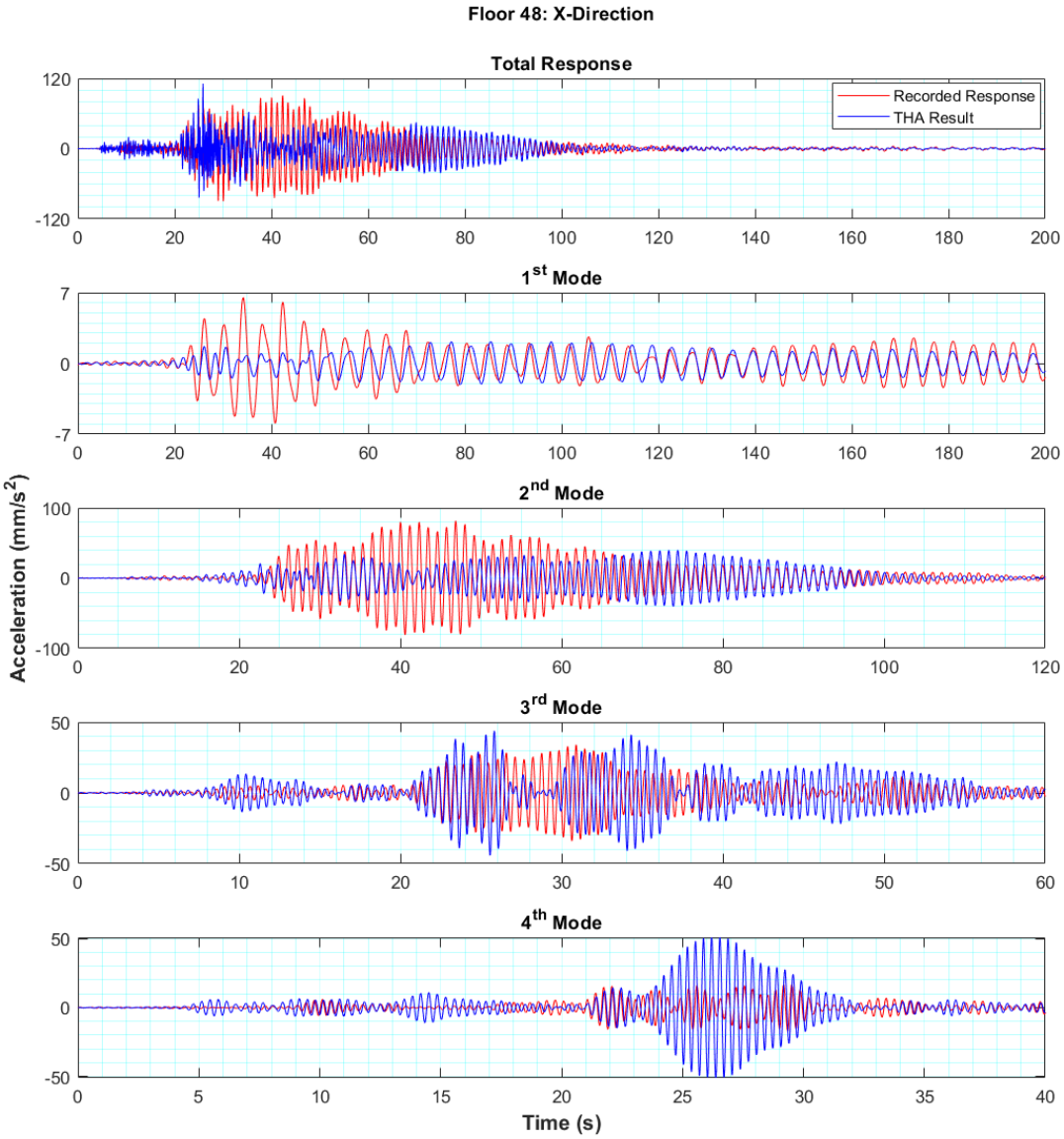

(a)

Figure 4.9 Simulated versus recorded modal acceleration responses of floor 48 for the Canakkale earthquake: (a) X and (b) Y directions

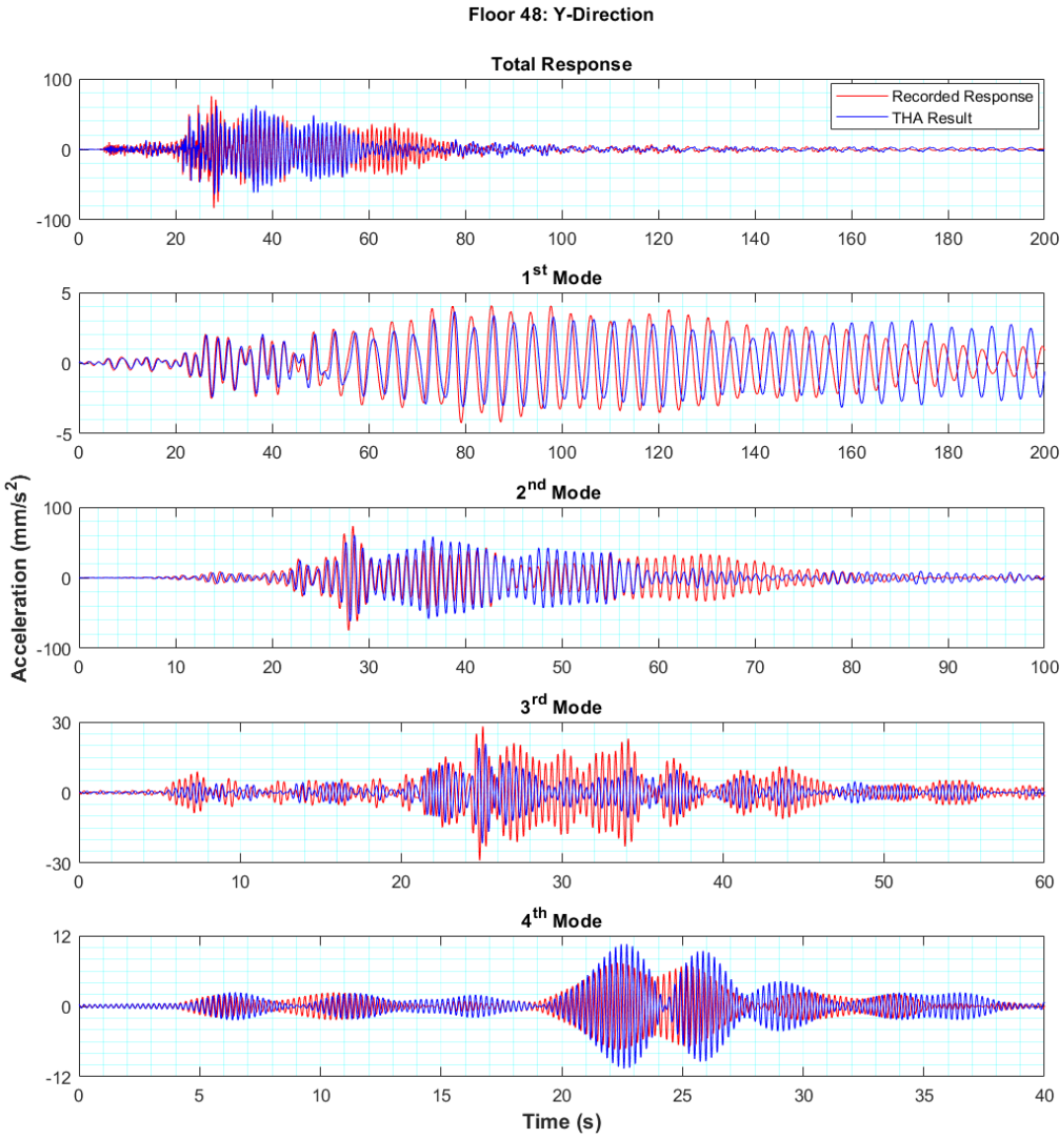

(b)

Figure 4.9 Simulated versus recorded modal acceleration responses of floor 48 for the Canakkale earthquake: (a) X and (b) Y directions (continued)

In the X direction, the simulated first-mode response significantly underestimates the recorded response between 20 and 70 s. However, this has an insignificant effect on the total response since the contribution of the first mode to the total response is limited. In any case, the simulated first-mode response matches the recorded response beyond 70 s and eventually dominates the total response after 120 s. The

simulated second-mode response underestimates the recorded response between 35 and 60 s significantly and overestimates the recorded response between 70 and 90 s, which cause the discrepancy between the simulated and recorded total responses in these ranges. The simulated third-mode response in general overestimates the recorded response, except between 26 and 30 s where the simulated response significantly underestimates the recorded response. The third-mode response dies out after 60 s. The fourth mode is practically excited only for a short duration between 21 and 30 s. The simulated fourth-mode response significantly overestimates the recorded response between 24 and 32 s.

In the Y direction, the simulated first-mode response almost perfectly matches the recorded response up to 160 s, thereafter overestimates the recorded response. However, similar to the X direction, the contribution of the first mode to the total response is limited. The simulated second-mode response also almost perfectly matches the recorded response up to 58 s, thereafter underestimates the recorded response for about 20 s, which causes the discrepancy between the simulated and recorded total responses in this range. The simulated third-mode response in general follows the recorded response but underestimates the recorded response. The third mode response dies out after 60 s. The simulated fourth-mode response also in general follows the recorded response but overestimates the recorded response after 22 s.

Table 4.2 compares the maximum values of the simulated and recorded total and modal floor accelerations for the Canakkale earthquake. The differences in the total responses in the X and Y directions are largely due to the differences in the second mode responses, which dominate the total responses.

Table 4.2 Comparison of the maximum values of the simulated and recorded floor accelerations for the Canakkale earthquake

		Maximum Floor Accelerations (mm/s^2)									
		X-Direction					Y-Direction				
		Total	Mode				Total	Mode			
Floor	Response		1	2	3	4		1	2	3	4
48	Recorded	91	6.5	81	34	17	83	4.2	75	29	7.4
	Simulated	111	2.2	40	44	51	64	3.6	61	22	11
40	Recorded	37	5.3	29	10	12	21	3.2	16	8.6	7.5
	Simulated	42	1.7	14	8.3	33	19	2.7	14	5.5	6.8
30	Recorded	59	3.5	40	27	5.3	45	2.1	38	20	3.1
	Simulated	44	1.2	19	32	8.5	35	1.6	32	14	1.5
20	Recorded	66	1.9	64	12	9.5	52	1.3	49	8.9	5.6
	Simulated	47	0.7	32	16	32	42	1.0	41	6.3	5.9
10	Recorded	57	1.4	43	24	11	40	1.1	26	19	6.9
	Simulated	64	0.9	21	27	38	31	1.1	22	14	7.4
G	Recorded	20	1.8	16	6.2	7.6	30	1.2	12	11	3.3
	Simulated	35	1.0	12	17	12	27	1.2	12	10	2.8

4.4.2 Simulated versus Recorded Istanbul Earthquake Responses

Figure 4.10 compares the simulated acceleration responses with the recorded responses of the instrumented floors when the finite element model is subjected to the Istanbul earthquake ground motions. The vibration amplitudes increase from the ground floor to floor 20, then decrease between floors 20 and 40. The amplitudes eventually peak at floor 48. These show that higher mode effects exist in the response of the building to the earthquake.

In the X direction, the simulated responses are in good agreement with the recorded responses up to 100 s whereas they significantly overestimate the recorded responses between 100 and 150 s.

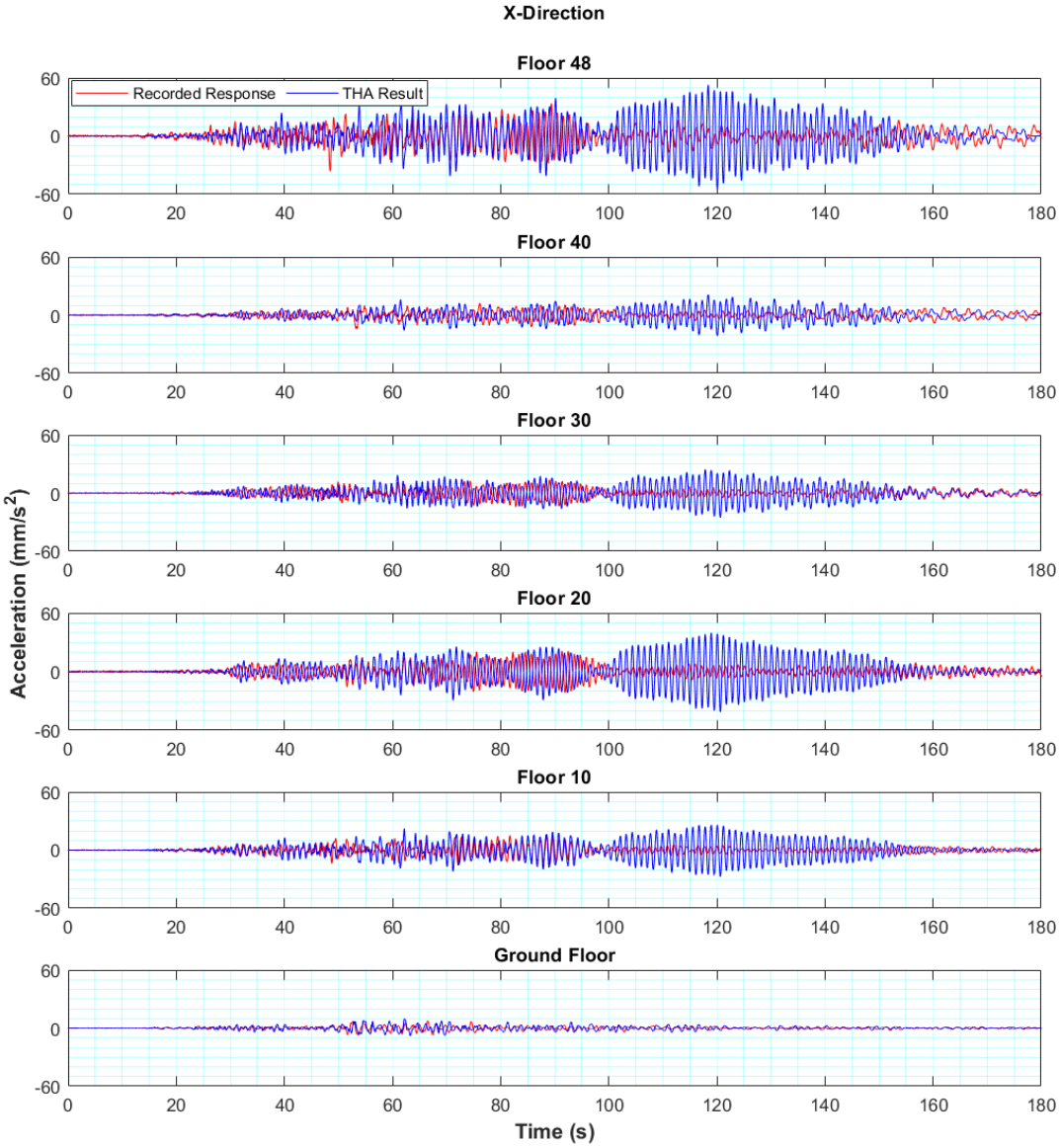

(a)

Figure 4.10 Simulated versus recorded acceleration responses of the instrumented floors for the Istanbul earthquake: (a) X and (b) Y directions

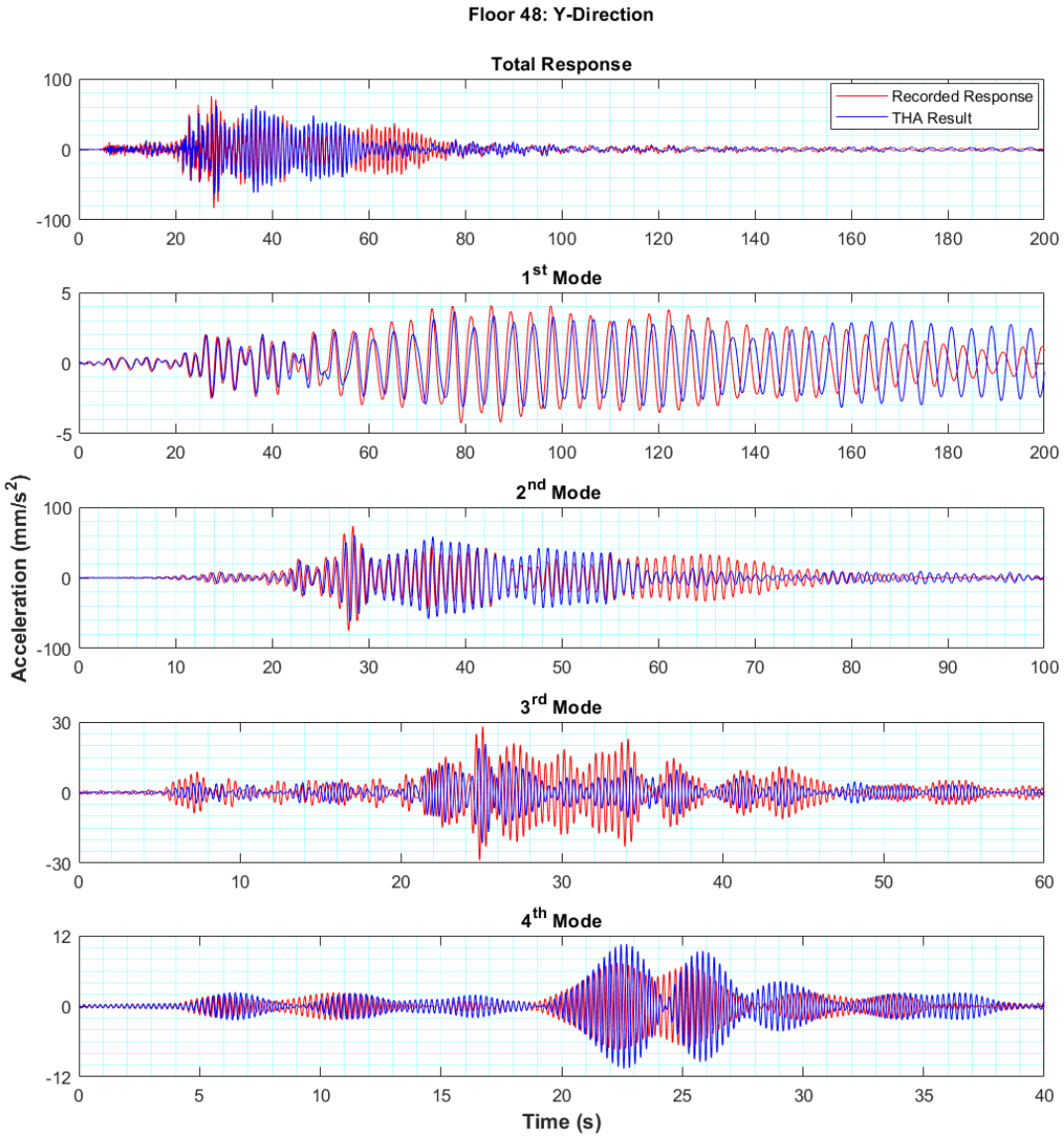

(b)

Figure 4.10 Simulated versus recorded acceleration responses of the instrumented floors for the Istanbul earthquake: (a) X and (b) Y directions (continued)

In the Y direction, the simulated responses are in better agreement with the recorded responses. Especially at the ground floor, the simulated responses almost perfectly follow the recorded responses. However, at the upper floors, there are differences between 30 and 50 s, where the simulated responses slightly underestimate the recorded responses. Similar to the X direction, these differences are more evident at floors 48 and 20, again indicating possible higher mode effects.

To examine the torsional responses, the recorded responses by accelerometers #7 and #8, two horizontal accelerometers placed parallel on floor 40, are compared in Figure 4.11. The amplitudes and the frequency content are almost the same; hence, the torsional responses are insignificant during the Istanbul earthquake.

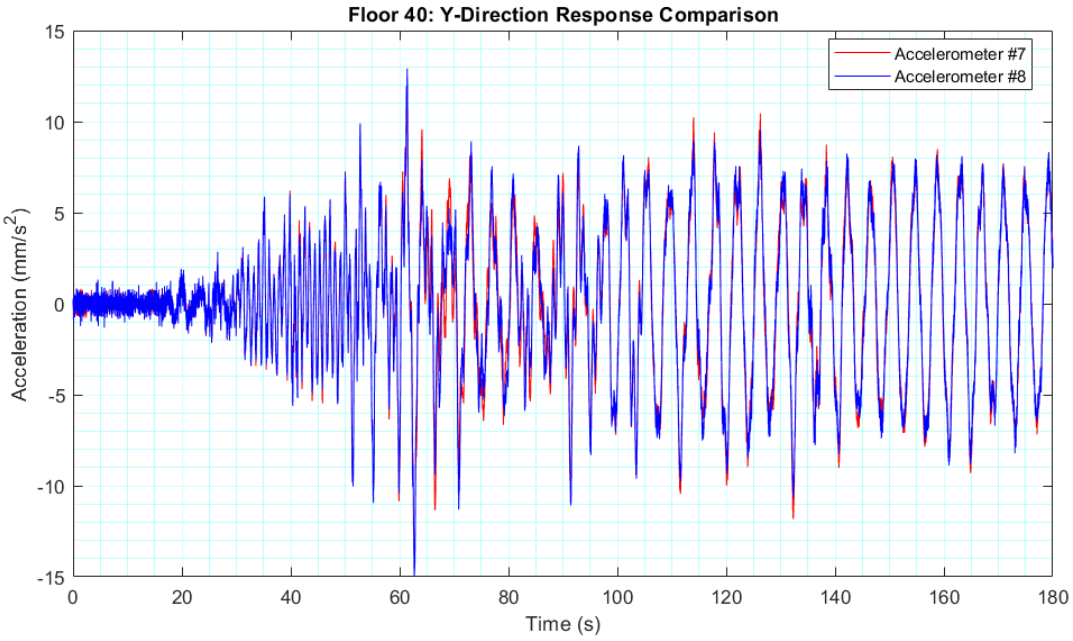

Figure 4.11 Comparison of the accelerations recorded by accelerometers #7 and #8 during the Istanbul earthquake

Figure 4.12 shows the STFT of the recorded acceleration response of floor 48. The second translational modes in the X and Y directions (with the identified natural frequencies of 0.90 and 1.08 Hz, respectively; see Table 3.1) significantly contribute to the building response and eventually damp out after three minutes. The first translational modes in the X and Y directions also have noticeable contributions and continue to contribute after all higher modes damp out. On the other hand, the third and fourth translational modes have limited contributions during the earthquake. Although the torsional response amplitudes are insignificant, a rich frequency content is apparent.

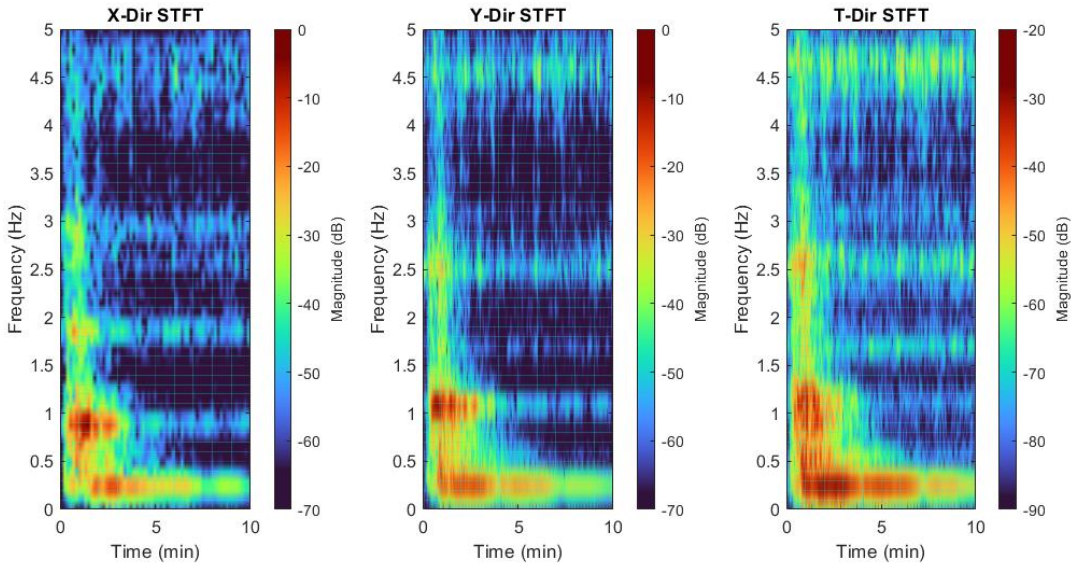

Figure 4.12 STFTs of the recorded floor 48 accelerations during the Istanbul earthquake.

Figure 4.13 shows the simulated and recorded modal acceleration responses of floor 48 in the X and Y directions. The second translational modes dominate the total responses while the first translational modes have noticeable contributions. The third and fourth translational modes, on the other hand, have limited contributions to the total responses.

In the X direction, the simulated first-mode response matches the recorded response and eventually dominates the total response after 200 s. The simulated second-mode response overestimates the recorded response between 100 and 150 s significantly, which cause the discrepancy between the simulated and recorded total responses in this range. The second-mode response dies out after 160 s. The simulated third-mode response significantly overestimates the recorded response between 60 and 120 s. However, the contribution of the third mode to the total response is limited. The third-mode response dies out after 120 s. The simulated fourth-mode response does not match the recorded response. However, this has an insignificant effect on the total response since the contribution of the fourth mode to the total response is limited and the fourth mode is practically excited only for a short duration.

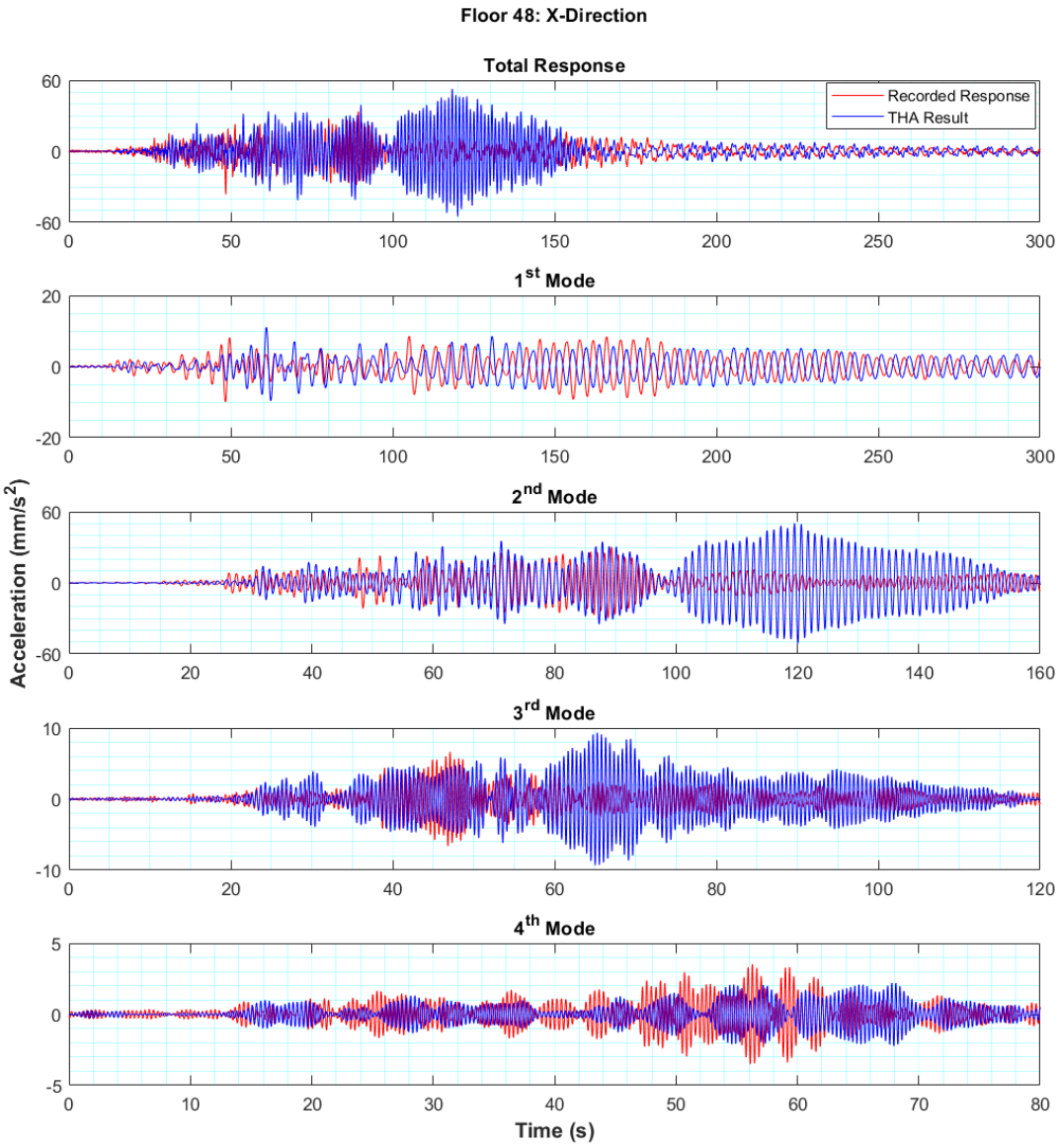

(a)

Figure 4.13 Simulated versus recorded modal acceleration responses of floor 48 for the Istanbul earthquake: (a) X and (b) Y directions

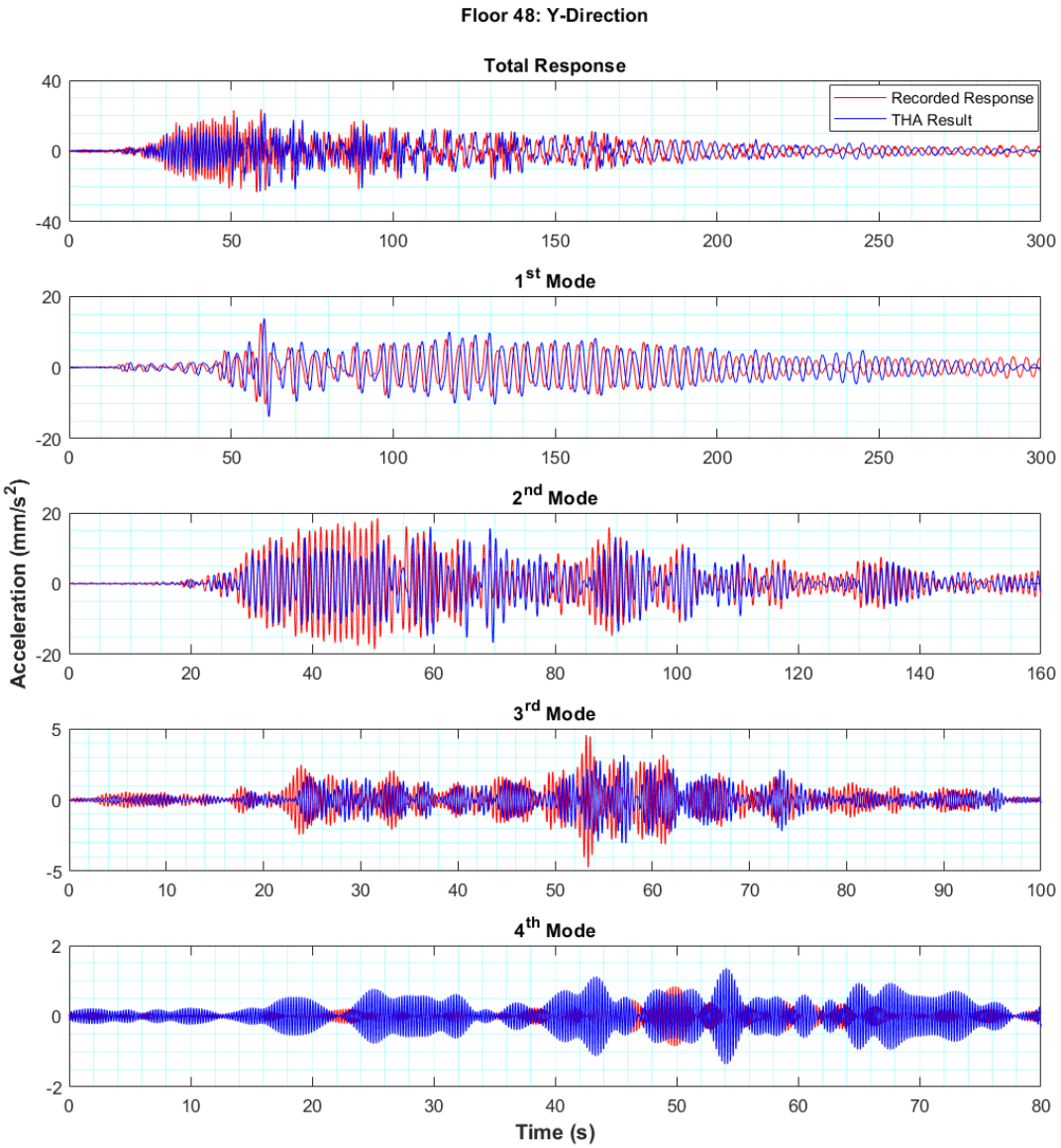

(b)

Figure 4.13 Simulated versus recorded modal acceleration responses of floor 48 for the Istanbul earthquake: (a) X and (b) Y directions (continued)

In the Y direction, the simulated first-mode response almost perfectly matches the recorded response except for a slight phase difference. Similar to the X direction, the first-mode response completely dominates the response after 200 s. The simulated second-mode response matches the recorded response except between 30 and 50 s, where it underestimates the recorded response, which causes the discrepancy

between the simulated and recorded total responses in this range. The simulated third-mode response in general follows the recorded response but underestimates the recorded response. The simulated fourth-mode response significantly overestimates the recorded response. However, these discrepancies in the third and fourth modes have insignificant effects on the total response since their contributions to the total response are limited.

Table 4.3 compares the maximum values of the simulated and recorded total and modal floor accelerations for the Istanbul earthquake. The differences in the total responses in the X and Y directions are largely due to the differences in the second mode responses, which dominate the total responses.

Table 4.3 Comparison of the maximum values of the simulated and recorded floor accelerations for the Istanbul earthquake

		Maximum Floor Accelerations (mm/s^2)									
		X-Direction					Y-Direction				
		Total	Mode				Total	Mode			
Floor	Response		1	2	3	4		1	2	3	4
48	Recorded	36	10	30	6.6	3.5	24	12	19	4.7	0.8
	Simulated	55	11	51	9.3	2.2	23	14	17	3.2	1.4
40	Recorded	14	7.4	10	1.9	1.9	15	10	5.3	1.4	0.9
	Simulated	21	7.8	18	1.5	1.5	13	10	4.6	0.8	0.9
30	Recorded	14	4.0	13	5.4	0.6	14	5.4	11	4.5	0.3
	Simulated	25	3.8	23	6.9	0.4	13	4.8	7.7	2.1	0.2
20	Recorded	22	2.4	21	2.5	1.7	15	3.4	14	1.4	0.8
	Simulated	41	2.6	41	2.4	1.3	13	3	11.5	0.9	0.7
10	Recorded	16	2.7	15	4.8	1.9	14	4.4	9	3.5	0.8
	Simulated	28	3.9	27	6.3	1.6	13	4.6	7.9	2.1	0.9
G	Recorded	7.5	3.7	5.9	1.8	1.2	9.0	5.5	6	1.6	0.3
	Simulated	10	4.7	8	2.7	0.7	8.8	5.7	5.9	1.4	0.3

Overall, the simulated Istanbul earthquake responses are more accurate than the simulated Canakkale earthquake responses.

4.5 Simulated Earthquake Responses using the Specified Damping Ratio in TBEC 2018

TBEC 2018 specifies the damping ratio as 2.5% for the design of tall buildings, which is generally higher than the identified damping ratios in this study. Hence, in this section, this value is used for the first four modes in each direction in the time history analyses for the Canakkale and Istanbul earthquakes to see how the simulated responses in the previous section will be impacted. The damping ratios for all other modes are set to 5% to be consistent with the analyses in the previous section.

4.5.1 Simulated versus Recorded Canakkale Earthquake Responses

Figure 4.14 compares the simulated and recorded acceleration responses of the instrumented floors when the finite element model is subjected to the Canakkale earthquake ground motions. When this figure is compared with Figure 4.6, it is evident that the simulated response amplitudes are significantly reduced. This effect is more obvious in the latter parts of the responses; with increased damping, the accelerations damp out faster. In the X direction, the simulated responses do not overestimate the recorded responses between 70 and 90 s with higher damping, showing that the damping is higher in this interval compared to the rest of the response history. This indicates that damping ratio was not constant during the whole record. In the Y direction, the simulated responses are better compared to the X direction, similar to the previous analysis. Furthermore, they look better compared to the previous simulated responses.

Figure 4.15 compares the simulated and recorded modal acceleration responses of floor 48. The first-mode and second-mode simulated responses are significantly

reduced since the specified damping ratio in TBEC 2018 is considerably higher than the identified damping ratios for these modes.

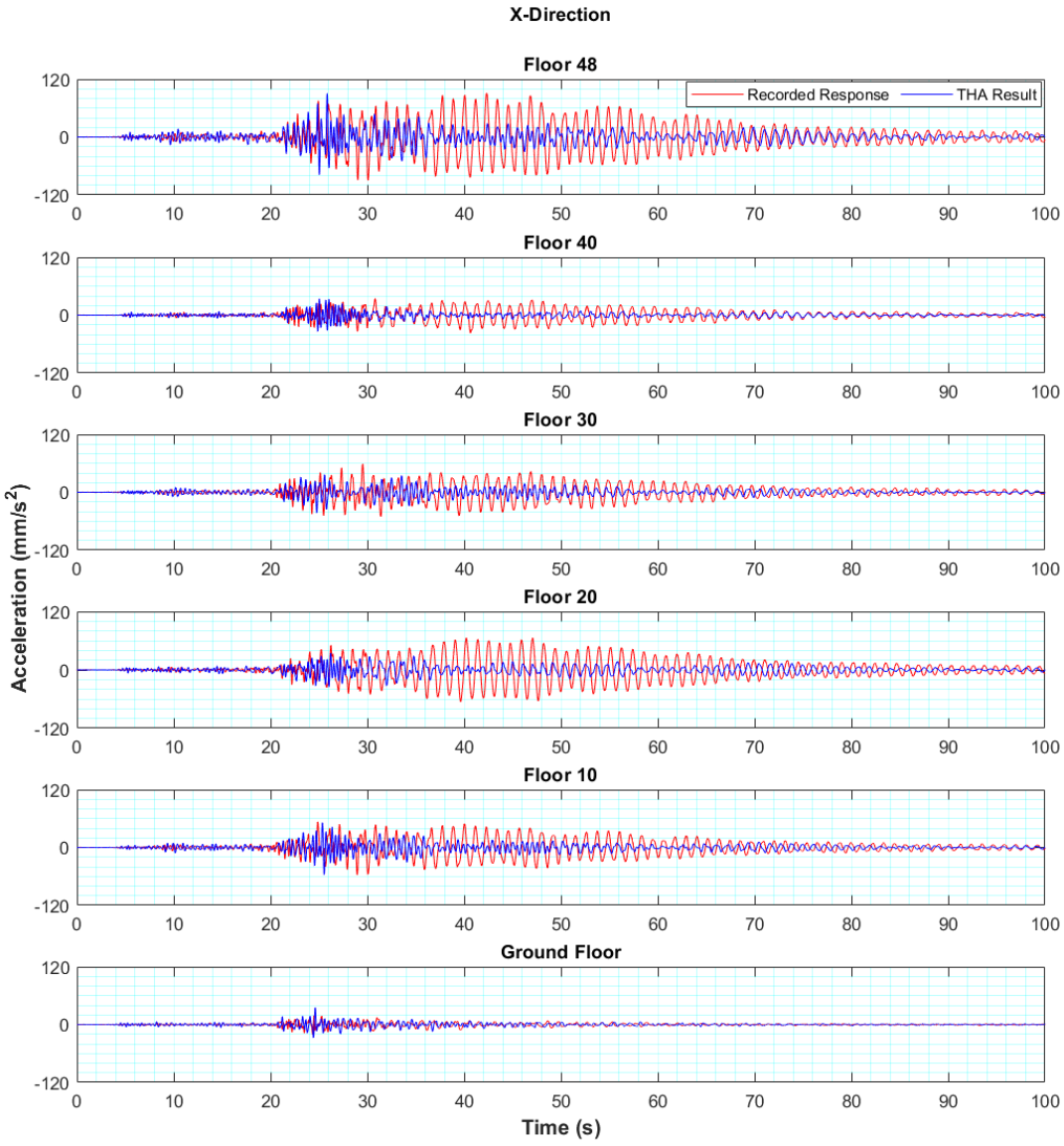

(a)

Figure 4.14 Simulated versus recorded acceleration responses of the instrumented floors for the Canakkale earthquake: (a) X and (b) Y directions

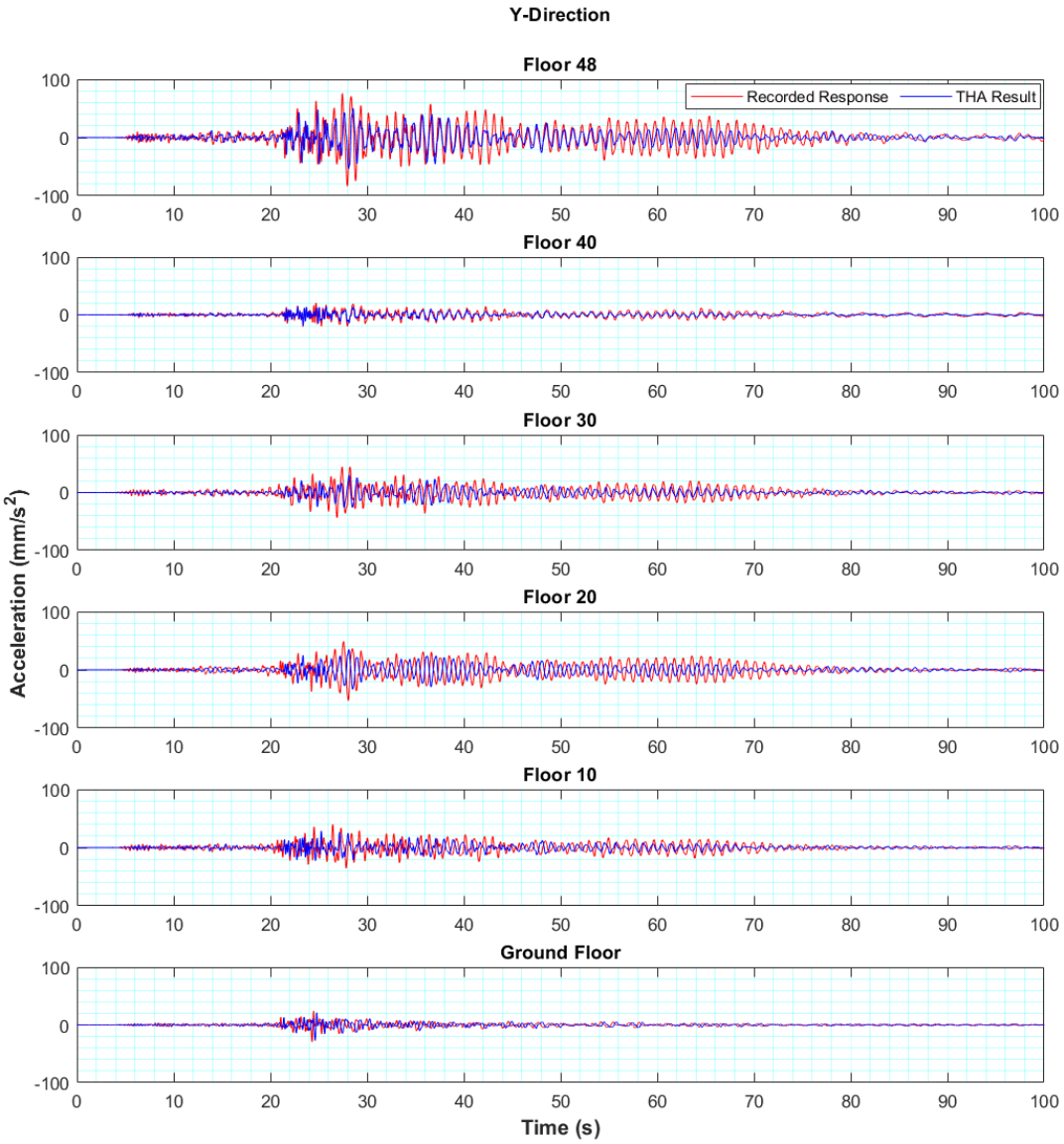

(b)

Figure 4.14 Simulated versus recorded acceleration responses of the instrumented floors for the Canakkale earthquake: (a) X and (b) Y directions (continued)

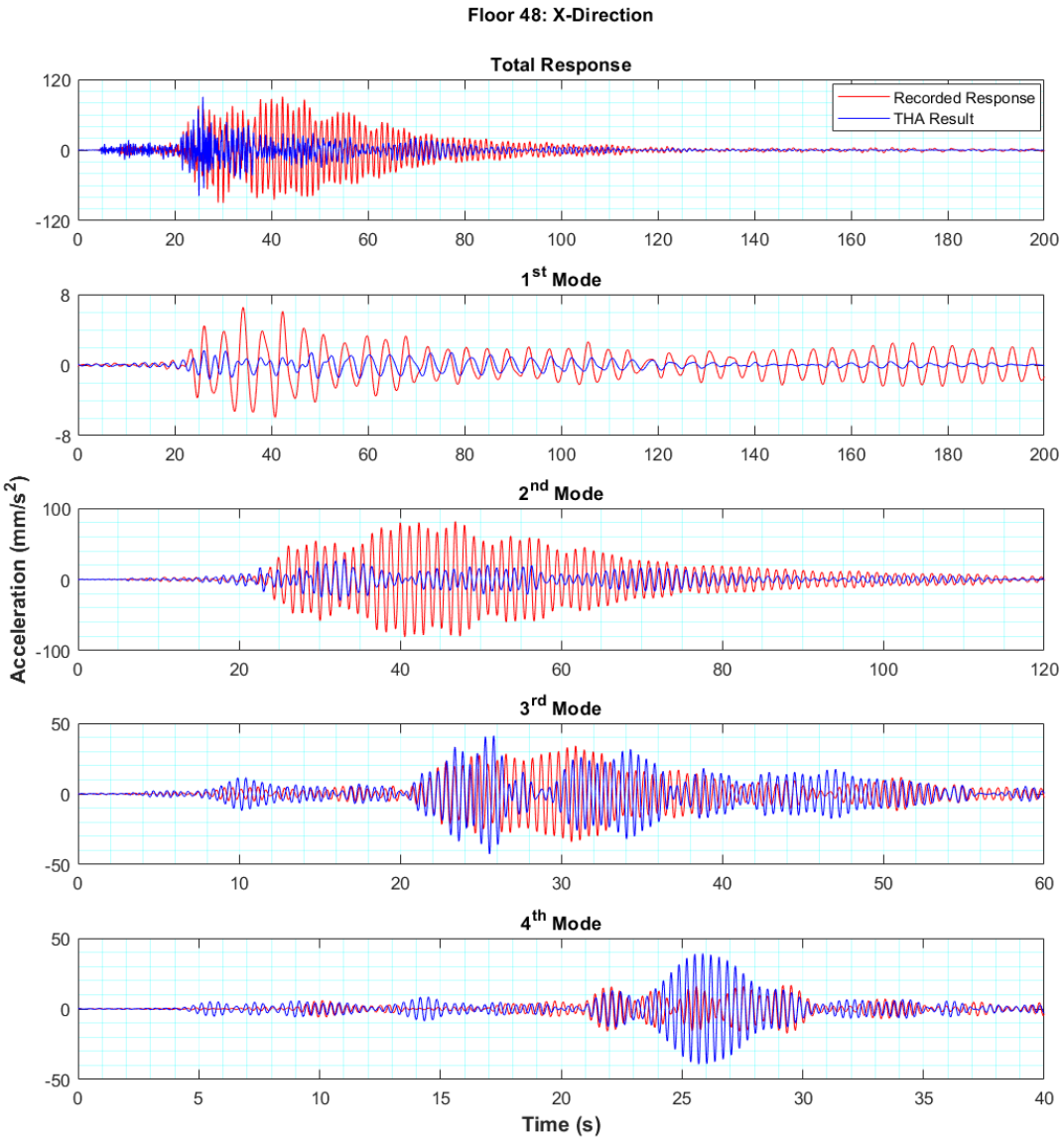

(a)

Figure 4.15 Simulated versus recorded modal acceleration responses of floor 48 for the Canakkale earthquake: (a) X and (b) Y directions

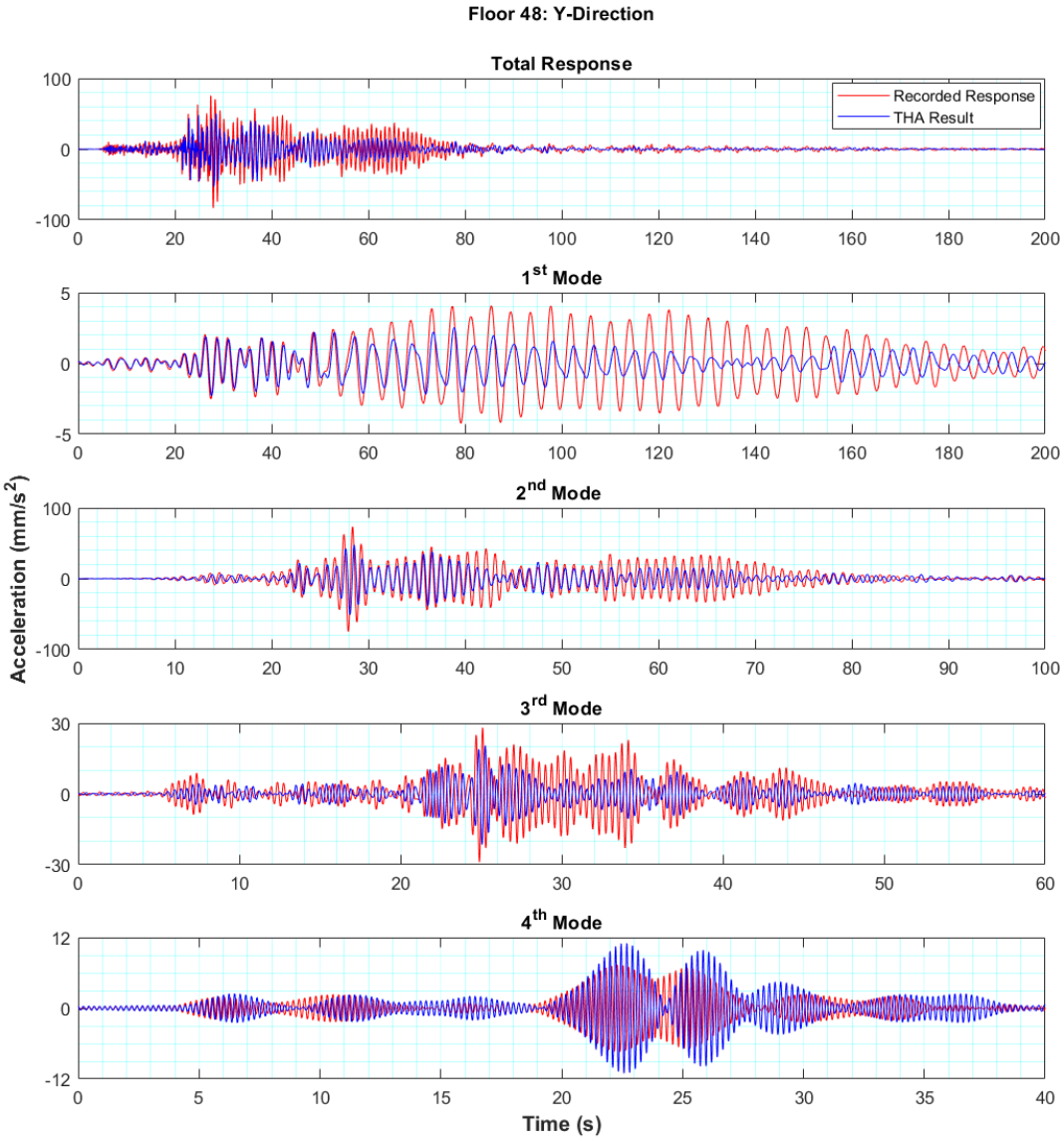

(b)

Figure 4.15 Simulated versus recorded modal acceleration responses of floor 48 for the Canakkale earthquake: (a) X and (b) Y directions (continued)

4.5.2 Simulated versus Recorded Istanbul Earthquake Responses

Figure 4.16 compares the simulated and recorded acceleration responses of the instrumented floors when the finite element model is subjected to the Istanbul earthquake ground motions. When this figure is compared with Figure 4.10, it is evident that the simulated response amplitudes are significantly reduced. This effect is more obvious in the latter parts of the responses; with increased damping, the accelerations damped out faster. In the X direction, the simulated responses do not overestimate the recorded responses between 100 and 150 s anymore, which shows that the damping is higher in this interval compared to the rest of the response history. Hence, damping is not constant during the whole record. In the Y direction, the simulated responses do not match the recorded responses anymore, which shows that the damping ratio is not as high as 2.5% during the Istanbul earthquake.

Figure 4.17 compares the simulated and recorded modal acceleration responses of floor 48. The first-mode and second-mode simulated responses are significantly reduced since the specified damping ratio in TBEC 2018 is considerably higher than the identified damping ratios for these modes.

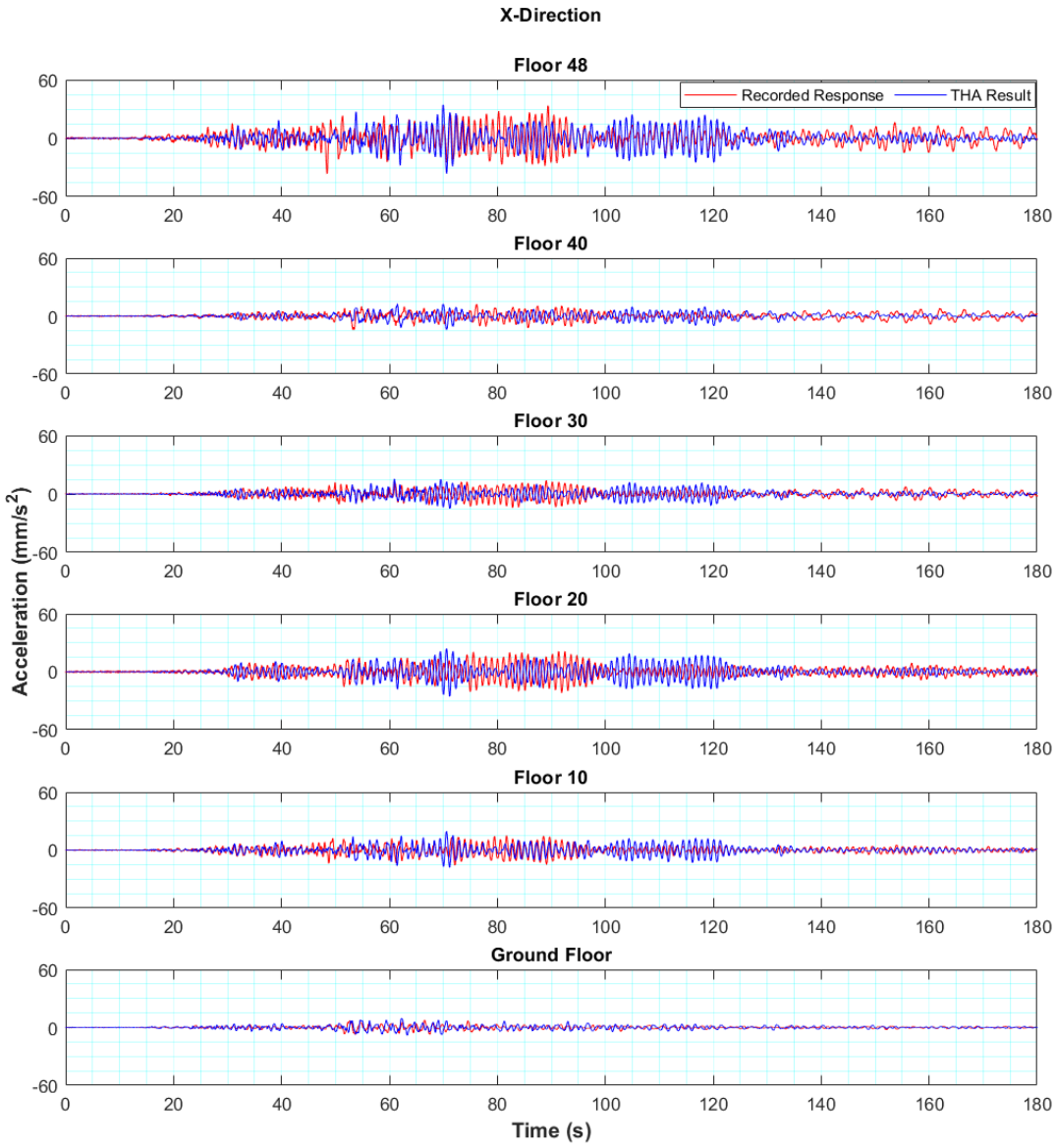

(a)

Figure 4.16 Simulated versus recorded acceleration responses of the instrumented floors for the Istanbul earthquake: (a) X and (b) Y directions

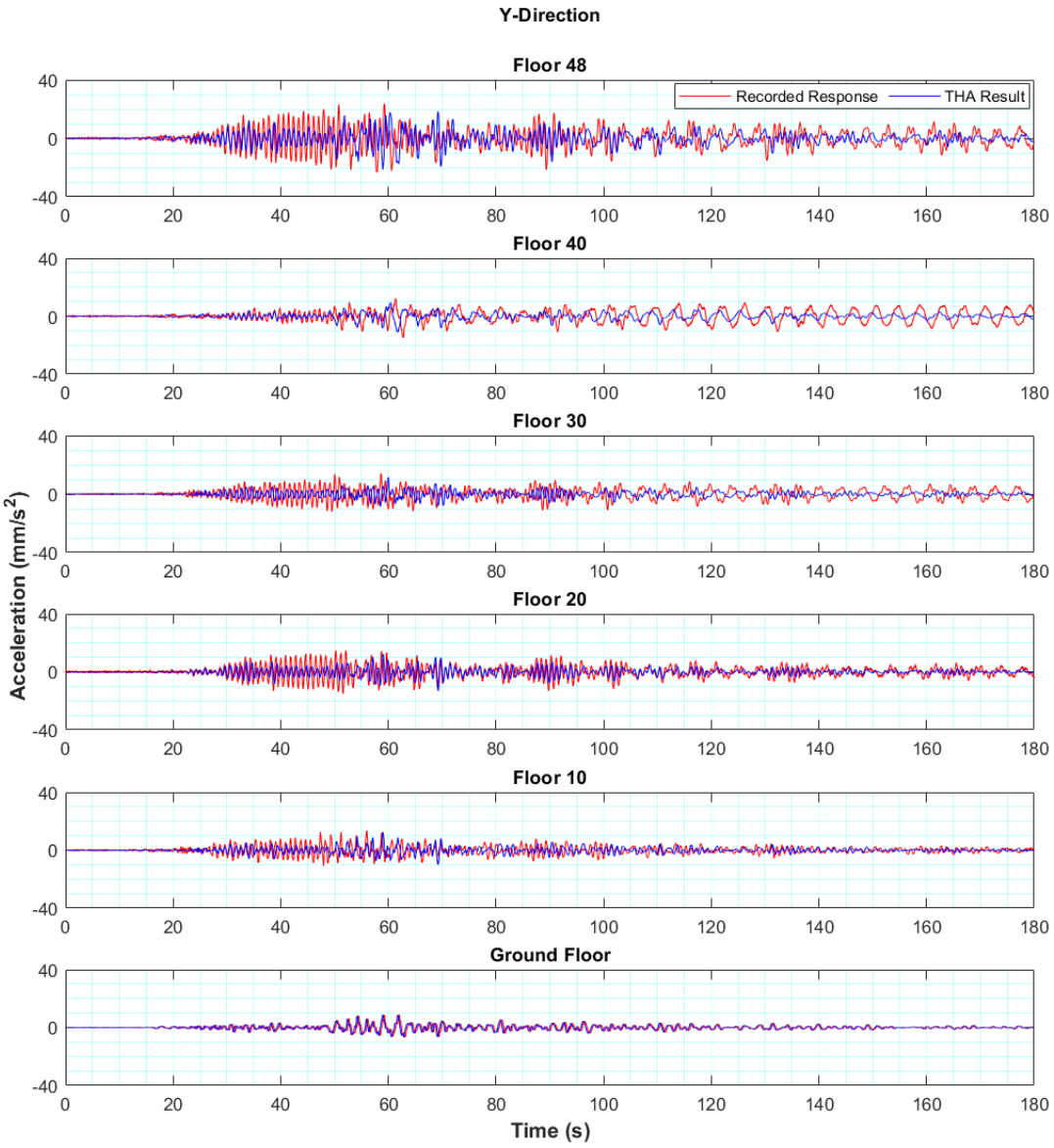

(b)

Figure 4.16 Simulated versus recorded acceleration responses of the instrumented floors for the Istanbul earthquake: (a) X and (b) Y directions (continued)

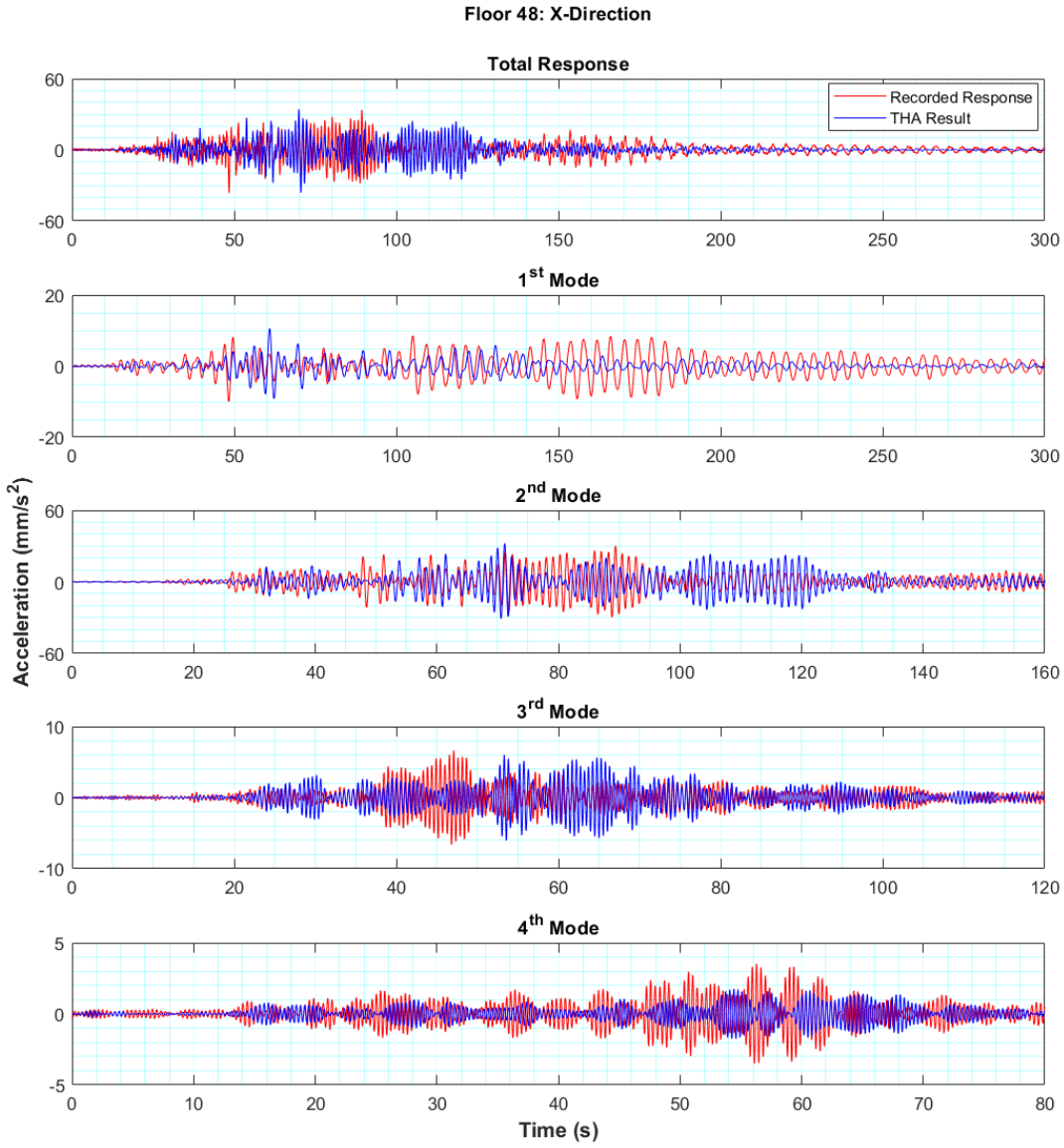

(a)

Figure 4.17 Simulated versus recorded modal acceleration responses of floor 48 for the Canakkale earthquake: (a) X and (b) Y directions

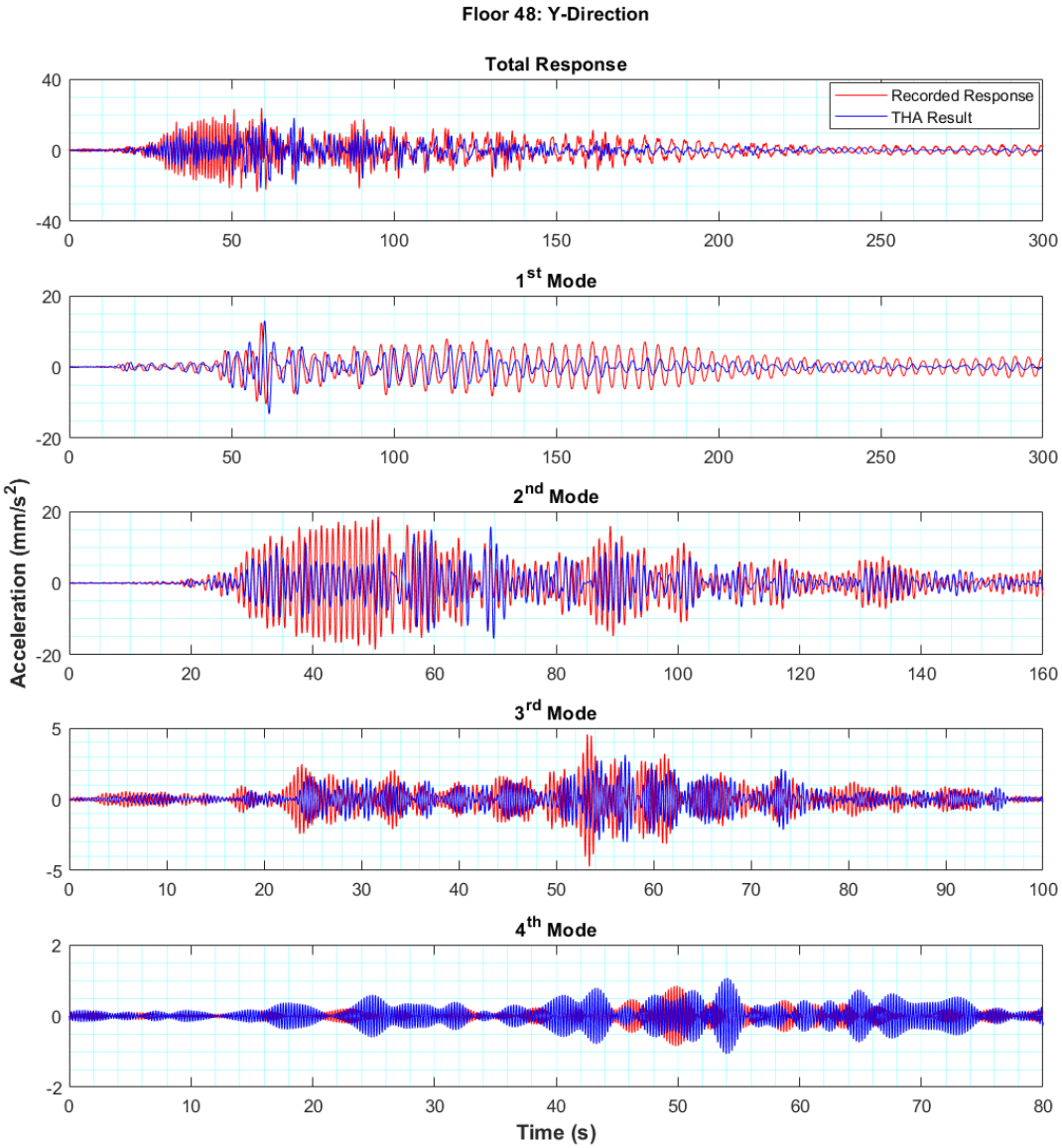

(b)

Figure 4.17 Simulated versus recorded modal acceleration responses of floor 48 for the Canakkale earthquake: (a) X and (b) Y directions (continued)

4.6 Summary

In this chapter, the existing 3-D finite element model of the Mistral Izmir Office Tower and two earthquake strong motion records of the building used in this study were presented. The Canakkale earthquake ground motions were expected to excite the higher modes, while the Istanbul earthquake ground motions were expected to excite the lower modes. Then, the time history analyses were performed using the identified modal damping ratios to reproduce the recorded responses at the instrumented floors. In general, the simulated responses in the Y direction were found to be more accurate than those in the X direction. The second translational modes in both directions were significantly excited and dominated the total responses during both earthquakes. Finally, to evaluate the impact of the damping ratio on the structural response, time history analyses were repeated using the code-specified damping ratios in the finite element model, which were generally higher than the identified damping ratios. Hence, the vibration amplitudes were reduced. The damping was observed to be not constant during the duration of the strong motion records.

CHAPTER 5

SUMMARY, CONCLUSIONS AND FUTURE RESEARCH

5.1 Summary

With the release of TBEC 2018, it became mandatory to install real-time SHM systems on tall buildings in Turkey. AFAD funded two research projects to develop the guidelines for these systems. Mistral Izmir Office Tower was instrumented as part of the research project undertaken at Middle East Technical University. This study focused on the identification of damping ratios of this instrumented tall building from its ambient vibration records. First, examples of instrumented tall buildings, with a particular focus on the reported damping values, and damping estimation methods were reviewed. Then, an algorithm was developed using the random decrement method to identify the modal damping ratios of the building. Using the finite element model of the building developed as part of a previous study, linear elastic time history analyses were performed to reproduce the structural responses of the building under the 2019 M_w 5.0 Ayvacik, Canakkale and M_w 5.8 Marmara Sea, Istanbul earthquakes.

5.2 Conclusions

The dynamic properties of the instrumented tall building under ambient vibrations were identified for the first four modes in the E-W and N-S translational directions and in the torsional direction. The first natural periods of the building are 4.17 s, 4.00 s and 1.72 s and the second natural periods of the building are 1.11 s, 0.93 s and 0.59 s in the E-W, N-S and torsional directions, respectively. The important parameters of the random decrement method that impact the identified damping values were studied and the following parameters were selected:

- Triggering condition was selected as level-crossing with overlap.
- Threshold level was selected as 0.5σ.
- Segment length was selected as 20 vibration cycles.
- Bandpass filter width was selected as 10%.

In addition, the number of segments used in each computation was monitored and kept above 500.

The mean values of the identified modal damping ratios over two separate weeks are 0.64%, 0.65% and 0.55% for the first modes and 0.64%, 0.95% and 2.05% for the second modes in the E-W, N-S and torsional directions, respectively, with CoVs in the order of 0.10–0.40. The random decrement method was found to be robust in identifying the modal damping ratios. The identified modal damping ratios were compared with the values from code and other formulations in literature. In general, the identified damping ratios from ambient vibration records were lower than the calculated values recommended for seismic or wind design of tall buildings, pointing the amplitude dependency of damping.

To simulate the recorded responses of the building under Canakkale and Istanbul earthquakes, linear elastic time history analyses were performed using the identified modal damping ratios. The simulated responses in the Y direction were more successful in predicting the recorded responses than those in the X direction, which significantly underestimated and overestimated the recorded responses at several occasions. The Canakkale earthquake ground motions were expected to excite the higher modes, while the Istanbul earthquake ground motions were expected to excite the lower modes. The STFTs of the building responses revealed that the second translational modes in both directions were excited the most during both earthquakes and dominated the total responses showing the importance of higher mode effects in tall buildings. During both earthquakes, the torsional responses of the building were found to be insignificant compared to the translational responses.

When the 2.5% damping ratio specified in TBEC 2018 was used in the finite element model, the vibration amplitudes were reduced considerably. In general, the code-

specified damping ratio was found to be too high for the dominant modes excited during both earthquakes. Furthermore, the damping was observed to be not constant during the duration of the strong motion records.

5.3 Future Research

The scope and limitations of this study point to the following topics that can be studied in the future:

- the reliability of the random decrement method in estimating modal damping ratios
- the identification of modal damping ratios under ambient vibrations using other system identification methods
- the identification of modal damping ratios under earthquake excitations
- the amplitude dependency of damping ratios
- the simulations of the recorded strong motion responses of the building using more advanced analysis methods

REFERENCES

AFAD [2018]. Turkish Building Earthquake Code 2019, *Official Gazette, No: 30364 (in Turkish).* Disaster and Emergency Management Authority, Ankara, Turkey.

Brincker R, Zhang L, Andersen P [2001a]. Modal identification of output-only systems using frequency domain decomposition. *Smart Materials and Structures*, 10(3): 441–445. doi: 10.1088/0964-1726/10/3/303

Brincker R, Ventura CE, Andersen P [2001b]. Damping Estimation by Frequency Domain Decomposition. In *Proceedings of IMAC 19: A Conference on Structural Dynamics, February 5-8, 2001, Hyatt Orlando, Kissimmee, Florida*, (pp. 698–703). Society for Experimental Mechanics.

Casiano MJ [2016]. *Extracting Damping Ratio From Dynamic Data and Numerical Solutions, NASA/TM—2016–218227.* Huntsville, Alabama, USA. Available at: http://www.sti.nasa.gov (Accessed: 1 January 2022).

Chopra AK [2012]. *Dynamics of Structures: Theory and Applications to Earthquake Engineering*, (4th ed.). Prentice Hall.

Cole HA [1973]. On-line failure detection and damping measurement of aerospace structures by random decrement signatures. *NASA Contractor Reports*. Available at: https://ntrs.nasa.gov (Accessed: 1 August 2021).

Computers and Structures Inc. [2018]. ETABS Version 18.0.1, Walnut Creek, California, USA. Available at: https://www.csiamerica.com/products/etabs (Accessed: 1 September 2022).

Celebi M [2006]. Recorded earthquake responses from the integrated seismic monitoring network of the Atwood Building, Anchorage, Alaska. *Earthquake Spectra, 22*(4): 847–864. doi: 10.1193/1.2359702

Celebi M [2017]. Study of Responses of 64-Story Rincon Building to Napa, Fremont, Piedmont, San Ramon Earthquakes and Ambient Motions. *Earthquake Spectra* 33(3): 1125–1148. doi: 10.1193/031616EQS041M

Celebi M, Kaya Y, eds. [2022]. Seismic monitoring solutions for buildings. In *Sensor Technologies for Civil Infrastructures* (Issue 1). Elsevier Ltd. doi: 10.1016/b978-0-08-102706-6.00004-0

Celebi M, Swensen D, Haddadi H [2021]. Response study of a 51-story-tall Los Angeles, California building inferred from motions of the Mw7.1 July 5, 2019 Ridgecrest, California earthquake. *Bulletin of Earthquake Engineering*, 19(4): 1797–1814. doi: 10.1007/s10518-021-01053-9

Celebi M, Huang M, Shakal A, Hooper J, Klemencic R [2013]. Ambient response of a unique performance-based design tall building with dynamic response modification features. *The Structural Design of Tall and Special Buildings, 22*(10): 816–829. doi: 10.1002/tal.1093

CTBUH [2023]. Mistral Izmir Office Tower. (n.d.). https://www.skyscrapercenter.com/building/mistral-office-tower/14978. (Accessed:1 April 2023).

Dunand F, Bard PY, Chatelain JL, Gueguen P, Vassail T, Farsi MN [2002]. Damping and frequency from randomdec method applied to in situ measurements of ambient vibrations: evidence for effective soil structure interaction. *12th European Conference on Earthquake Engineering*.

Gumus O [2021]. *Guidelines For Structural Health Monitoring Systems On Tall Buildings And A Case Study*, M.S. Thesis, Middle East Technical University, Ankara, Turkey.

Gumus O, Celik OC [2019]. Structural Health Monitoring System on a 216 m Tall Building in Izmir Per the New Turkish Building Earthquake Code, in

Proceedings of the Fifth International Conference on Earthquake Engineering and Seismology, October 8–11. Ankara, Turkey.

Ha T, Shin SH, Kim H [2020]. Damping and natural period evaluation of tall RC buildings using full-scale data in Korea. *Applied Sciences (Switzerland)*, 10(5). doi: 10.3390/app10051568

He Y, Li Q, Zhu H, Han X, He Y, Li X [2018]. Monitoring of structural modal parameters and dynamic responses of a 600m-high skyscraper during a typhoon. *Structural Design of Tall and Special Buildings*, *27*(6): 1–15. doi: 10.1002/tal.1456

ISO [1984] "6897: 1984" Guidelines for the evaluation of the response of occupants of fixed structures, especially buildings and offshore structures, to low-frequency horizontal motion (0.063 to 1.0 Hz).

Jeary AP [1986]. Damping in tall buildings—a mechanism and a predictor. *Earthquake Engineering & Structural Dynamics, 14*(5): 733–750. doi: 10.1002/eqe.4290140505

Kijewski T, Kareem A [2000]. Reliability of Random Decrement Technique For Estimates of Structural Damping. *8th ASCE Specialty Conference on Probabilistic Mechanics and Structural Reliability*, 1: 1–6.

Kijewski T, Kareem A [2002]. On the reliability of a class of system identification techniques: Insights from bootstrap theory. *Structural Safety*, *24*(2–4): 261–280. doi: 10.1016/S0167-4730(02)00028-0

Li QS, Zhou K, Li X [2020]. Damping estimation of high-rise buildings considering structural modal directions. *Earthquake Engineering & Structural Dynamics*, *49*(6): 543–566. doi: 10.1002/eqe.3253

Limongelli MP, Celebi M, eds. [2019]. Seismic Structural Health Monitoring. From Theory to Successful Applications. In *Springer Tracts in Civil Engineering*.

Los Angeles Tall Buildings Structural Design Council [2020]. *An Alternative Procedure for Seismic Analysis and Design of Tall Buildings Located in the Los Angeles Region.* Los Angeles, California, USA.

Mikael A, Gueguen P, Bard PY, Roux P, Langlais M [2013]. The analysis of long-term frequency and damping wandering in buildings using the Random decrement Technique. *Bulletin of the Seismological Society of America*, *103*(1): 236–246. doi: 10.1785/0120120048

Petrovic B, Dikmen SU, Parolai S [2018]. Real data and numerical simulations-based approaches for estimating the dynamic characteristics of a tunnel formwork building. *Bulletin of Earthquake Engineering*, *16*(3): 1633–1656. doi: 10.1007/s10518-017-0250-3

Rodrigues J, Brincker R [2005]. Application of the random decrement technique in operational modal analysis. *Proceedings of the 1st International Operational Modal Analysis Conference, IOMAC 2005*.

Safak E, Cakti E [2014]. Simple techniques to analyze vibration records from buildings, in *Proceedings of the 7th European Workshop on Structural Health Monitoring, July 8–11. Nantes, France.*

Shan J, Zhang H, Shi W, Lu X [2020]. Health monitoring and field-testing of high-rise buildings: A review. *Structural Concrete*, *21*(4): 1272–1285. doi: 10.1002/suco.201900454

Shi W, Shan J, Lu X [2012]. Modal identification of Shanghai World Financial Center both from free and ambient vibration response. *Engineering Structures*, *36*: 14–26. doi: 10.1016/j.engstruct.2011.11.025

Su J, Xia Y, Weng S [2020]. Review on field monitoring of high-rise structures. In *Structural Control and Health Monitoring, 27*(12): 1–24. doi: 10.1002/stc.2629

Tamura Y, Suda K, Sasaki A [2000]. Damping in buildings for wind resistant design. *Int. Symp. on Wind and Structures for the 21st Century*, Techno-Press, Daejeon, Korea, 115–130.

Tamura Y [2012]. Amplitude Dependency of Damping in Buildings and Critical Tip Drift Ratio. *International Journal of High-Rise Buildings, 1*(1): 1–13. doi: 10.1061/41000(315)39

Tamura Y, Kareem A [2013]. Advanced structural wind engineering. In *Advanced Structural Wind Engineering*. doi: 10.1007/978-4-431-54337-4

Tanaka T, Yoshizawa S, Osawa Y, Morishita T [1969]. Period and damping of vibration in actual buildings during earthquakes. *Bulletin of the Earthquake Research Institute, 47*: 1073–1092.

The MathWorks Inc [2019]. MATLAB. Available at: www.mathworks.com/products/matlab. (Accessed:1 April 2020).

Trifunac MD, Todorovska MI [2001]. Evolution of accelerographs, data processing, strong motion arrays and amplitude and spatial resolution in recording strong earthquake motion. In *Soil Dynamics and Earthquake Engineering, 21*(6): 537–555. doi: 10.1016/S0267-7261(01)00013-6

USGS [2023]. NSMP History. (n.d.). https://earthquake.usgs.gov/monitoring/nsmp/history/. (Accessed:1 January 2023).

Zhang J, Li Q [2019]. Identification of modal parameters of a 600-m-high skyscraper from field vibration tests. *Earthquake Engineering and Structural Dynamics*, *48*(15): 1678–1698. doi: 10.1002/eqe.3219.

Zhou K, Li QS [2021]. Reliability analysis of damping estimation by random decrement technique for high-rise buildings. *Earthquake Engineering and Structural Dynamics*, *50*(5): 1251–1270. doi: 10.1002/eqe.3396.